770-R-1

PRE-SUNRISE CHANGES IN VLF RADIO WAVES IONOSPHERICALLY REFLECTED NEAR VERTICAL INCIDENCE

GPO PRICE $ _____

CSFTI PRICE(S) $ _____

Hard copy (HC) $4.00

Microfiche (MF) .75

ff 653 July 65

FACILITY FORM 602

N65-35581 (ACCESSION NUMBER)

110 (PAGES)

CR-62375 (NASA CR OR TMX OR AD NUMBER)

1 (THRU)

(CODE)

13 (CATEGORY)

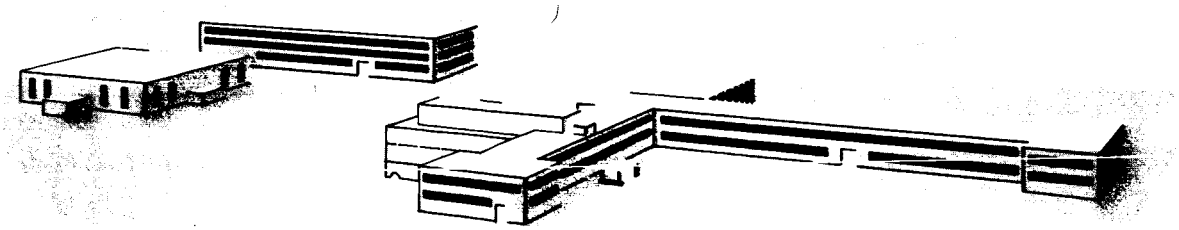

HRB

HRB-SINGER, INC.

SCIENCE PARK · STATE COLLEGE, PENNSYLVANIA

A SUBSIDIARY

"The following publication designations and their descriptions outline the system used by HRB-Singer, Inc., to differentiate the various types of technical publications."

Project No. Serial No.	
37 - 42	No letter designation is given to Interim Progress Reports.
37 - R - 42	"R" is designated to all technical reports completing a task on a current project.
37 - F	"F" is assigned to all Final Report designations.
53 - M - 46	"M" designation is assigned to all equipment operation and maintenance manuals.
P - 612	"P" is assigned to all proposals.
S - 24	"S" describes Special Publications.

HRB-SINGER, INC.
A SUBSIDIARY OF THE SINGER COMPANY
Science Park, State College, Pa.

770-R-1

PRE-SUNRISE CHANGES IN VLF RADIO WAVES IONOSPHERICALLY REFLECTED NEAR VERTICAL INCIDENCE

Contract No. NASW-1109
National Aeronautics and Space Administration
Washington, D.C.

June 1965

Copy No. 1 of 65 Copies

Prepared By:
J. M. Musser
C. F. Sechrist, Jr.

Reverse (Page ii) Blank

ABSTRACT

This report describes the results of steep-incidence VLF measurements conducted at Wallops Island, Virginia, which complemented D-region rocket experiments carried out by the University of Illinois. The VLF data reveal indirectly the variability of non-deviative absorption caused by the formation of the C-layer prior to ground sunrise.

On the basis of several electron density distributions and plausible collision frequency profiles, the non-deviative absorption of several assumed C-layers is computed. Also, the results of full-wave solutions by the U.S. Navy Electronics Laboratory and the Radio and Space Research Station (Slough) are presented. The implications of the theory and experiment conclude this report.

Reverse (page iv) Blank

TABLE OF CONTENTS

TABLE OF CONTENTS (Cont'd)

LIST OF ILLUSTRATIONS

LIST OF ILLUSTRATIONS (Cont'd)

A. INTRODUCTION

VLF recordings of the amplitude and relative phase of the abnormal component of the NSS (21.4 kc/s) skywave were made at Wallops Island, Virginia, during the week of 12 July 1964. Also, recordings of the amplitude and phase of the normal and abnormal components were made during the weeks of 8 November and 15 November 1964. These ground-based, steep-incidence VLF measurements complemented D-region rocket experiments by the University of Illinois, which were conducted prior to and following ground sunrise on 15 July, near sunrise on 10 November, near sunset on 19 November, and when the solar zenith angle was near 60 degrees on 19 November. The rocket experiments were designed by Prof. S. A. Bowhill of the University of Illinois to study the role of photodetachment in the lower D-region and the change in ionospheric structure from nighttime to daytime. Since VLF amplitude and phase measurements near vertical incidence of the downcoming skywave constitute one of the most sensitive ways of determining the diurnal and seasonal variations of the lower boundary of the D-region, they proved useful adjuncts to the rocket measurements.

Following a description of the VLF experimental technique, the adjustments of the normal and abnormal antenna systems are described. The experimental data collected in July and November 1964 are presented with emphasis placed on the amplitude and phase variations occurring during the sunrise transition. Next, the current state of knowledge concerning the pre-sunrise changes in the lower ionosphere are reviewed, and some examples of theoretical and experimental C-layer electron density profiles are described.

Several C-layers are assumed having peak electron densities varying between 20 and 200 electrons per cm^3, and Sen-Wyller formulation of the absorption coefficient is utilized to compute the non-deviative C-layer absorption values; these values are compared with those derived from full-wave solutions carried out by NEL. Finally, several electron density profiles derived by Deeks are utilized in a full-wave solution by the Radio and Space Research Station (Slough) to compute the magnitudes of the reflection and conversion coefficients as a function of solar zenith angle. The implications of the VLF measurements, non-deviative absorption computations, and the full-wave solution are discussed and some tentative suggestions concerning the C-layer and the reflection of VLF waves near vertical incidence are presented.

Reverse (Page 2) Blank

B. DESCRIPTION OF EXPERIMENTAL TECHNIQUE

The electromagnetic field at the receiver is composed of a linearly polarized ground wave and an elliptically polarized downcoming skywave. The ground wave has its electric vector vertical and its magnetic vector horizontal and perpendicular to the plane of propagation. The skywave may be split into two linearly polarized components: one, which like the ground wave has the magnetic vector horizontal, is called the normally polarized component (normal component) of the skywave; the other has the electric vector horizontal and is called the abnormally polarized component (abnormal component) of the skywave. These various field components are shown in Figure 1A, where the subscripts are 0 for ground wave, 1 for normal component of sky wave and 2 for the abnormal component.

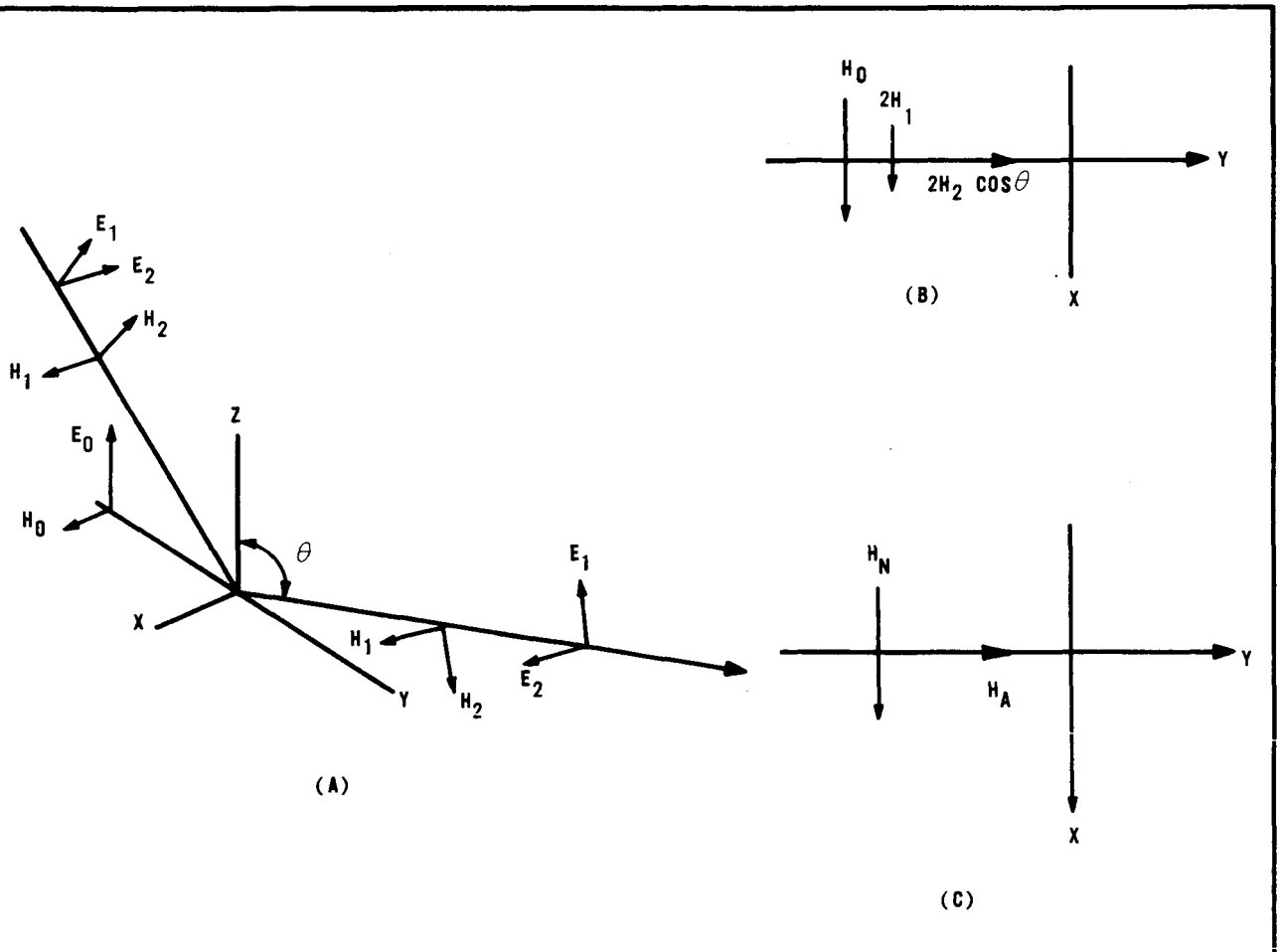

FIG. 1 COMPONENTS OF THE FIELD AT THE GROUND (BRACEWELL, 1952)

The total magnetic field at the ground is horizontal and, as shown in Figure 1B, consists of H_0, the ground wave, $2H_1$, the normally polarized sky-wave (doubled because of the contribution from the reflected wave), and a component $2H_2 \cos \theta$, the sum of the horizontally resolved parts of the incident and ground-reflected abnormally polarized waves.

The measurable quantities are H_N, the total normal component, and H_A, the abnormal component, of the horizontal magnetic field (Figure 1C) and they may be expressed as:

$$H_N = H_0 + 2H_1 \tag{1}$$

$$H_A = 2H_2 \cos \theta \tag{2}$$

In general, the two vectors are not in the same phase. Their result, thus, traces an elliptical locus, the horizontal-field ellipse.

1. REFLECTION AND CONVERSION COEFFICIENTS

The wave emitted from a VLF transmitter (e.g., NSS at 21.4 kc/s) with a vertical antenna is polarized with its electric vector parallel to the plane of incidence, but after reflection it is polarized with components both parallel and perpendicular to the plane of incidence. The strengths of these components, relative to the incident field, are denoted by the reflection coefficient $_{\parallel}R_{\parallel}$ and the conversion coefficient $_{\parallel}R_{\perp}$. These coefficients are defined in terms of an assumed model in which reflection takes place sharply from a plane boundary with no absorption or refraction at lower levels; and the ground reflection coefficient is assumed to be unity.

Reflection and conversion coefficients may be calculated from the equations

$$\frac{2H_1^{(1)}}{H_o} = 2\frac{d}{S^{(1)}} \sin \theta^{(1)} \, (_{\parallel}R_{\parallel}) \tag{3}$$

$$\frac{H_A^{(1)}}{H_o} = 2\frac{d}{S^{(1)}} \sin \theta^{(1)} \cos \theta^{(1)} \, (_{\parallel}R_{\perp}) \tag{4}$$

where $d/S^{(1)}$ is the ratio of the paths traversed by the ground and one-hop sky-wave; the factor 2 allows for doubling by ground reflection, the sine and cosine factors allow respectively for the transmitter polar diagram and for resolving the magnetic field horizontally at the ground, and the superscripts indicate the once-reflected wave (Bracewell, 1952).

2. ISOLATION OF THE DOWNCOMING WAVE

The method of investigating the ionosphere by observing the changes of phase of the downcoming wave was in use at the Cavendish Laboratory (Weekes and Stuart, 1951) for many years, and the problems involved in isolating the downcoming wave by special antenna systems have been described in detail by Best et al., (1936). The method will be outlined briefly as follows:

In general, the electromagnetic field at the receiver consists of a ground wave with electric and magnetic fields, E_o and H_o, and a downcoming wave incident at angle θ with the normal component of the electric field (E_1 associated with H_1 perpendicular to it) in the plane of incidence and the abnormal component (E_2 associated with H_2) perpendicular to the plane of incidence. The downcoming wave is completely specified by these two components and the phase difference between them.

In order to measure the phase of one component, say E_1, relative to the much stronger ground wave, it is necessary to separate the two fields. To isolate the abnormal component, E_2, it is necessary only to use a well-designed loop antenna with its plane perpendicular to the plane of incidence.

If it is desired to observe the normal component, E_1, a loop antenna is positioned so that its plane is in the plane of incidence and it receives an emf proportional to

$$E_o + 2E_1$$

A vertical whip antenna receives an emf proportional to

$$E_o + 2E_1 \sin \theta$$

so that these two emf's may be added in the appropriate phase and amplitude so as to eliminate E_o and leave in the combined antenna system an emf proportional to

$$2E_1 (1-\sin \theta)$$

If there were no downcoming wave at a certain time (e.g., at midday), it would be possible to adjust the antenna systems to receive zero signal, and any signal received at other times would represent the downcoming wave alone. Some downcoming wave is , however, always present and the optimum adjustment of the antenna systems must then be made by a process of trial and error. Since the downcoming wave changes phase by several complete periods, the curve obtained by plotting phase and amplitude of the wave received on the antenna system on a polar plot should circle around the origin if there is only the downcoming wave present.

If there is some ground wave present, the curve obtained will appear to circle about a point which is separated from the origin by the vector representing the residual ground wave. These interference effects between the constant ground wave and the variable downcoming skywave are particularly noticeable during sunrise and sunset, when the downcoming wave varies steadily with time. Small adjustments are made on successive days until the interference effects are no longer noticeable. These adjustments are described in more detail in Best et al. (1936) and Bracewell (1952).

C. EXPERIMENTAL RESULTS

1. VLF MEASUREMENTS IN JULY 1964

During several hours preceding and following the July 15 rocket firings, VLF amplitude and phase data were recorded manually so that a plot of the abnormal phase and amplitude could be prepared quickly. Initially, the phase and amplitude data were plotted on polar-coordinate paper as shown in Figure 2; this is called an amplitude-phase diagram, or ABLIL which means abnormal loop induction locus.

An important feature of the ABLIL is the ability to determine accurately the extent of the ground wave suppression during the daytime. If there is a constant ground wave component present, the daytime ABLIL (in the form of a spiral) should be centered on the tip of the ground wave vector and its displacement from the origin represents the magnitude and phase of the ground wave. If there is only a skywave present, the locus of the vector should approximate a spiral centered on the origin as the reflecting layer varies through the day. At night the signal is too erratic for this technique to be useful; following sunrise the signal generally becomes quite stable and meaningful plots can be obtained.

Figure 3 shows an ABLIL for a 24-hour period between July 16 and 17. Note the high degree of variability at night and the reasonably steady behavior during the daytime.

In Figure 4, the amplitude and phase are plotted as a function of time and the solar zenith angle, around the sunrise transition period for July 15. Also, the time variation of the phase during the sunrise transition is presented for July 16. Note that the time of ground sunrise (GSR) and the times of various layer sunrises are indicated. One layer sunrise (LSR) corresponds to the time at which the earth's shadow reaches the nighttime reflection height of about 90 km. Another layer sunrise (LSR') corresponds to the time at which the ozone layer's shadow reaches the nighttime reflection height of 90 km.

Figure 5 illustrates the amplitude and phase behavior around the sunrise transition period for July 17. Note the presence of a plateau in the phase plot during the transition interval. It is believed that this plateau is caused by a recombination mechanism such as that described by Hargreaves (1962); this interpretation will be discussed in more detail in a subsequent section.

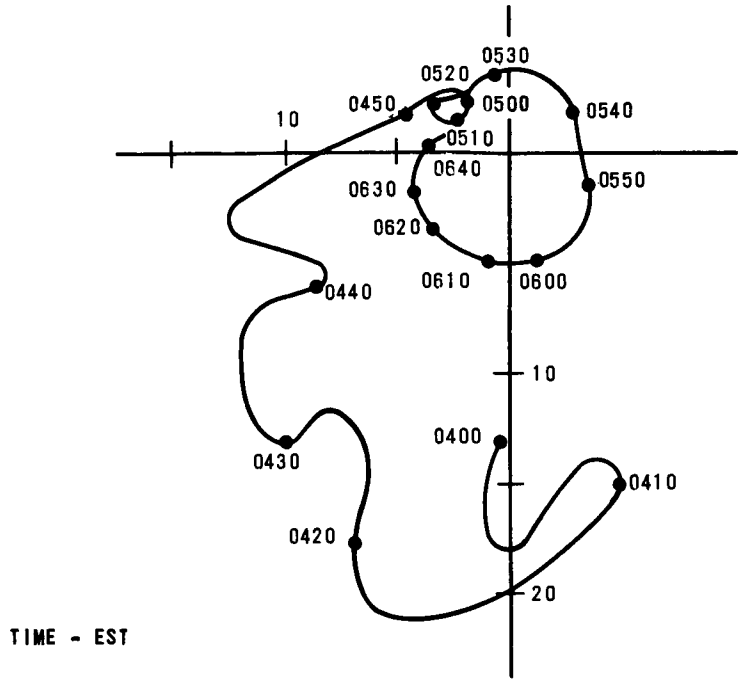

FIG. 2 ABLIL FOR JULY 15, 1964

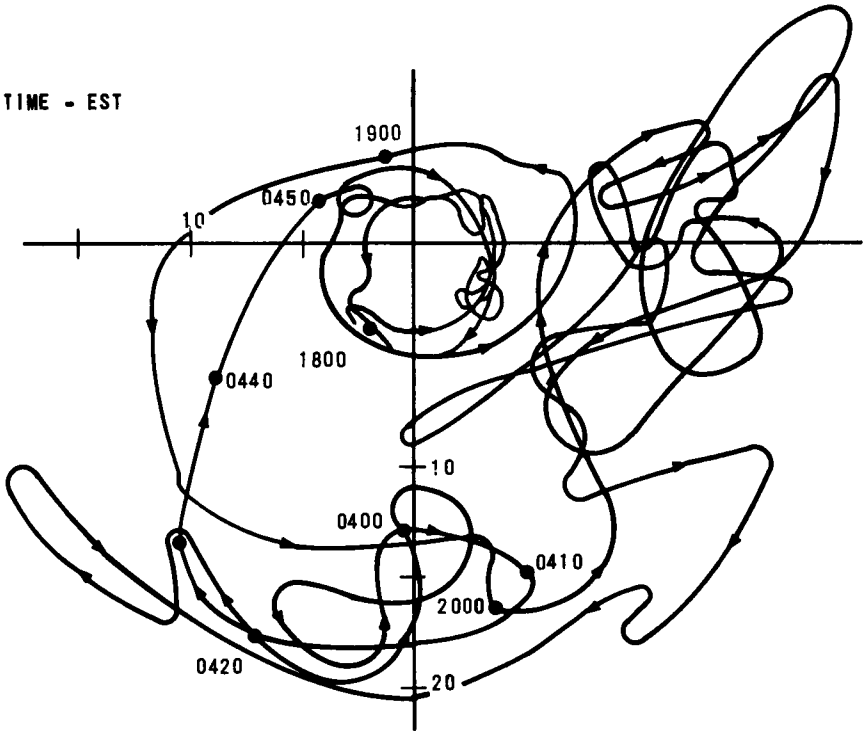

FIG. 3 ABLIL FOR JULY 16-17, 1964

On the basis of the propagation geometry and the measured amplitudes of H_A and H_o, the magnitude of the conversion coefficient was computed as a function of time from the VLF data for July 16-17. Figure 6 is a plot of $|R_{\perp}|$ for the time period between 1200 EST on July 16 and 1200 EST on July 17. Also shown in Figure 6 is a plot of the relative phase for the same interval; since the phase change relates to the height change of the reflecting layer, the right-hand ordinate gives the height change in km.

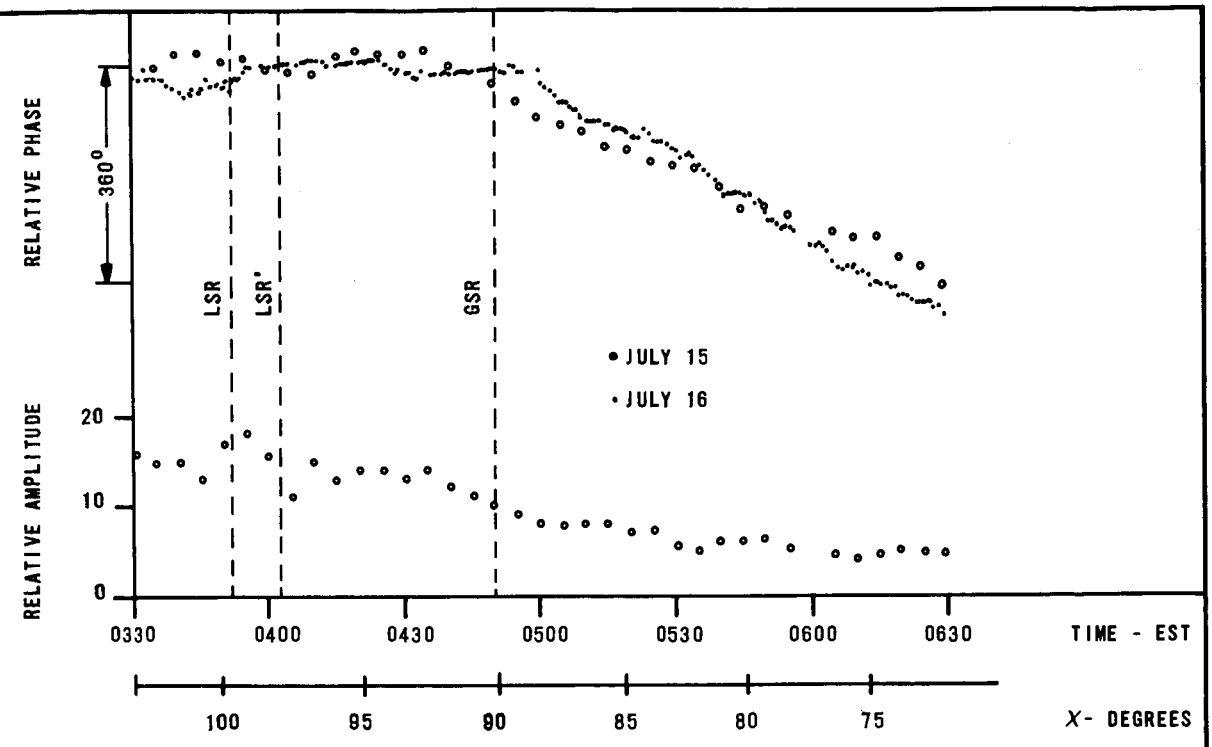

FIG. 4 ABNORMAL COMPONENT FOR JULY 15 AND 16, 1964

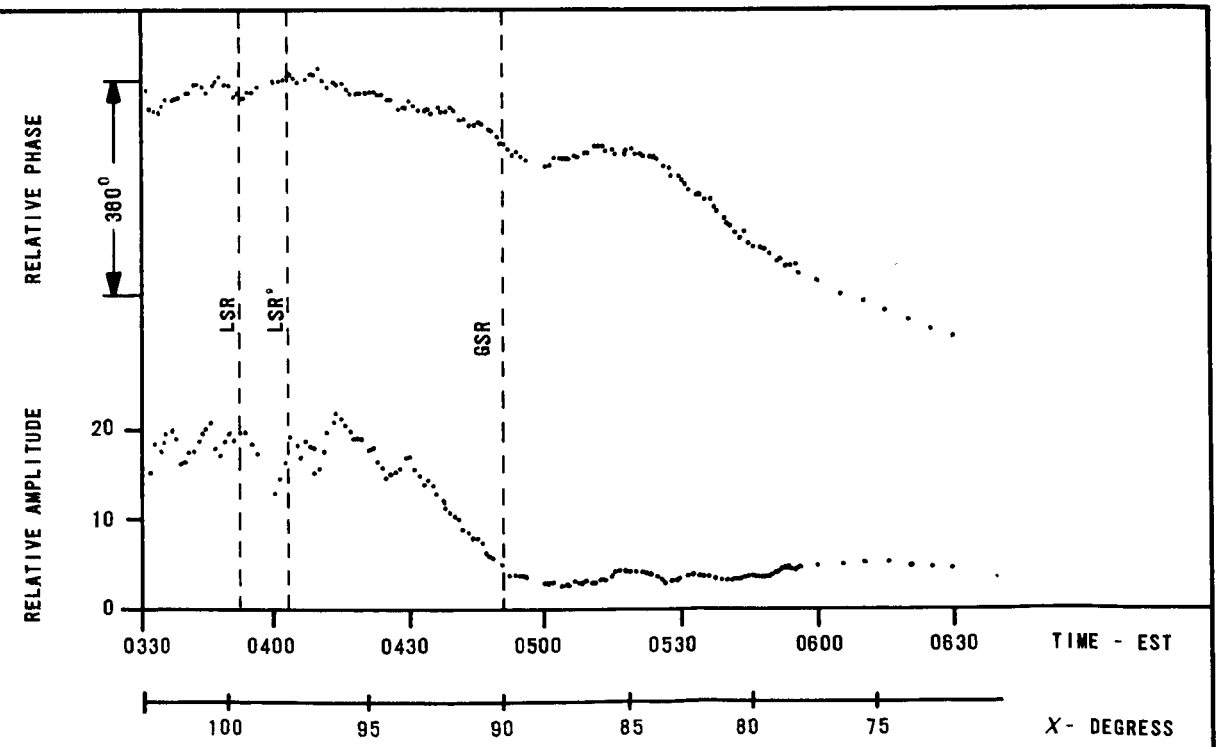

FIG. 5 ABNORMAL COMPONENT FOR JULY 17, 1964

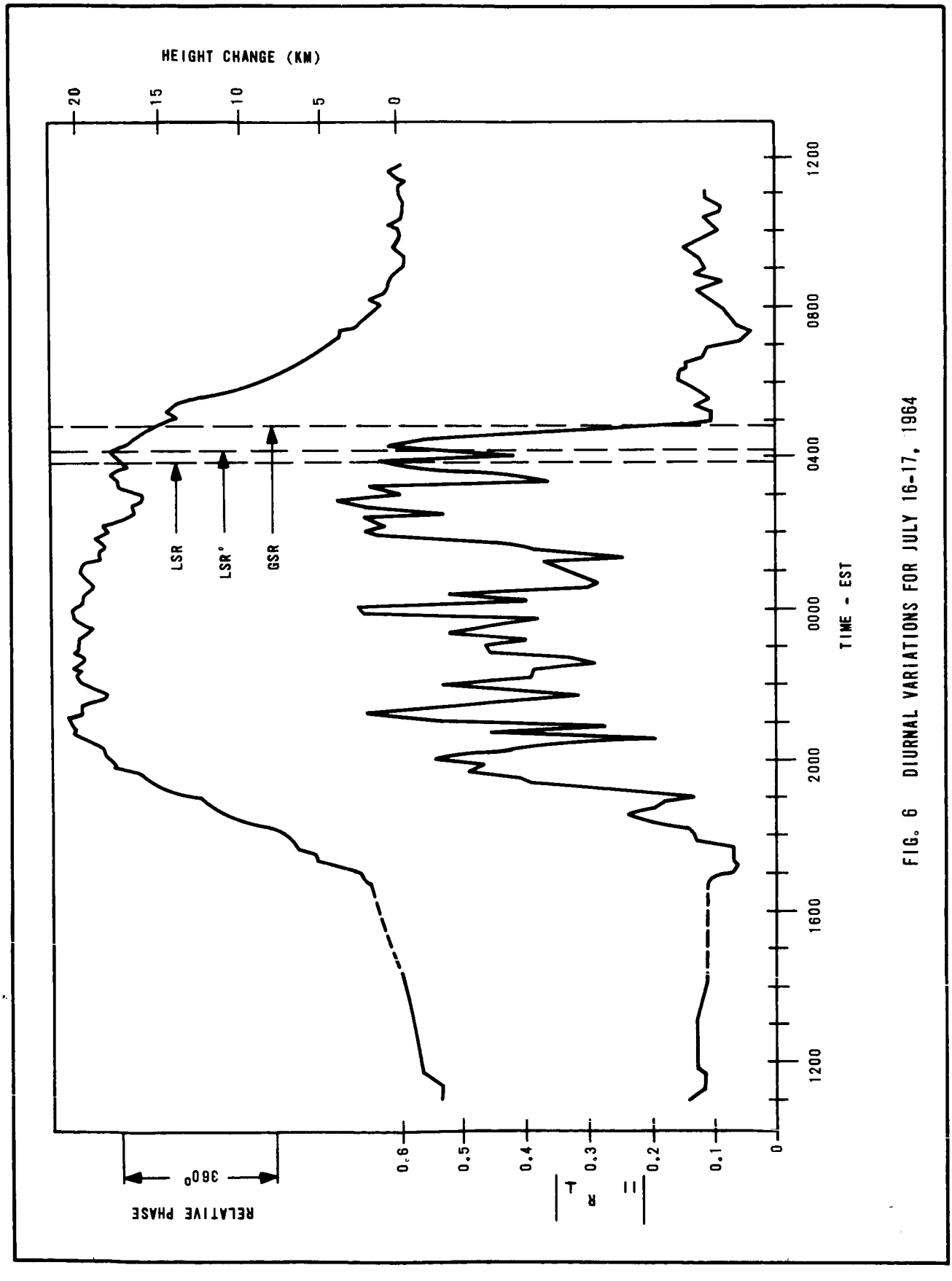

FIG. 6 DIURNAL VARIATIONS FOR JULY 16-17, 1964

2. VLF MEASUREMENTS IN NOVEMBER 1964

During the weeks of 8 November and 15 November 1964 recordings of the amplitude and relative phase of the normal and abnormal components were made. These measurements complemented D-region rocket experiments by the University of Illinois which were conducted near ground sunrise on 10 November, near sunset on 19 November, and when the solar zenith angle was near 60 degrees on 19 November 1964.

(a) Abnormal Component in November 1964

The data of November 12, 1964, are presented as a typical day representative of the data for each day of recording in November 1964. An ABLIL is shown in Figure 7 to illustrate the suppression of the ground wave. In Figure 8 the amplitude and phase of the abnormal component are plotted as a function of time and solar zenith angle. Note the phase did not begin to advance until nearly $\chi = 90^{\circ}$ at which time it advanced rapidly by about 360°; after this the solar control of the phase is evident from the log sec χ behavior as the phase advanced about 360° more. The noon amplitude is seen to be about 18 db below the average night amplitude.

(b) Normal Component in November 1964

Again the data for November 12 are presented. Figure 9 is a NORLIL which means normal loop induction locus; this illustrates the suppression of the ground wave on the normal loop/whip system. As seen in Figure 10 there is little change in the phase of the nighttime signal until $\chi = 90^{\circ}$; at that time the phase begins to advance rapidly by about 360°. Shortly after sunrise the phase retards by 35° and then remains constant throughout the day. The amplitude of the normal component is attenuated by about 18 db at sunrise but then increases again; the daytime and nighttime amplitude of the normal component are approximately equal.

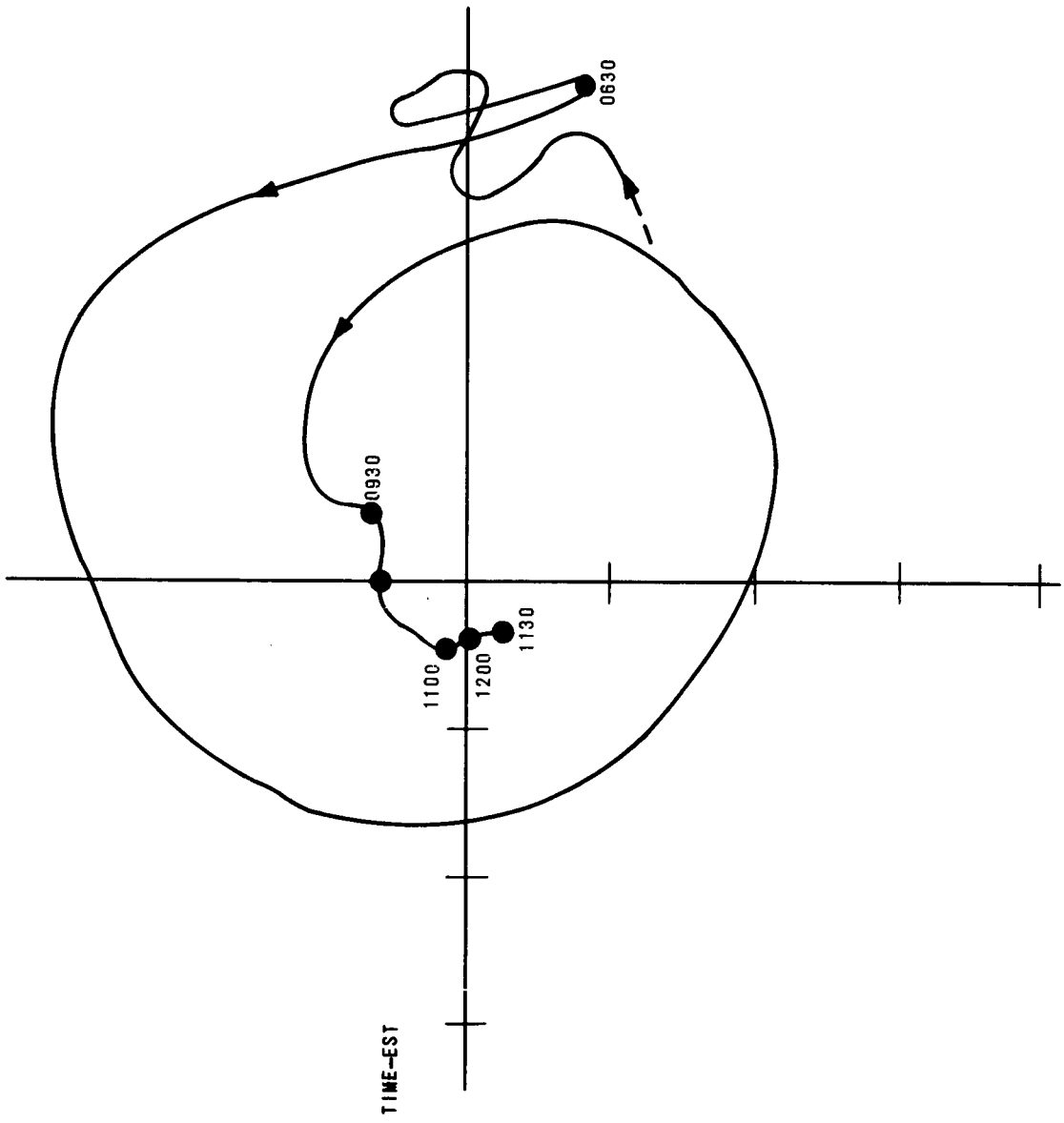

FIG. 7 ABLIL FOR NOV. 12, 1964

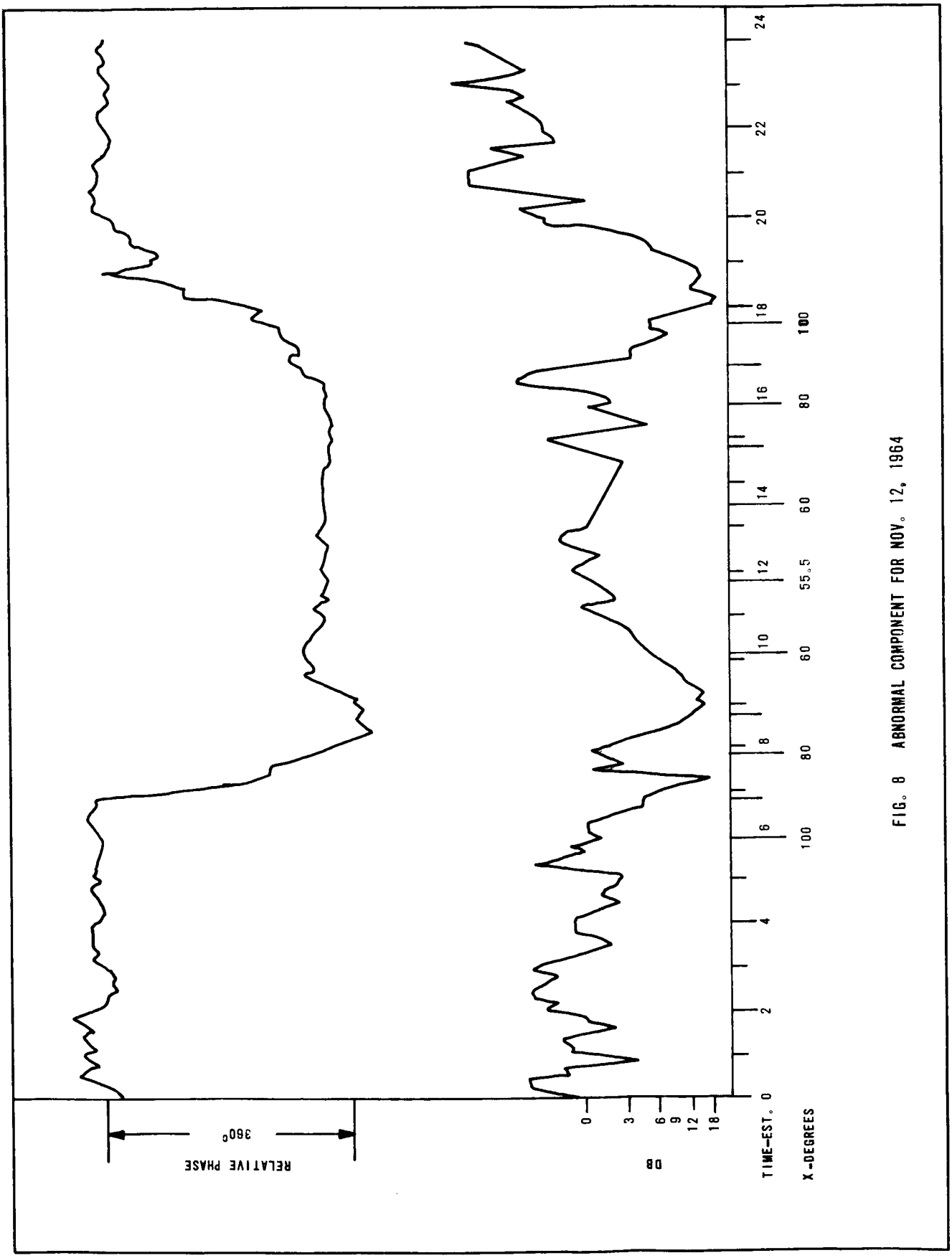

FIG. 8 ABNORMAL COMPONENT FOR NOV. 12, 1964

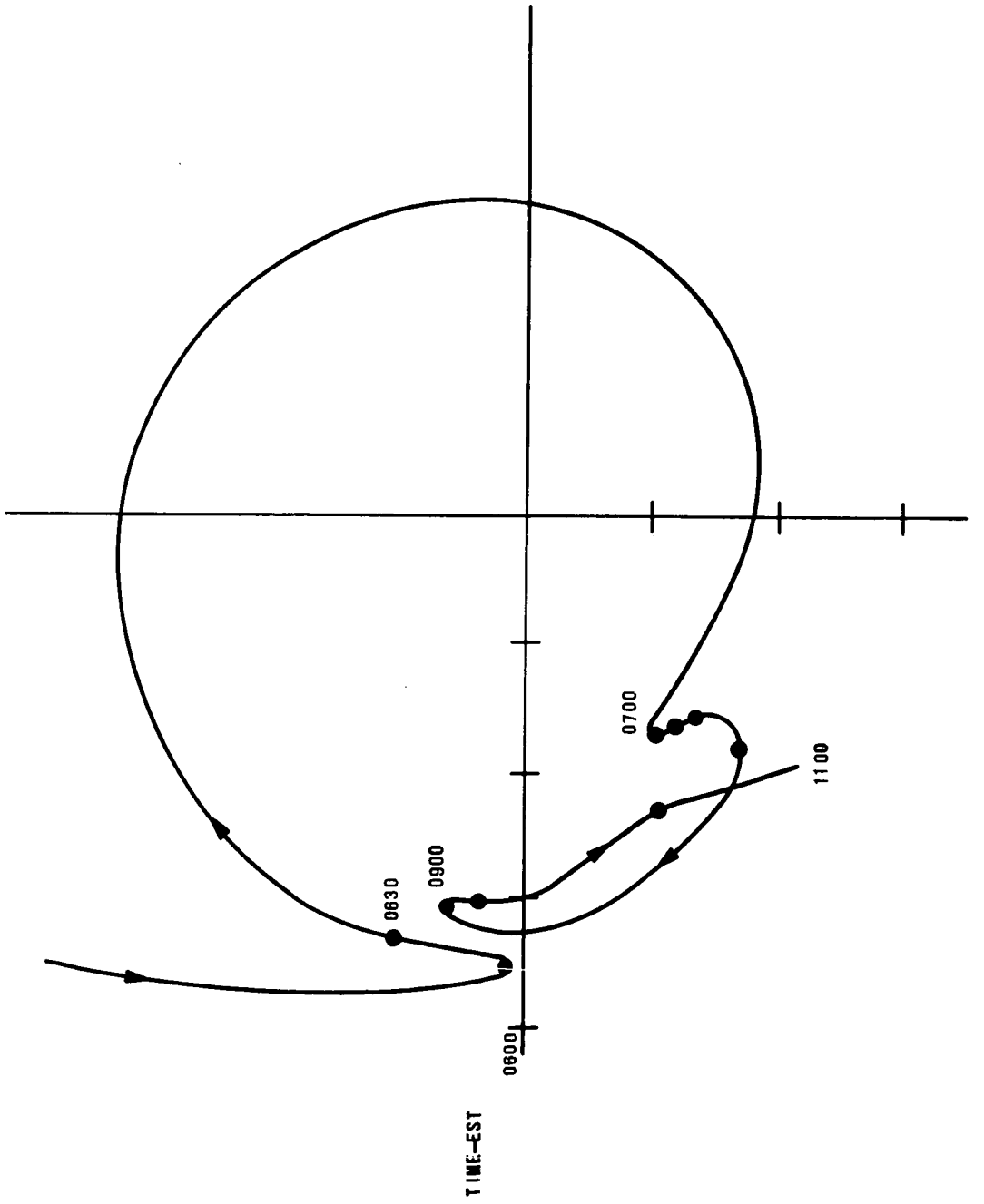

FIG. 9 NORLIL FOR NOV. 18, 1964

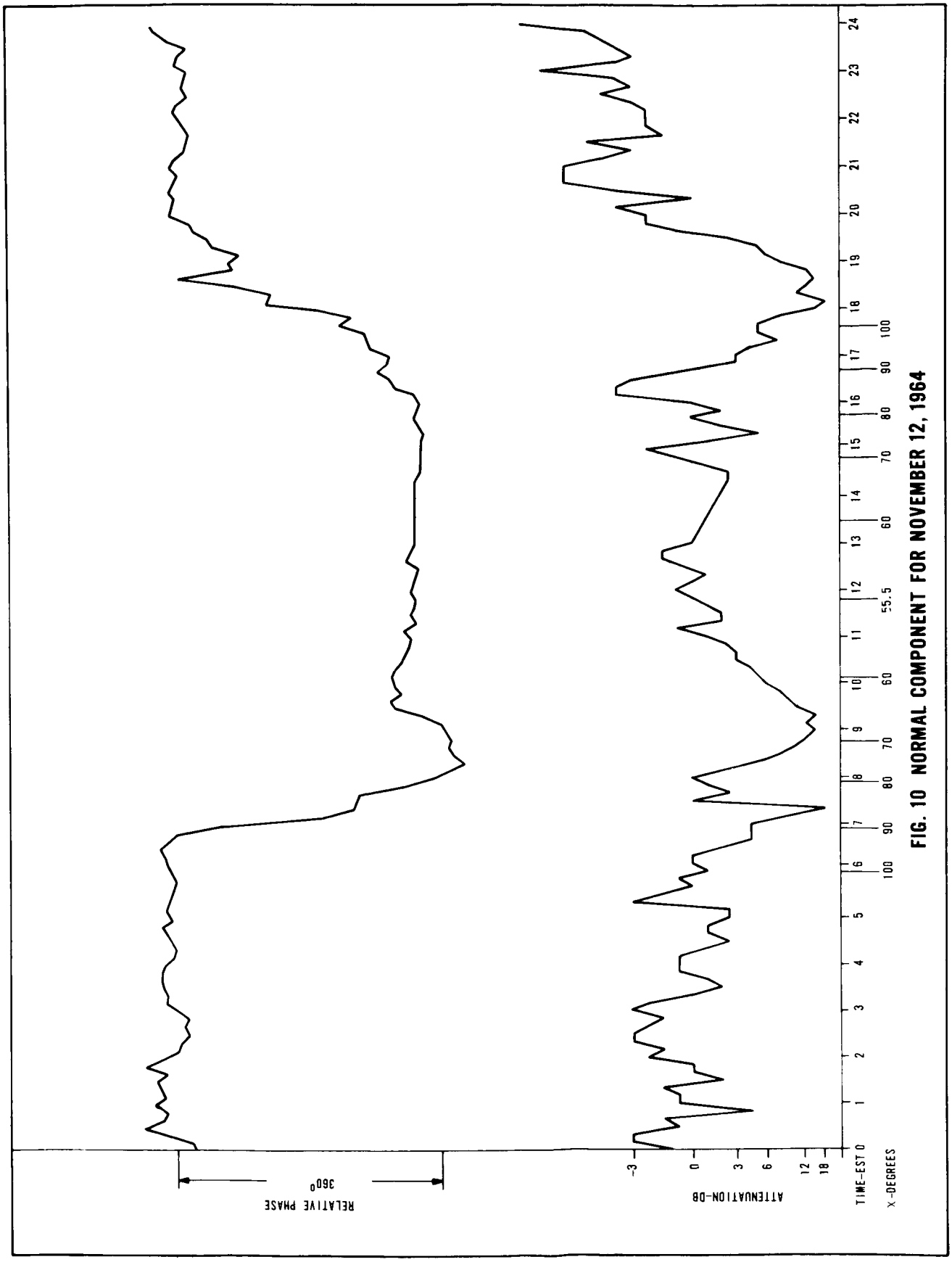

FIG. 10 NORMAL COMPONENT FOR NOVEMBER 12, 1964

D. THEORETICAL CONSIDERATIONS

1. PRE-SUNRISE CHANGES IN THE LOWER IONOSPHERE

Most of the observed changes in amplitude and phase of the abnormal component prior to and following ground sunrise were anticipated and agree with the extensive measurements of Bracewell, et al. (1951). From their results, it was concluded that waves of frequencies 16-113 kc/s, incident nearly vertically on the ionosphere, undergo a sudden decrease in amplitude about one hour before ground sunrise; but that no sudden change of phase occurs until near ground sunrise. The same waves, propagated over distances of 500-900 km, undergo similar changes of amplitude; but their phase also starts to change suddenly about one hour before ground sunrise at the midpoint of the propagation path. The start of the amplitude change occurred when the sun's zenith angle at the midpoint of the path was about 98°.

The explanation of the first above mentioned sunrise effect is likely as follows. The electron density produced before ground sunrise by the release of electrons from negative ions is not sufficient to reflect VLF waves transmitted at near vertical incidence; hence reflection does not take place at lower levels until after ground sunrise. However, the number of electrons produced is sufficient to increase the absorption and the wave is returned with reduced amplitude.

Bracewell, et al, (1951) reported that the pre-sunrise effects occur when the solar ultraviolet rays impinge on the atmosphere at a height of 90 km, and it can be shown that the solar rays would be tangential to a sphere situated about 30 km above the surface of the earth at the time when the effects are first noticed.

Following the work of Bracewell, et al. (1951), Brown and Petrie (1954) considered the effect of sunrise on the reflection height of low and very low frequency waves. By considering the geometry of the situation, they reasoned that the process of photoionization of atmospheric molecules cannot produce the observed effect since the relevant wavelengths are absorbed before reaching the 90 km nighttime reflection height. However, they asserted that electrons may be removed from negative oxygen ions (O_2^-) by visible and near infrared radiation which does reach the 90 km level prior to ground sunrise. Brown and

Petrie (1954) showed that the pre-sunrise effect at 90 km was explicable in terms of a negative ion, photodetachment phenomenon.

Moler (1960) stated that photodetachment begins immediately with the illumination, and the electron densities produced by cosmic rays quickly change from the night to the day values. The result is that a sharp discontinuity in the electron density profile develops at the position of the grazing solar rays. When the illumination reaches the region of negligible daytime electron densities (near 60 km) the sharp discontinuity disappears. At this time the maximum electron density gradient in the cosmic-ray-produced layer is at the daytime equilibrium position at the lowest inflection point in the profile. At ground sunrise, photoionization of nitric oxide by Lyman alpha begins and a second sharp gradient in the electron density profile is produced above the cosmic-ray-produced layer.

Reid and Leinbach (1962) and Reid (1961) suggested that the dominant negative ion during twilight was not O_2^-, but some ion with a much larger electron affinity, requiring ultraviolet light for efficient photodetachment. The effective screening region for ultraviolet light is the ozone layer, and when the solid earth shadow reaches 60 km (at the midpoint of the propagation path), the shadow of the top of this layer is in the neighborhood of 90 km, the nighttime reflection level; hence, it is likely that the effective shadow is not that of the the solid earth, but of an atmospheric layer, such as the ozone layer. Because the ozone layer is practically opaque to wavelengths below about 2900 Angstroms (an energy of 4.25 ev), Reid and Leinbach (1962) suggested that the effective negative ion must be one which requires at least 4.25 ev for photodetachment; they have suggested that NO_2^- and O_3^- are possible candidates.

Around sunrise, the cross-modulation observations of Barrington and Thrane (1962) require that electron densities of around 100 electrons/cm^3 exist between 60 and 70 km previous to or simultaneously with the appearance of such densities between 70 and 80 km; and there is some evidence which might suggest that this ionization which appears between 60 and 80 km around sunrise may have a broad maximum between 60 and 70 km. This conclusion is consistent with theoretical predictions by Nicolet and Aikin (1960) and Aikin (1962) which consider the production of electrons in the height range from 60 to 80 km by cosmic rays. During the sunrise period the density of free electrons at such heights would increase rapidly due to a photodetachment process. That electron

densities created in this manner, would occur before ionization at greater heights, due to solar Lyman alpha radiation, is of importance. Moreover, the resultant electron densities deduced from observations made at midday agree fairly well in the range from 60 to 75 km with those predicted by Nicolet and Aikin (1960), on the basis of these processes.

2. HOLT'S C-LAYERS

This section presents some results that were obtained by Barrington, et al. (1962) and by Holt (1963) with regard to electron density profiles in the lowest ionosphere. Essentially, Holt computed C-layer electron density profiles as a function of solar zenith angles between 90 and 100 degrees; these profiles were deduced from theoretical values for the variation of electron density with solar zenith angle (Reid, 1961). Of course, the electron densities depend on the value of the coefficient of collisional detachment, which determines the ratio between night and day values of the electron density; this coefficient and some of the other reaction coefficients involved are not well known, and Holt's calculations are, therefore, only approximate.

The form of the C-layer at the time of ground sunrise (or sunset) was established by Barrington, et al. (1962) from observations of ionospheric cross modulation. The resulting electron density profile at ground sunrise, is shown in Figure 11; in addition, Holt's computed profiles are illustrated in the same figure.

In a subsequent section of this report, Holt's C-layer profiles are utilized in computations of the non-deviative abosorption of a VLF skywave, ionospherically reflected near vertical incidence. Also, Holt's C-layer profiles are used in conjunction with a nighttime profile to compute the magnitudes of VLF reflection and conversion coefficients, on the basis of full-wave computations by the U.S. Navy Electronics Laboratory.

3. ROCKET C-LAYER PROFILE

The University of Illinois has conducted D-region rocket experiments at Wallops Island, Virginia, to study the role of photodetachment in the lower D-region and the change in ionospheric structure from nighttime to daytime. The development and decay of the ionosphere up to 160 km at sunrise and sunset has been observed in this series of rocket flights (Bowhill and Kleiman, 1964; Bowhill and Smith, 1965).

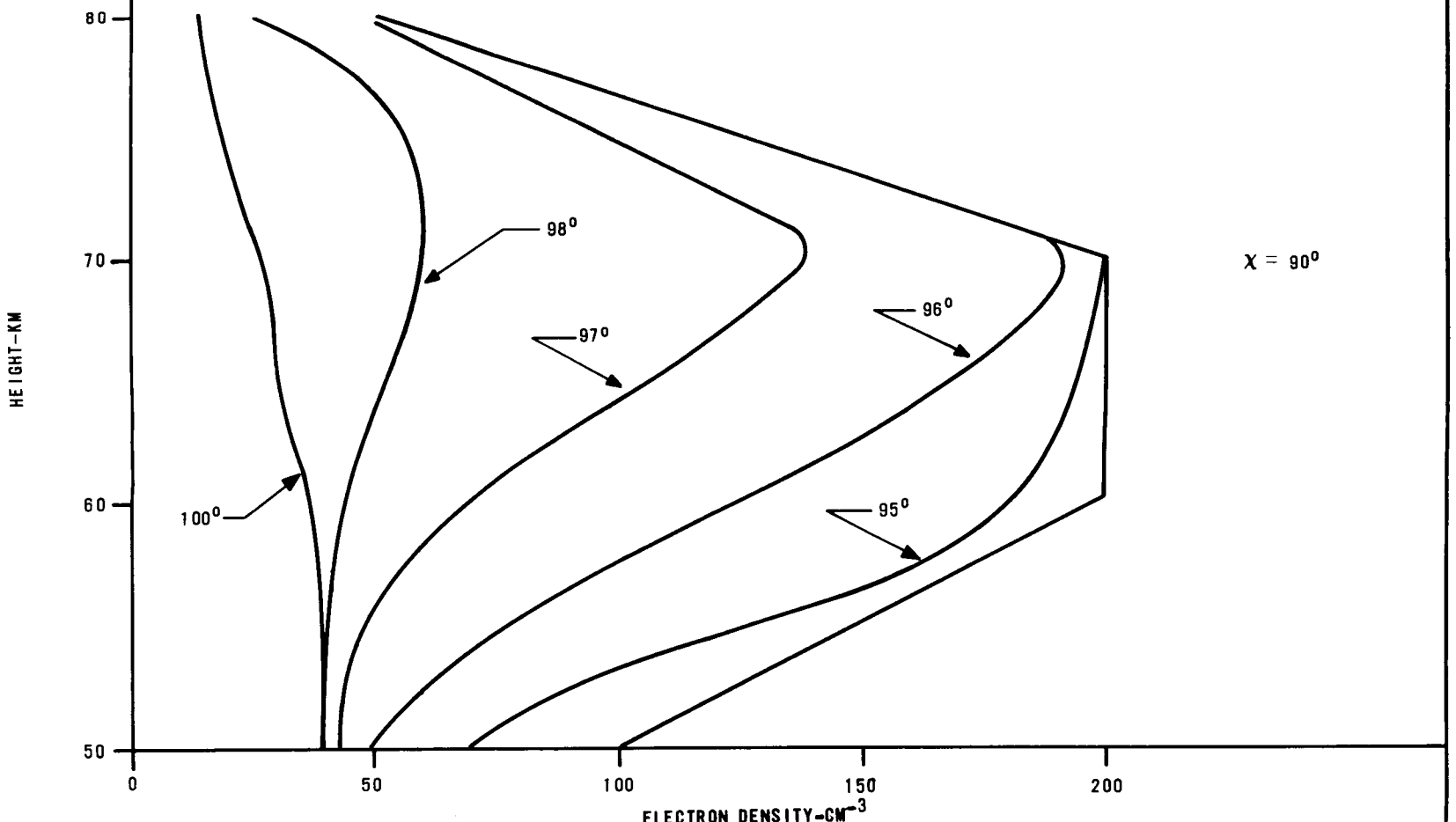

FIG. 11 ELECTRON DENSITY PROFILES DEDUCED FOR DIFFERENT SOLAR ZENITH ANGLES (O. HOLT, NDRE REPORT NO. 46)

Three flights on the morning of 15 July 1964, at solar zenith angles of about 108, 95 and 85 degrees show the rapid increase of the electron density below 85 km as solar ultraviolet radiation illuminates the region.

A further flight on the morning of 10 November 1964 confirmed the foregoing observation.

The rocket measurements, therefore, demonstrated that solar visible radiation did not result in photodetachment; it must be presumed that the negative ions in the D-region at night may not be O_2^- but may be O_3^- or NO_2^-.

Two rocket flights at zenith angles of about 77and 95 degrees on 19 November 1964 showed that the attachment of electrons at sunset takes place rapidly and the region can be regarded as being in equilibrium during the transition period (Bowhill and Smith 1965).

The C-layer profile obtained on 15 July 1964, when the solar zenith angle was 85 degrees, is shown in Figure 12. It should be noted that the electron density values were deduced by means of composite probe and propagation experiments on each rocket payload. This rocket C-layer profile will be utilized in computations of the non-deviative VLF-skywave absorption.

4. NON-DEVIATIVE ABSORPTION EQUATION

It is now well known that the discrepancy between classical magneto-ionic theory and generalized theory, in which the energy dependence of the electron collision frequency is taken into account, is appreciable in most of the lower ionosphere.

Sen and Wyller (1960) derived the following expression for the absorption coefficient for propagation along the geomagnetic field lines:

$$k = \frac{\omega}{c\sqrt{2}} \left[\frac{\omega_o^2 (\omega \pm \omega_H)}{\omega \nu_m^2} C_{3/2} \left(\frac{\omega \pm \omega_H}{\nu_m} \right) - 1 \right.$$

$$\left. + \left(\left\{ 1 - \frac{\omega_o^2 (\omega \pm \omega_H)}{\omega \nu_m^2} C_{3/2} \left(\frac{\omega \pm \omega_H}{\nu_m} \right) \right\}^2 \right. \right. \qquad (1)$$

(Continued on next page)

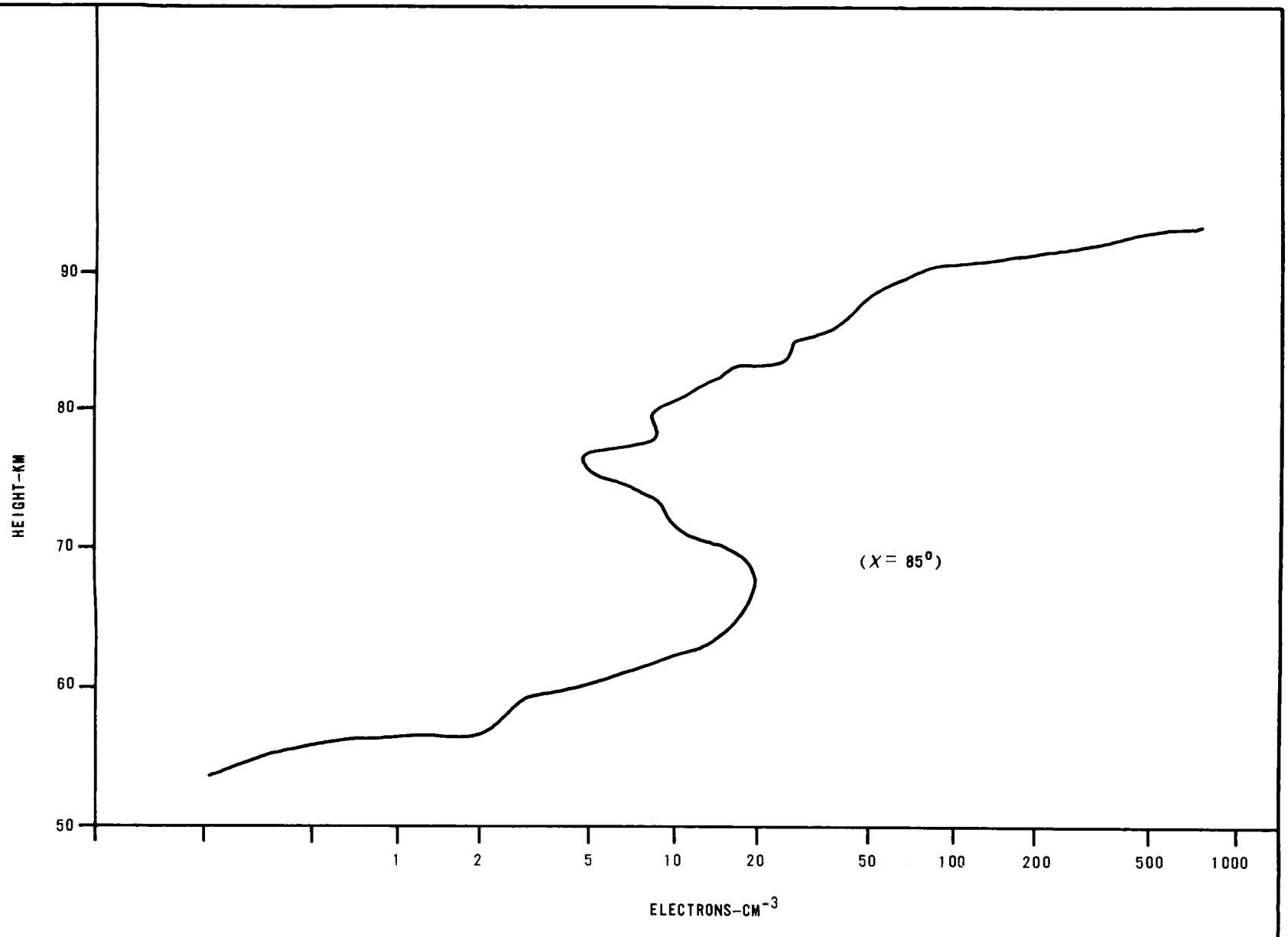

FIG. 12 C-LAYER PROFILE FOR 15 JULY 1964 AT WALLOPS ISLAND, VIRGINIA (BOWHILL, ET AL., 1964)

$$+\frac{25\,\omega_o^4}{4\omega^2\nu_m^2}\left\{C_{5/2}\left(\left(\frac{\omega\pm\omega_H}{\nu_m}\right)\right\}^2\right)^{1/2}\Bigg]^{1/2} \qquad (1)\ \text{cont'd}$$

At riometer frequencies such that ω is greater than ν, the absorption coefficient should be proportional to the collision frequency. However, it will be shown that, if the collision frequency ν is greater than the wave frequency ω, the collisions will prevent the electrons from moving in the electric field and thereby absorbing energy from it. For such high values of ν the absorption coefficient may be expected to decrease with increasing ν (Hultqvist, 1963).

In equation (1), ν_m is the collision frequency for monoenergetic electrons of energy kT (k is Boltzman's constant and T is absolute temperature) and ω_o is the plasma frequency ($\omega_o^2 = 4\pi N e^2/m$). Burke and Hara (1963) have tabulated the semiconductor integrals $C_{3/2}(x)$ and $C_{5/2}(x)$.

If the C-layer electron densities are of the order of 100 electrons per cm^3 or less, then it can be shown that equation (1) can be reduced to the following simple expression:

$$k \simeq \frac{5\omega_o^2}{4c\nu_m} C_{5/2}\left(\frac{\omega\pm\omega_H}{\nu_m}\right) = \frac{5\pi Ne^2}{mc\,\nu_m} C_{5/2}\left(\frac{\omega\pm\omega_H}{\nu_m}\right) \qquad (2)$$

For a direction of propagation different from that of the geomagnetic field lines the general expression for the complex refractive index given by Sen and Wyller has to be used. The calculations of k are then perfectly rigorous with no simplifying assumptions involved in their deduction from the generalized theory. However, according to Barrington and Thrane (1962) equation (2) is valid also in the quasilongitudinal case, if ω_H is replaced with ω_L where $\omega_L = \omega_H \cos\theta$, and θ is the angle between the direction of propagation and the geomagnetic field.

In actual computations of the non-deviative, VLF skywave absorption, the following expression was used:

$$A(db) = (2 \sec \theta)\ 1.15 \int_{h_1}^{h_2} \frac{C_{5/2}\left(\frac{\omega_L}{\nu_m}\right) N}{\nu_m}\, dh \qquad (3)$$

In equation (3), the term (2 sec θ) is necessary because the reflected VLF skywave tranverses the non-deviative C-layer twice, and because the angle of incidence is θ degrees. N is the electron density in electrons per cm^3, h_1 and h_2 are the lower and upper height limits, respectively, of the C-layer; little or no non-deviative absorption occurs below h_1 or above h_2. In practice, h_1 = 50 km and h_2 = 80 km, approximately. The angle of incidence assumed for calculations of absorption was 45^o. However, θ is about 40 degrees at nighttime and 50 degrees during the daytime.

5. COLLISION FREQUENCY PROFILES

Figure 13 shows most of the important determinations of the altitude variation of collision frequency, all measurements having been normalized to values of ν_m (Deeks, 1964). Note that the Kane (1961) profile, which is frequently assumed in computations of non-deviative absorption, corresponds quite closely with Deeks' profile and that obtained by Fejer and Vice (1958). In particular, the results of Belrose (calculated and from partial reflections, 1962), Hall, Kane (July 1957), Landmark and Lied (August 1962) are very close, and the results of Kane (November 1956), Fejer and Vice, Landmark and Lied (December 1962), and Belrose (November 1961) are grouped together but are about 50 percent smaller than the other values. Since the first group are predominantly measurements made in the summer and the second group in winter, this suggests a seasonal variation in the collision frequency profile. A factor of about 2.5 to 3 is necessary to include all these values of ν_m. In Figure 14 we have plotted the Kane (1961) profile of collision frequency. In addition, summer and winter profiles are plotted such that all of the summer and winter determinations of ν lie between these two profiles. Actually, the ratio of the Kane-to-winter values is 1.9, and the ratio of the summer-to-Kane values is 1.7.

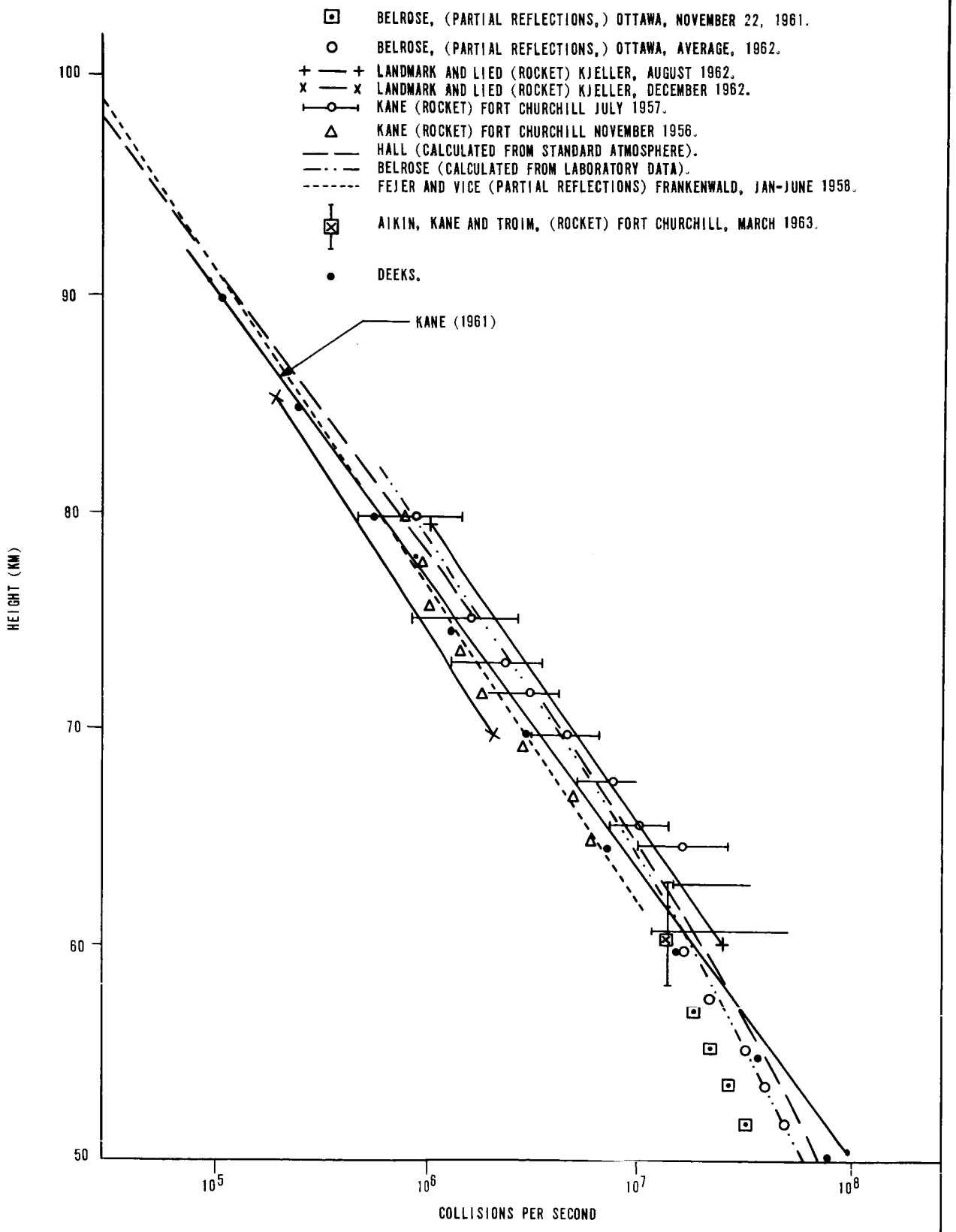

FIG. 13 ELECTRON COLLISION FREQUENCY PROFILES (AFTER DEEKS, 1964)

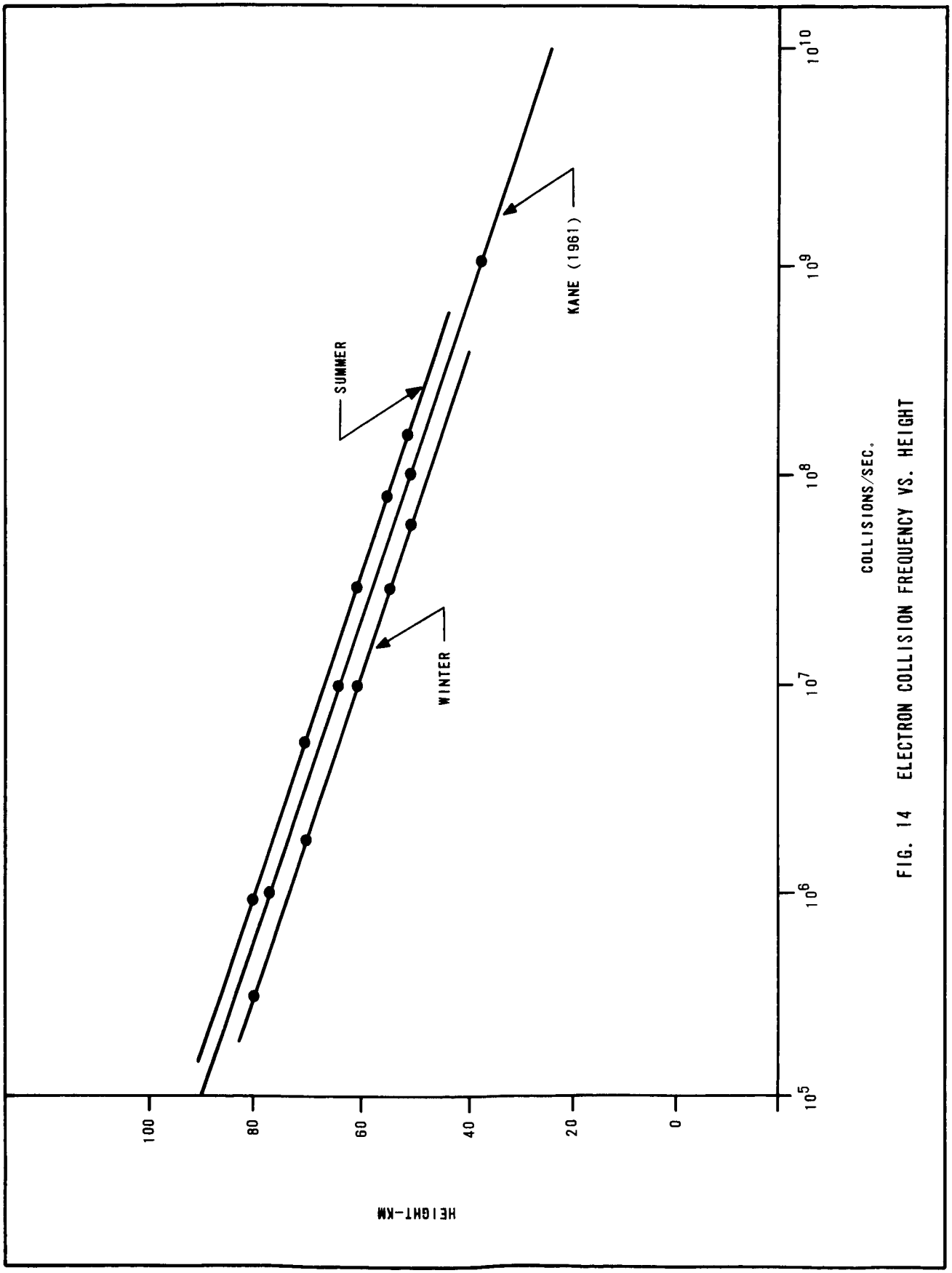

FIG. 14 ELECTRON COLLISION FREQUENCY VS. HEIGHT

In a later section, the summer and winter (extreme) collision frequency profiles are utilized to compute the non-deviative VLF skywave absorption produced by several assumed C-layer, electron density profiles. Furthermore, the Fejer and Vice profile is used in full-wave calculations to be presented in a later section of this report.

6. RESULTS OF FULL-WAVE COMPUTATIONS AND NON-DEVIATIVE C-LAYER ABSORPTION CALCULATIONS

In Figure 15, we have plotted Deeks' nighttime electron density profile (Deeks, 1964) between 80 and 120 km. Between 50 and 80 km, we have plotted four of Holt's C-layers with peak electron densities ranging from 50 to 200 electrons per cm^3. The U.S. Navy Electronics Laboratory computed the magnitudes of the reflection ($_{||}R_{||}$) and conversion ($_{||}R_{\perp}$) coefficients based on a full-wave computer program, the five profiles presented in Figure 15 and the propagation conditions which exist on the NSS to Wallops Island path. In particular the following parameters were assumed in the full-wave computations:

Propagation path length = 145 km

Wave Frequency = 21.4 kc/s

Geomagnetic Field Induction = 0.56 gauss

Geomagnetic Dip Angle = 70 degrees

Angle between plane of incidence and geomagnetic meridian = 30 degrees

As stated earlier, the collision frequency profile of Fejer and Vice, which is practically exponential, was assumed in the full-wave computations.

The results of the full-wave and absorption computations are presented in Table 1. It is interesting to note the following significant points concerning these tabulated results: First, the magnitude of the reflection coefficient ($_{||}R_{||}$) is almost an order of magnitude lower than the magnitude of the conversion coefficient ($_{||}R_{\perp}$) for Deeks' nighttime profile and Holt's profiles for zenith angles of 98 and 97 degrees. Second, the reflection coefficient

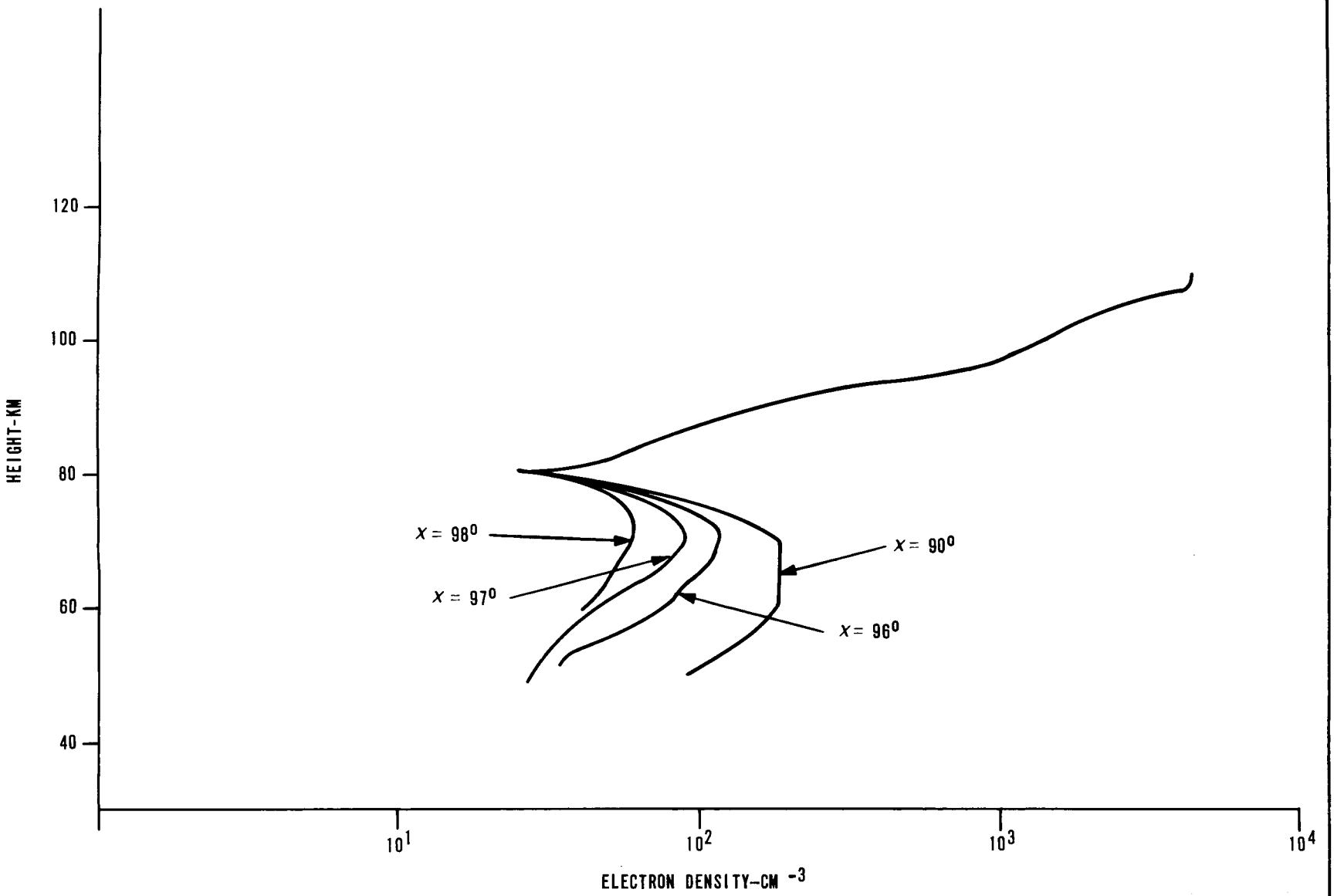

FIG. 15 DEEKS' NIGHT AND HOLT'S SUNRISE ELECTRON DENSITY PROFILES

TABLE 1 RESULTS OF FULL-WAVE COMPUTATIONS BY NEL AND NON-DEVIATIVE C-LAYER ABSORPTION

ELECTRON DENSITY PROFILE	FULL-WAVE THEORY				ABSORPTION (DB)	
	$\lvert {}_{\parallel}R_{\parallel} \rvert$	DB	$\lvert {}_{\parallel}R_{\perp} \rvert$	DB	SUMMER	WINTER
DEEKS' NIGHT	0.088	0	0.408	0	0	0
HOLT (X = 100°)	--	--	--	--	1.5	3.3
HOLT (X = 98°)	0.020	12.8	0.224	5.1	4.8	6.3
HOLT (X = 97°)	0.0223	12	0.105	12	11.8	13.5
HOLT (X = 96°)	0.0222	12	0.052	18	18.1	21.3
HOLT (X = 90°)	0.0156	15	0.036	21	20.9	26.7
BOWHILL (X = 85°)	--	--	--	--	1.42	1.54

magnitude is practically constant at 0.02 for zenith angles of 98, 97 and 96 degrees. Third, the non-deviative absorption values for summer are less than the winter values. Fourth, they compare remarkably well with the values derived from the conversion coefficient ($ {}_{\parallel}R_{\perp} $). That is, Deeks' nighttime profile is assumed to yield 0 db absorption, and the db absorption values tabulated in the column to the right of the $\lvert {}_{\parallel}R_{\perp} \rvert$ column are normalized such that they represent the db absorption relative to Deeks' night profile.

On the basis of these tabulated values, it appears that $\lvert {}_{\parallel}R_{\parallel} \rvert$ is not very sensitive to changes in the C-layer profile. However, it is quite obvious that $\lvert {}_{\parallel}R_{\perp} \rvert$ suffers non-deviative absorption because of the presence of the C-layer below the reflection level of the abnormal component of the VLF sky-wave. This result suggests that the normal component of the VLF skywave is reflected from the bottom of the C-layer and that the abnormal component is reflected from the D-layer. This matter will be discussed in more detail in a later section of this report.

7. DEEKS' ELECTRON DENSITY PROFILES

D.G. Deeks (1964) estimated how the electron density profile in the D-region changes as a function of time of day, season, and sunspot cycle, assuming an undisturbed ionosphere.

In Figure 16, electron density distributions for nighttime and solar zenith angles from 90° 50' to 58° 52' are presented for the case of minimum sunspot number and equinoxes. Figure 17 shows winter noon ($\chi = 75^{\circ}$) and summer noon ($\chi = 29^{\circ}$) profiles. These profiles are considered by Deeks to be first order approximations at the latitude of 52 degrees; and they represent the profiles which have to be assumed to match experimental VLF results and computed results when Maxwell's equations are solved exactly through the ionosphere. Most of the full-wave computing has been done at 16 kc/s and 50 kc/s, and calculated reflection coefficients and phase heights agree with measured values within experimental error. Figure 16 and 17 display order of magnitude estimates of how the profiles change during undisturbed and sunspot minimum conditions in England.

The profiles in Figure 16 show how the electron density changes between ground sunrise and noon at equinox and at sunspot minimum conditions. The important feature seems to be that the ionization below 70 kms is produced in the hour before ground sunrise, and that above 70 kms is produced in the 2 or 3 hours after ground sunrise.

8. RESULTS OF FULL-WAVE COMPUTATIONS BY RADIO AND SPACE RESEARCH STATION (SLOUGH)

On the basis of Deeks' electron density distributions presented in Figure 16 and 17, the exponential collision frequency profile of Deeks and the geometry of the NSS-to-Wallops Island propagation path, the Radio and Space Research Station (Slough, England) computed magnitudes of the VLF reflection and conversion coefficients; these are plotted in Figure 18 as a function of solar zenith angle.

In this figure, it can be seen that, at night, the conversion coefficient magnitude is about four times that of the reflection coefficient; following ground sunrise ($\chi = 90^{\circ}$), the conversion coefficient magnitude decreases to 0.2 and remains there until about $\chi = 75^{\circ}$; after this, it drops again to about

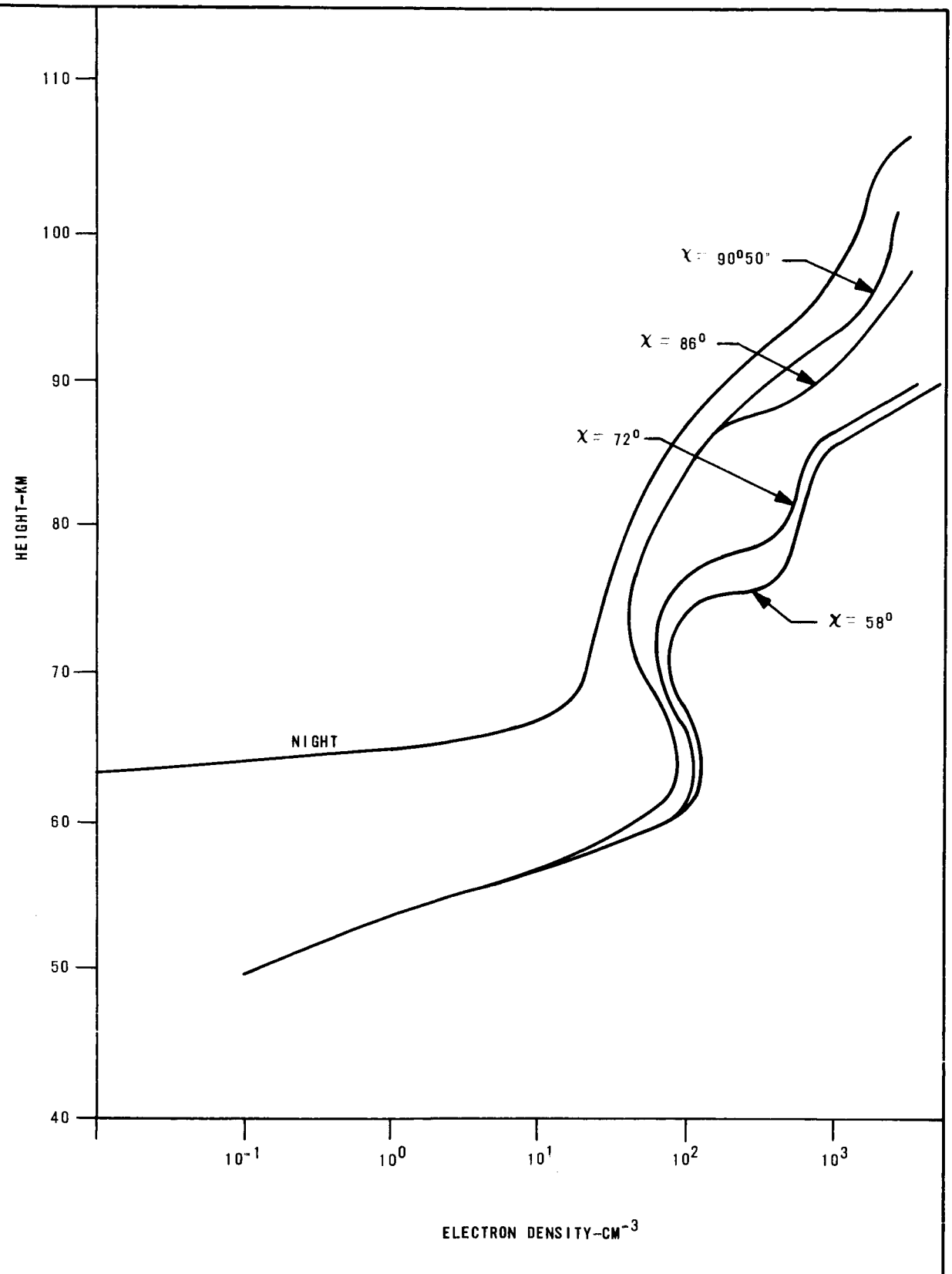

FIG. 16 DEEKS' NIGHT AND HOLT'S SUNRISE ELECTRON DENSITY PROFILES

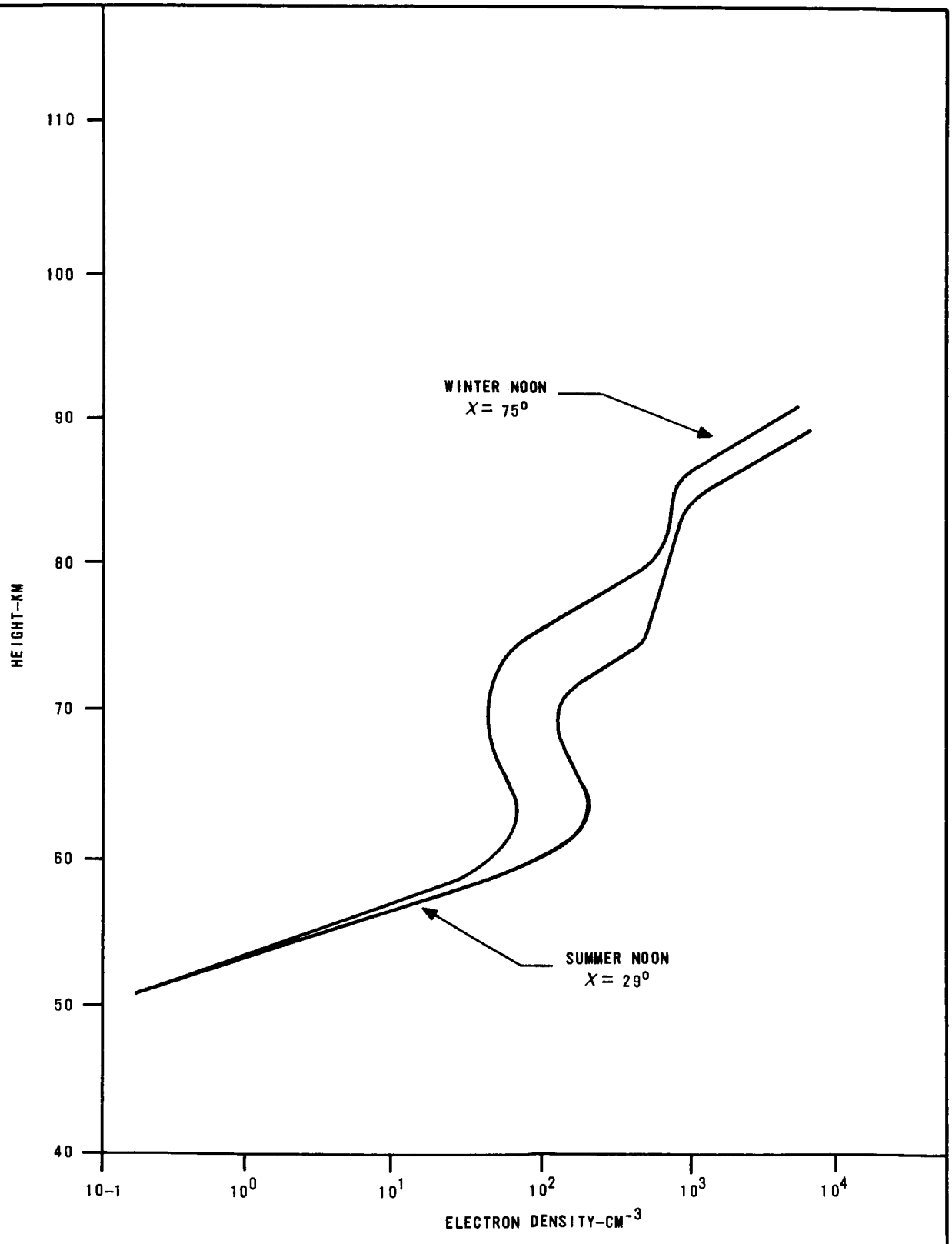

FIG. 17 DEEKS' ELECTRON DENSITY PROFILES (1964)

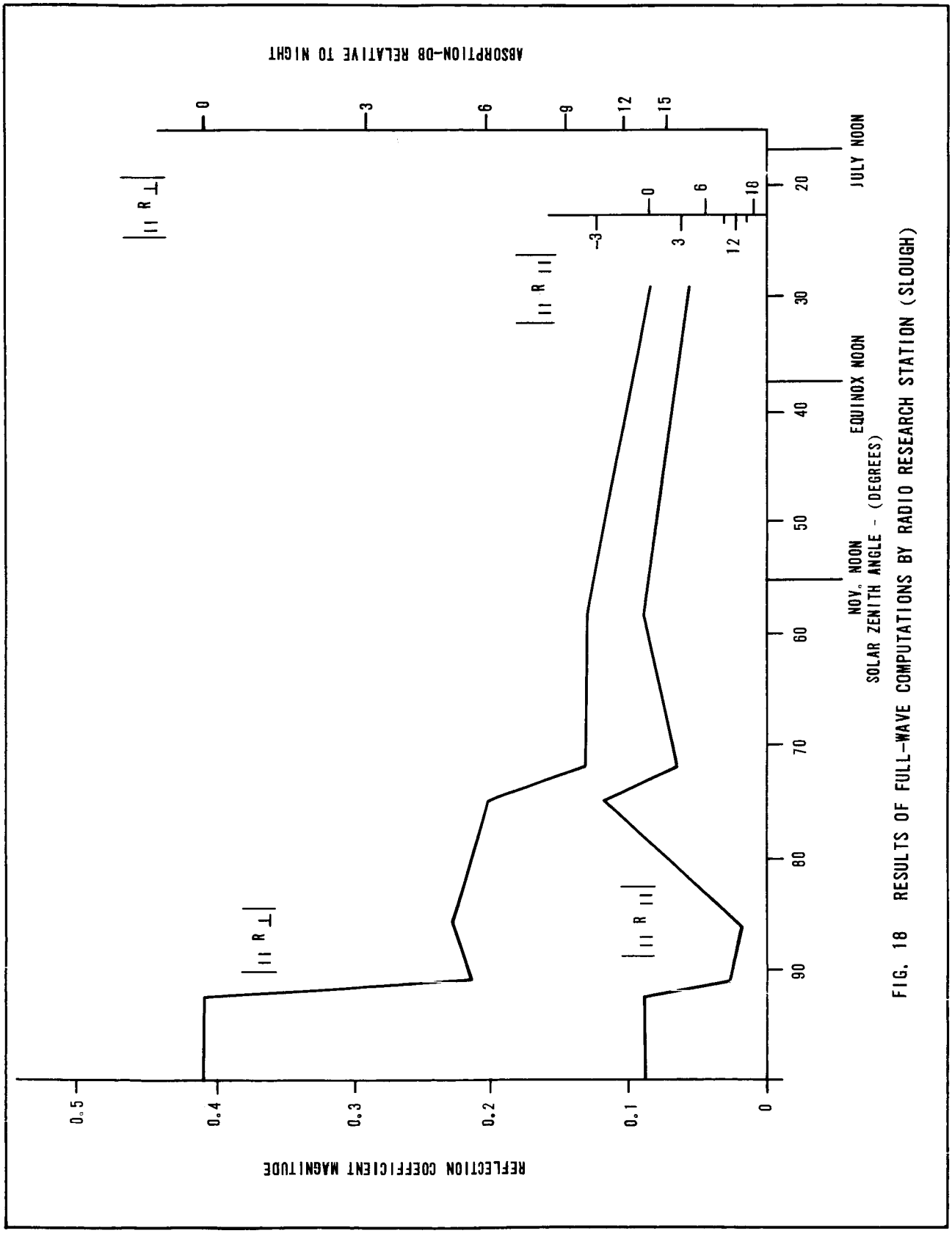

FIG. 18 RESULTS OF FULL-WAVE COMPUTATIONS BY RADIO RESEARCH STATION (SLOUGH)

0.1 at $\chi = 70^{\circ}$ and slowly decreases to $\chi = 30^{\circ}$. The ordinates at the right of Figure 18 give the db absorption values relative to the nighttime condition.

Note that the reflection coefficient magnitude is always less than the conversion coefficient magnitude, and that it is about 0.1 during night and day; however, the sunrise and sunset transitions produce a deep minimum (12 db below the night value) which is followed at $\chi = 75^{\circ}$ by a maximum (3 db above the night value). Following a zenith angle of 70°, the reflection coefficient magnitude remains essentially constant and slightly less than the nighttime value.

The zenith angles for November noon, equinox noon and July noon, for the NSS-to-Wallops Island path, are indicated in Figure 18; these are 55°, 38° and 16°, respectively.

It should be noted here that the 12 November 1964 VLF data agree semi-quantitatively with the full-wave results shown in Figure 18. For example, the amplitude of the abnormal component at noon is roughly 18 db below the average nighttime amplitude; also, the amplitude increases following ground sunrise but begins to decrease again starting at $\chi = 75^{\circ}$. This behavior is repeated during the sunset transition.

Concerning the amplitude of the normal component on 12 November 1964, it is significant that nighttime and midday values are quite comparable. Furthermore, during the sunrise and sunset transitions minima of about 18 db were observed; and, at ground sunset ($\chi = 90^{\circ}$) there was a maximum of 3 db above the nighttime amplitude.

Hence, there is a suprising consistency between the full-wave results and the November 1964 experimental data.

E. DISCUSSION OF RESULTS

Bracewell and Bain (1952) summarized the results of a series of 16 kc/s propagation experiments made over path lengths from 90 to 535 km. For the shorter paths they found that measured diurnal phase changes could be explained in terms of a relatively strong layer D_α which remained at a constant height during the night but descended during the day with decreasing solar zenith angle. For paths longer than 300 km, the received signal showed a rapid change in phase during the hour preceding ground sunrise and the hour after ground sunset, with high phase stability during the intervening hours. They concluded that reflection from a weak lower layer D_β (which appears about an hour before sunrise and descends to the daytime equilibrium position by sunrise) dominates the propagation mechanism for the longer paths. Figure 19 shows the Bracewell and Bain (1952) model of the diurnal height variations of the layer D_α and D_β observed over England during the equinoxes.

One of the significant differences between the English VLF results and the July 1964 data presented in this report concerns the commencement time of the pre-sunrise amplitude and phase changes. The English workers have consistently reported that the pre-sunrise changes start when the solar zenith angle is about 98 degrees. However, the pre-sunrise decrease in the amplitude of the abnormal components for 15 July 1964 began at about $\chi = 93^\circ$; and the decrease on 17 July 1964 began around $\chi = 93^\circ$ to 94°, although the July 17th phase of the abnormal component appears to advance beginning around $\chi = 97^\circ$. Of course, one must be cautious about stating that the July 17th amplitude decrease started at $\chi = 93^\circ$ or 94°, because of the uncertainties due to the relatively large nighttime amplitude fluctuations. Furthermore, it is obvious that the paucity of July 1964 data precludes detailed comparisons with the very extensive English results.

In the light of the rocket C-layer electron density profiles measured by Bowhill, et al. (1964), it is clear that electron detachment effects in the 60-90 km height interval occur in the twilight periods. Furthermore, it is possible to detect them by studying the pre-sunrise changes in VLF radio waves ionospherically reflected near vertical incidence. For 16 kc/s transmissions over fairly short ground distances the amplitude does not, on the average, start to decline until the upper boundary of the solid earth's shadow, moving downward, has

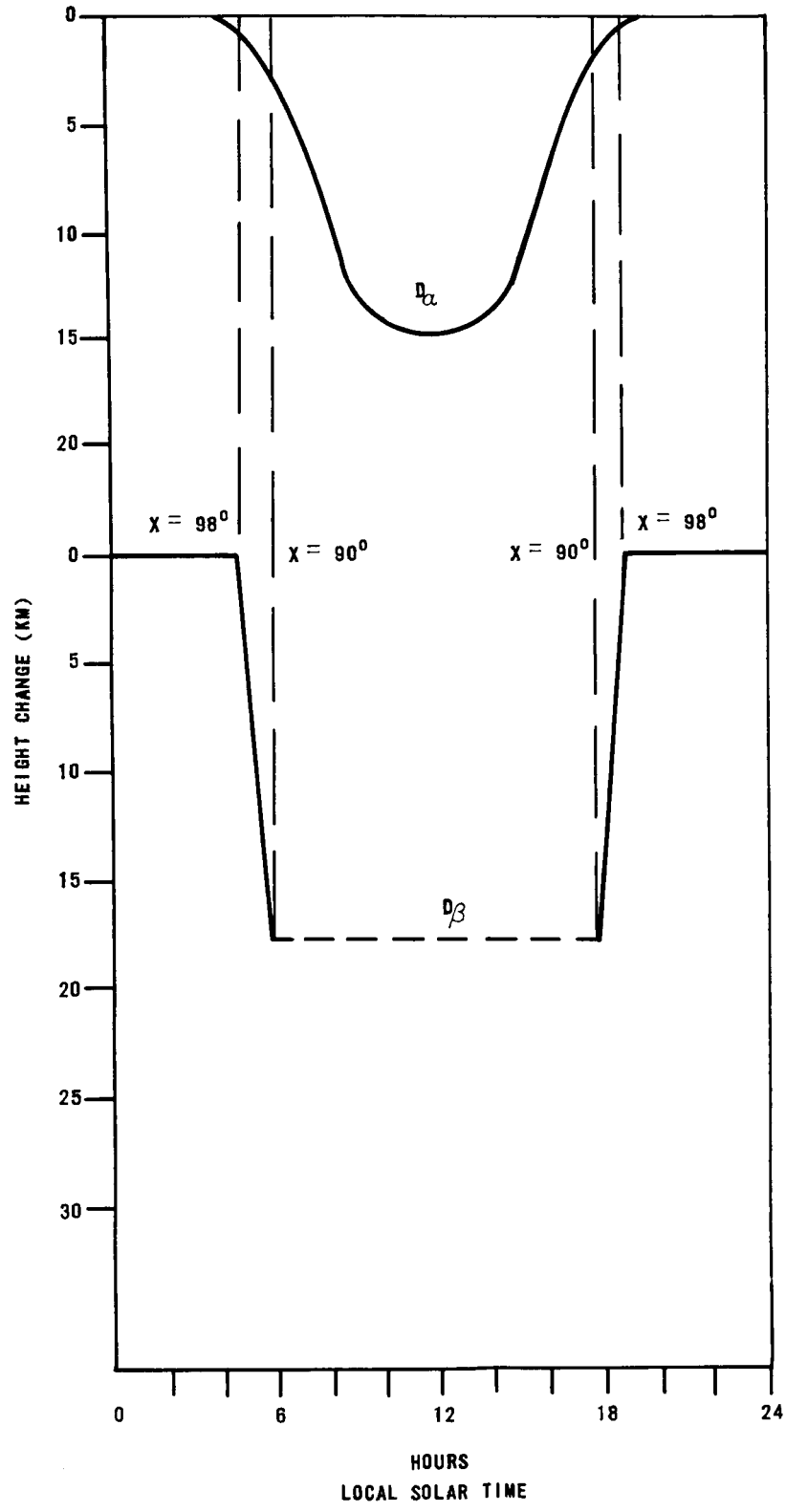

FIG. 19 DIURNAL BEHAVIOR OF THE IONOSPHERIC LAYERS $D\alpha$ AND $D\beta$ DURING THE EQUINOXES, ACCORDING TO BRACEWELL AND BAIN (1952)

reached an altitude of about 60 km at sunrise (Bracewell, 1952). It should be noted that, at the same time, a 30 km ozone layer shadow is at 90 km which is the nighttime VLF reflection height; and this situation corresponds to a solar zenith angle of 98 degrees. It is, therefore, clear that the electron detachment in the lowermost, cosmic-ray-produced C-layer increases the non-deviative attention of the VLF skywave. At steep angles of incidence, the VLF phase starts to advance a few minutes after ground sunrise (Bracewell, et al., 1951); this means that the C-layer absorption produced prior to ground sunrise is undoubtedly non-deviative in nature.

Based on the July 1964 VLF data, it is believed that the C-layer can be highly variable in nature from day to day; this variability has been observed by Belrose and Burke (1964) at Ottawa by means of the partial reflection technique. Also, Barrington et al. (1963) reported on the diurnal and seasonal variations in D-region electron densities derived from observations of cross modulation; their measurements showed considerable variation from day to day. Also, Deeks (1964) deduced that C-layer peak electron densities were roughly 60 and 200 electrons per cm^3 at winter and summer noon, respectively; this suggests a rather significant decrease in C-layer electron densities from summer to winter, and it may explain the apparent lack of non-deviative C-layer absorption in the November 1964 VLF data.

Furthermore, Gregory (1965) reported on measurements of electron densities in the mesosphere at Christchurch, N.Z. ($43^{\circ}S$); relatively constant values exist in summer, but large variations occur in winter. During the period 21-29 June 1963, isopleths of electron density descended and ascended by approximately 10 km, while stratospheric temperatures rose and fell by $10^{\circ}C$. Both effects are ascribed to atmospheric vertical motion. Gregory believes that "major disturbances of the winter westerly circulation in the mesosphere, possibly extending into the lower thermosphere, cause a redistribution of ionizable photo-chemical constituents, particularly by virtue of vertical motion, and possibly through turbulent transport." While the production of electrons in the C-layer is still due to cosmic rays, and solar ultraviolet radiation photodetaches electrons from the negative ions, "actual values of electron density must now be presumed to be determined by the redistribution of ionizable constituents and negative ions due to mass transport."

The observed plateau in the abnormal phase plot, following ground sun-

rise on July 17, is believed to be due to a recombination effect similar to that described by Hargreaves (1962) and Wagner (1964). They pointed out that near sunrise it is necessary to take nonequilibrium conditions into account; that is, Hargreaves (1962) considered the aeronomic processes of the lower D-region, and predicted a partial decay of ionization following sunrise. In terms of VLF propagation, this would cause a temporary amplitude decrease and temporary phase retardation (reflection height increase), following the formation of the cosmic-ray-produced layer (C-layer) in the lower D-region. Hargreaves (1962) noted that the temporary layer was more apparent in winter than in summer, and was variable from day to day, also.

Therefore, following ground sunrise, we should expect to find that the VLF amplitude decreases while the phase retards (reflection height increases) slightly; that is exactly what appears to happen in the July 17 phase and amplitude plots. Note the gradual increase of the amplitude during the 60-minute period following ground sunrise. Furthermore, the phase plateau observed in these data is then followed by a further phase advance which may be attributed to the lowering of the upper D-layer; this layer is probably formed by the photoionization of atmospheric nitric oxide by solar Lyman-alpha radiation.

Hargreaves (1962) showed that if the ratio of the negative ion density and electron density was greater at night than in the daytime, and if the electron recombination coefficient exceeded the ion recombination coefficient, then the electron density in the C-layer should be greater at sunrise than when the layer has reached equilibrium; therefore, recombination with positive ions in the lower D-region near sunrise appears to be the explanation for the temporary plateau observed in the July 17 phase data. Figure 20 shows the theoretical sunrise and day equilibrium C-layers predicted by Hargreaves.

In connection with, the above mentioned recombination effect in the C-layer, it should be noted that the phase of the normal component (November 1964 data) exhibits a similar effect; that is, following ground sunrise, the normal component phase advances temporarily and then retards slightly to a daytime equilibrium value. The difference between the phase near ground sunrise and the daytime equilibrium phase is roughly 70 degrees; this corresponds to an apparent height change of 2 km, which is consistent with the height change postulated by Hargreaves.

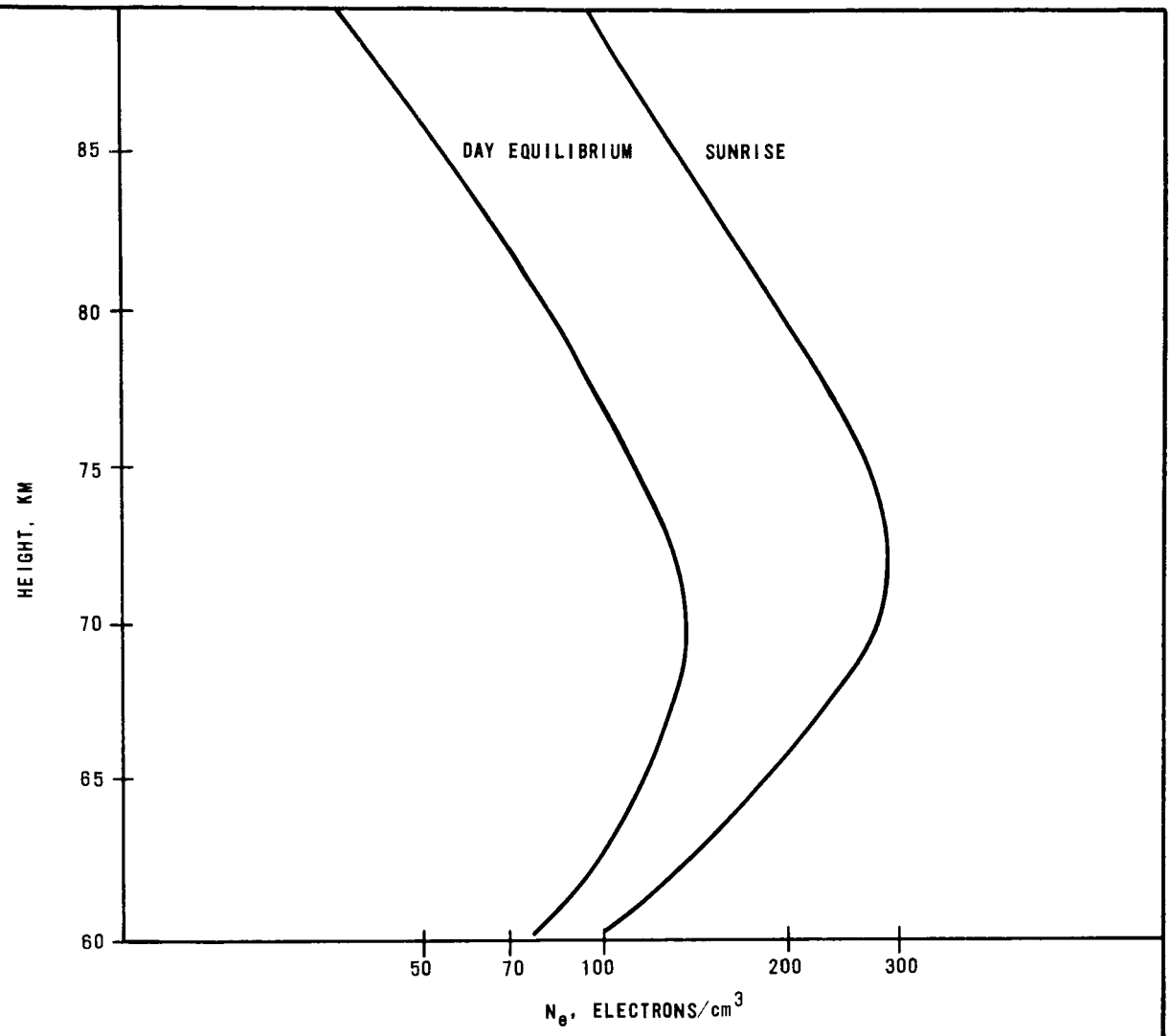

FIG. 20 THEORETICAL C-LAYERS

Based on the full-wave computations, the calculations of non-deviative C-layer absorption, and the experimental VLF data, it is suggested that only the abnormal component of the NSS skywave suffers non-deviative absorption; this is apparent from Table 1 which compares the full-wave results and the values of non-deviative absorption for various assumed C-layers. The reflection coefficient magnitude is not very sensitive to changes in the C-layer, while the conversion coefficient magnitude varies in a manner consistent with the non-deviative absorption caused by the C-layer electron density. Furthermore, the November VLF data, for the normal component, reveal that the phase is essentially constant during the daytime; this suggests that the reflecting layer is not subject to solar control. Therefore, it is believed that the normal

component is reflected from the bottom of the C-layer (which is produced by galactic cosmic rays) and that the abnormal component is reflected from the D-layer which is indeed under the direct control of solar Lyman-alpha radiation.

Finally, it should be noted that the amplitude of the normal component in November is about the same during daytime and nighttime with the exception of the sunrise and sunset transitional periods. This behavior is very apparent in Figure 18 which illustrates the variation of the reflection coefficient magnitude as a function of the solar zenith angle. Also, note that the conversion coefficient is consistently greater than the reflection coefficient, and that their magnitudes approach each other at the lower zenith angles; this result suggests that the downcoming skywave polarization is not circular in general, but that circular polarization is closely approached at summer noon.

F. CONCLUSIONS

To summarize, we have examined the results of ground-based, steep-incidence VLF measurements conducted concurrently with D-region rocket experiments, and obtained reasonable agreement between theory and experiment. The chief conclusions applicable to this particular theoretical and experimental work are as follows:

1. Amplitude and relative phase measurements of the normal and abnormal components of the downcoming VLF skywave are most useful adjuncts to D-region, direct rocket measurements.

2. The rocket electron density profiles enable a calibration of the VLF measurements against actual electron density-height profiles; it has been difficult to interpret VLF measurement of skywaves due to the uncertainties associated with full-wave solutions of the coupled wave equations. Having an actual profile available on one or two occasions may well serve to illuminate the whole problem.

3. Computation of the non-deviative, C-layer absorption utilizing rocket electron density profiles, and comparison of the absorption measured by means of a steep-incidence VLF experiment enables one to calibrate the in situ measurements of electron density vs. height, assuming a plausible collision frequency profile is used.

4. Non-equilibrium conditions in the C-layer at sunrise may be observed indirectly by means of VLF measurements; in particular the effect of electron recombination with positive ions may be discerned in the VLF phase data following ground sunrise. The magnitude and duration of this effect agree semi-quantitatively with Hargreaves' prediction that the lower D-region (C-layer) electron density decays to a daytime equilibrium value following ground sunrise.

5. It is probable that the abnormal component of the VLF skywave is reflected from the D-layer and suffers non-deviative absorption in traversing the C-layer during the daytime.

6. It is probable that the normal component of the VLF skywave is reflected from the bottom of the C-layer during the daytime.

7. The polarization of the downcoming VLF skywave is elliptical, in general; however, near summer midday, full-wave computations reveal that the normal and abnormal component magnitudes are about equal.

8. The daytime and nighttime magnitudes of the normal component are roughly equal; this is consistent with the full-wave results which reveal that the daytime and nighttime reflection coefficient magnitudes are about equal. There are exceptions to this in both the theory and experiment during the sunrise and sunset transitions.

9. There is a high degree of variability in C-layer electron densities from day to day and season to season as manifested by the highly variable extent of non-deviative C-layer absorption of the VLF skywave.

10. The pre-sunrise decrease in the amplitude of the abnormal component of the VLF skywave is a very sensitive indication of the extent of the C-layer electron density, The July 15 and 17 data revealed pre-sunrise amplitude decreases commencing at solar zenith angles of about 93 and 98 degrees, respectively, whereas the November data revealed no apparent pre-sunrise changes in either amplitude or phase. At this time, it is not apparent what mechanism produces the amplitude decrease commencing at χ = 93 to 94 degrees; it is suspected that there is a dearth of detachable negative ions in the 60 to 80 km height range because of a redistribution of negative ions by means of vertical motions in the atmosphere.

11. The pre-sunrise drop in the abnormal amplitude of the VLF skywave is a very useful precursor, and the extent of the decrease permits one to make rough estimates regarding the C-layer electron densities. Furthermore, this precursor may be utilized as a trigger in future rocket electron density experiments to study the variability and formation of the C-layer of the ionosphere.

12. There is a need for additional VLF amplitude and phase measurements at various angles of incidence; the pre-sunrise decrease in the VLF amplitude, commencing around χ = 93 to 94 degrees, requires further study because this effect has not been reported by other workers.

ACKNOWLEDGEMENTS

This research was sponsored by the National Aeronautics and Space Administration under Contract NASW-1109. The authors acknowledge the encouragement of Prof. S.A. Bowhill, of the University of Illinois, who suggested the steep-incidence VLF measurements at Wallops Island. We wish to thank Mr. R. Christie of the Radio and Space Research Station (Slough, England) and Dr. J.S. Belrose of the Defense Research Telecommunications Establishment (Ottawa, Canada) for their helpful suggestions regarding the adjustment of the abnormal loop antenna. Also, the authors gratefully acknowledge the cooperation and full-wave computational results generously furnished by Mr. J.A. Ratcliffe, Mr. D.G. Deeks, and Mr. B.R. May at the Radio and Space Research Station (Slough), and by Dr. E.E. Gossard and Mr. W.F. Moler at the U.S. Navy Electronics Laboratory in San Diego, Calif.

APPENDIX A

SOLAR ZENITH ANGLE

The equation relating the zenith angle of the sun (χ) to the observer's position on the earth, the hour of day, and the solar declination has been given by Chapman (1931) and Swider (1962) as:

$$\cos \chi = \cos \delta \cos \psi \sin \theta + \sin \delta \cos \theta$$

where

χ = solar zenith angle

δ = solar declination

ψ = hour angle

θ = colatitude of observer

In terms of the observer's latitude (ϕ) rather than the colatitude,

$$\cos \chi = \cos \delta \cos \psi \cos \phi + \sin \delta \sin \phi \qquad \text{(see Fig. A. 1)}$$

As the zenith angle of the sun is dependent on the solar declination, the hour angle corresponding to each χ value varies with the seasons. The zenith angle and hour angle must be calculated for each day of interest. The variance over a period of a week is only 4 minutes in December and is negligible in June; therefore, the calculation has been made only once for each series of VLF measurements.

The reflection point of the NSS-Wallops path is located at 38° 28' N, 75° 58' W. Local noon and solar declination at the reflection point are as follows:

Date	Solar Declination	Local Noon (EST)
July 15, 1964	+21° 32'	12:10
Nov. 15, 1964	-18° 19'	11:48

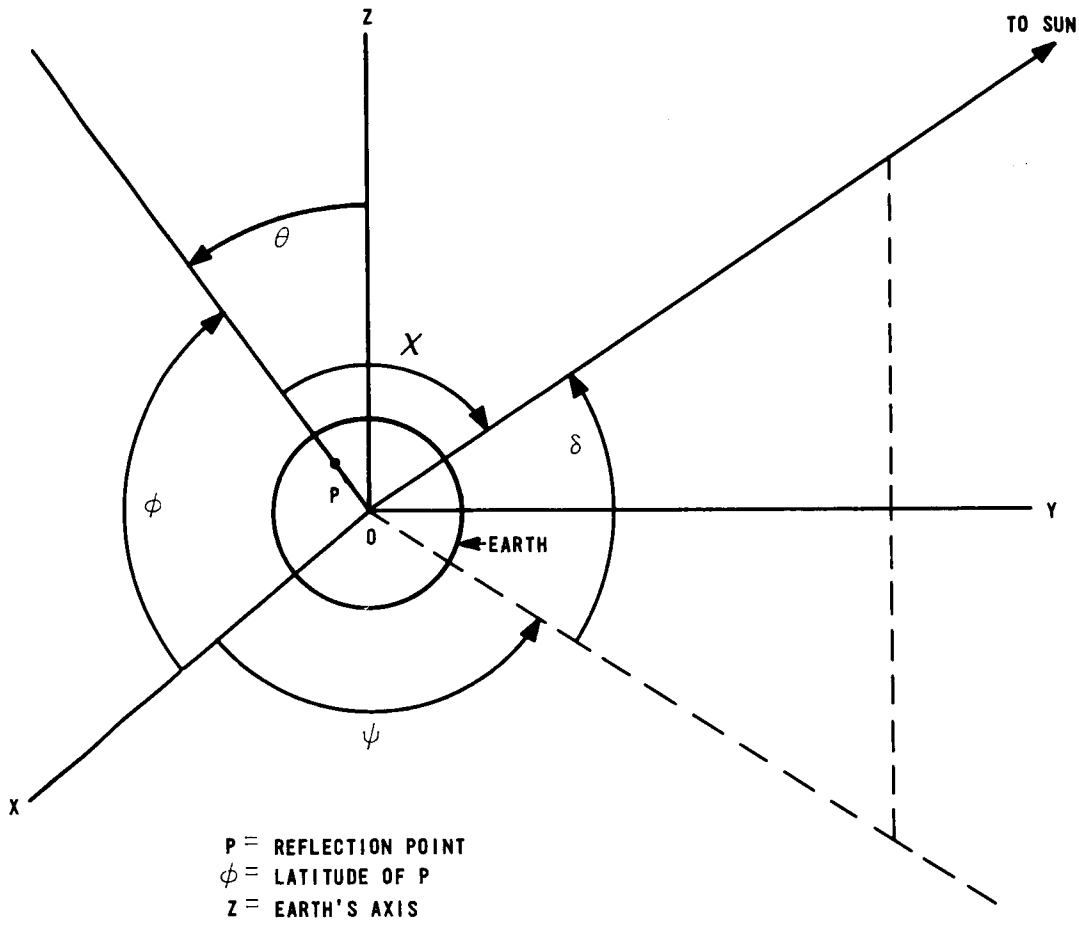

FIG. A.1 THE SOLAR ZENITH ANGLE

For these days the Eastern Standard Times of various zenith angles are as follows:

χ (degrees)	July 15, 1964	Nov. 15, 1964
100	0350 - 2018	0559 - 1741
95	0421 - 1947	0621 - 1714
90	0451 - 1917	0649 - 1647
85	0519 - 1849	0718 - 1617
80	0546 - 1822	0747 - 1549
75	0613 - 1754	0819 - 1516
70	0640 - 1728	0840 - 1456
60	0713 - 1654	1001 - 1335

At local noon ($\psi = 0$) the zenith angle is at its minimum value and the sun is due south. The equation of the zenith angle for this case is:

$$\cos \chi = \cos \delta \cos (0^{\circ}) \cos \phi + \sin \delta \sin \phi$$
$$= \cos (\phi - \delta)$$

or

$$\chi = \phi - \delta$$

For the VLF reflection point (near Cambridge, Md.) the minimum zenith angle for each case is:

Date	χ min.	Local Noon (EST)
July 15, 1964	16° 56'	12:10
Nov. 15, 1964	56° 47'	11:48
Autumnal Equinox	38° 28'	11:56
Vernal Equinox	38° 28'	12:11
Summer Solstice	15° 01'	12:06
Winter Solstice	61° 55'	12:02

APPENDIX B

SUNRISE GEOMETRY

For steep-incidence VLF propagation, three meanings can be associated with the term sunrise. Ground sunrise (GSR) refers to the time at which the sun's rays are tangent to the earth's surface below the reflection point, or $\chi = 90^{\circ}$. Layer sunrise (LSR) corresponds to the time at which the earth's shadow reaches the nighttime reflection height of about 90 km. Another layer sunrise (LSR') corresponds to the time at which the ozone layer's shadow reaches 90 km (Fig. B. 1). The ozone layer's height has been assumed to be 30 km in this report.

Each of the various sunrises has a particular value of χ associated with it. From Figure B. 2 it may be seen that solving each right triangle associated with a sunrise for α will yield χ since

$$\chi = 90^{\circ} + \alpha, \quad \text{and cos } \alpha \text{ is } \frac{ON}{OP}.$$

For our work a spherical earth of radius 6371 km has been employed. As well as finding the χ value associated with each sunrise, we have also followed the earth and ozone layer shadows to a 50 km reflection height and calculated the associated χ values; they are as follows:

Reflection Point Height	χ Earth's Shadow	χ Ozone Layer Shadow
95 km	99° 51'	98° 8'
90 km	99° 34'	97° 49'
85 km	99° 19'	97° 29'
80 km	99° 2'	97° 8'
75 km	98° 45'	96° 46'
70 km	98° 27'	96° 23'
65 km	98° 9'	95° 59'
60 km	97° 50''	95° 31'

(Continued on next page)

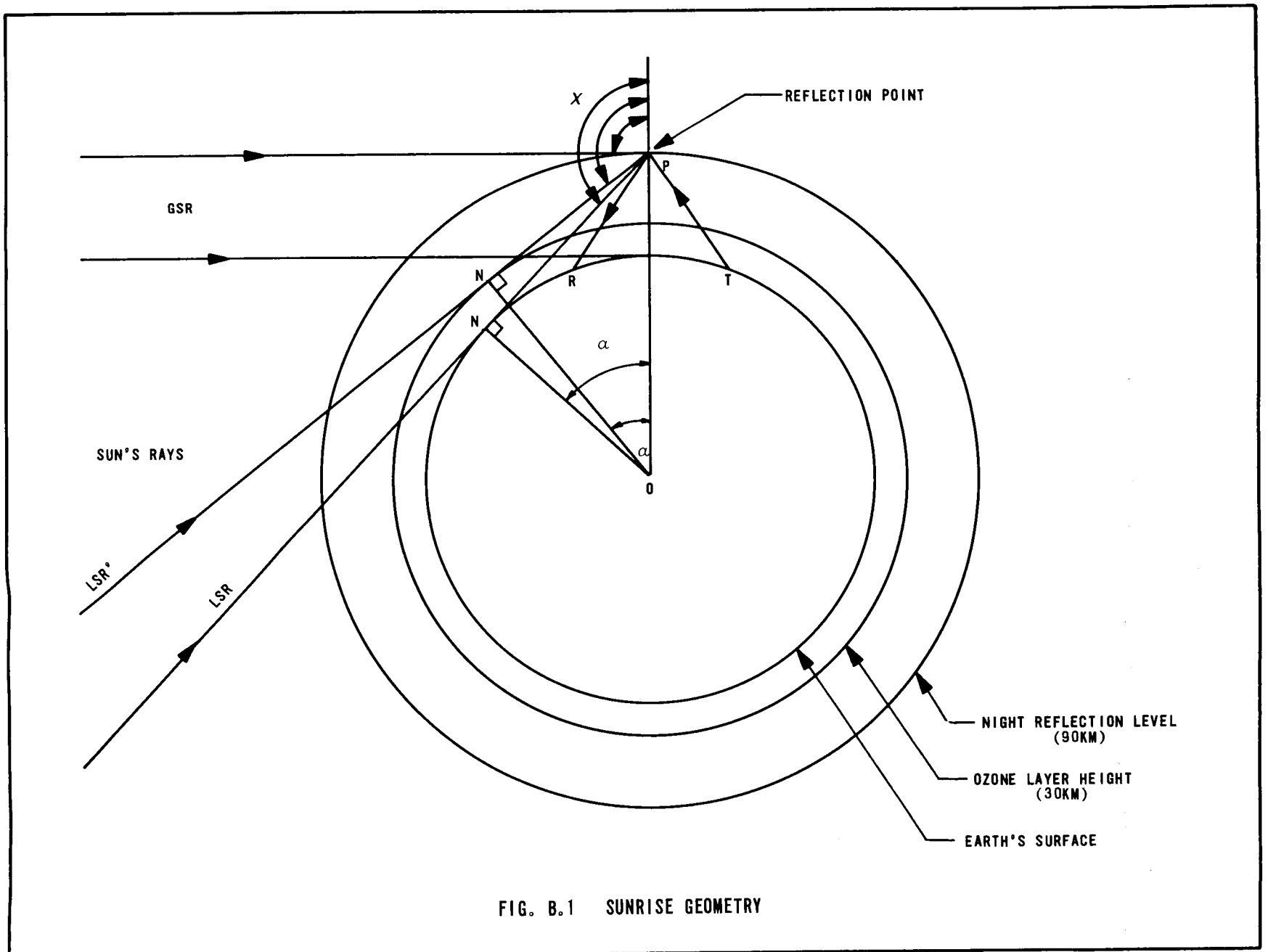

FIG. B.1 SUNRISE GEOMETRY

Reflection Point Height	χ Earth's Shadow	χ Ozone Layer Shadow
55 km	97° 30'	95° 3'
50 km	97° 9'	94° 31'

One should note that the earth's shadow is at 60 km when the ozone layer's shadow reaches 90 km, the nighttime reflection level.(Fig. B. 2).

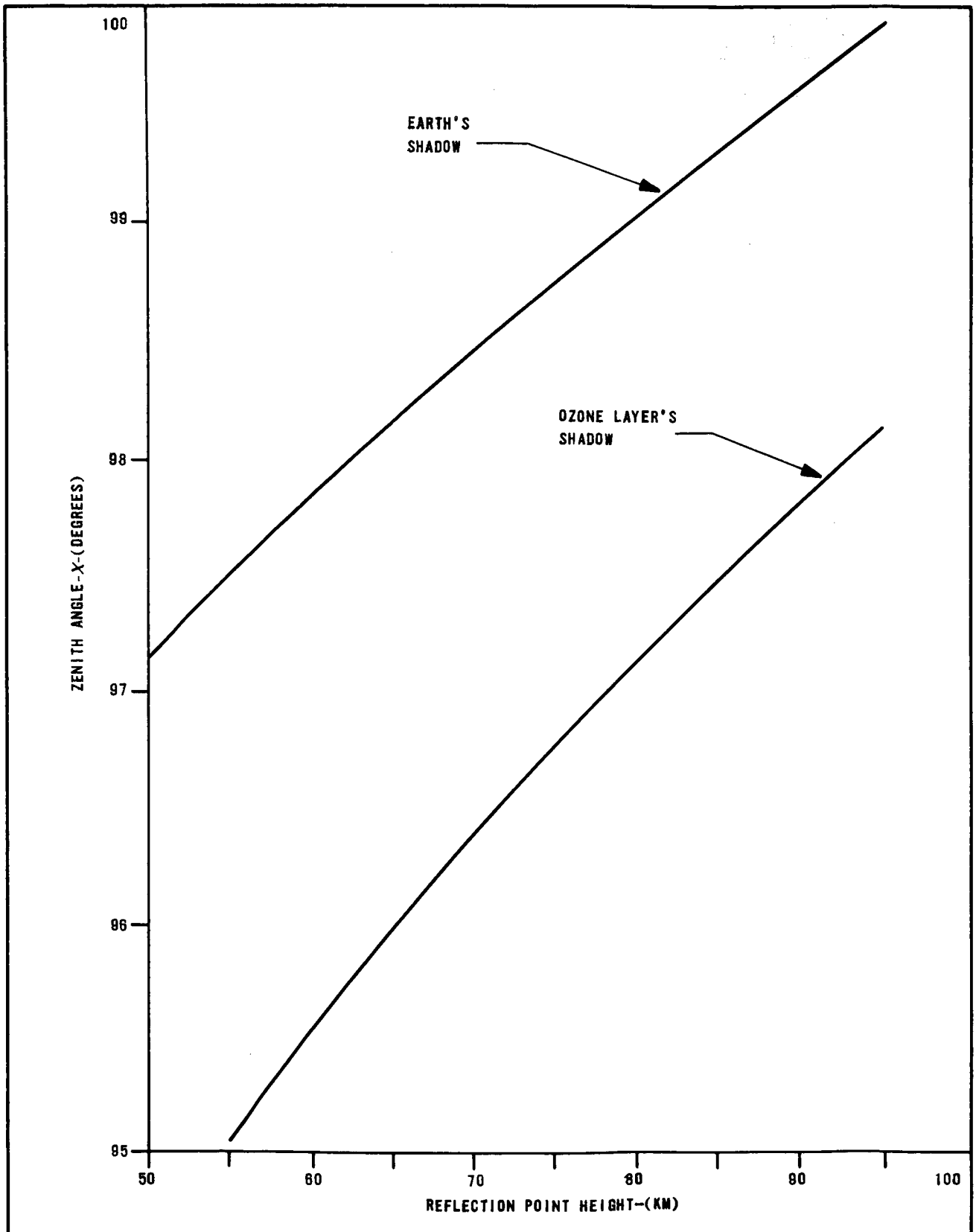

FIG. B.2 LAYER SUNRISE

APPENDIX C

ADJUSTMENT OF THE ANTENNA SYSTEMS

Abnormal Loop System

The loop antennas used are manufactured by the Stoddart Aircraft Radio company for use with low-frequency field intensity meters. Measurements have shown this antenna to be well balanced and have negligible vertical effect. A toroidal transformer is used immediately after the loop to transform from push-pull (balanced) to single-ended coaxial line to the receiver. This transformer was found to have greater than 80 db common-mode rejection.

To facilitate adjustment of this antenna, a mirror is mounted in the plane of the loop as shown in Fig. C. 1. At a distance of about 100 ft. from the loop antenna, a surveyor's transit is erected, leveled, and turned to the azimuth of the propagation path, the great-circle path from transmitter to receiver. The antenna is then oriented so that the cross hairs in the eyepiece of the transit telescope are centered on the image of the transit telescope in the mirror. Experience has shown this adjustment to be satisfactory in rejecting the ground wave.

Normal Loop/Whip System

The normal loop is orientated with its electrical plane parallel to the plane of incidence; in this position it receives an emf proportional to the normal component, E_1, of the downcoming skywave. However, in this position the normal loop is also responsive to the ground wave, E_o, and it receives an emf proportional to

$$E_o + 2 E_1$$

A vertical whip antenna receives an emf proportional to

$$E_o + 2E_1 \sin \theta$$

where θ is the angle of incidence of the skywave. These two may be added in the appropriate phase and amplitude so as to eliminate E_o and leave an emf proportional to

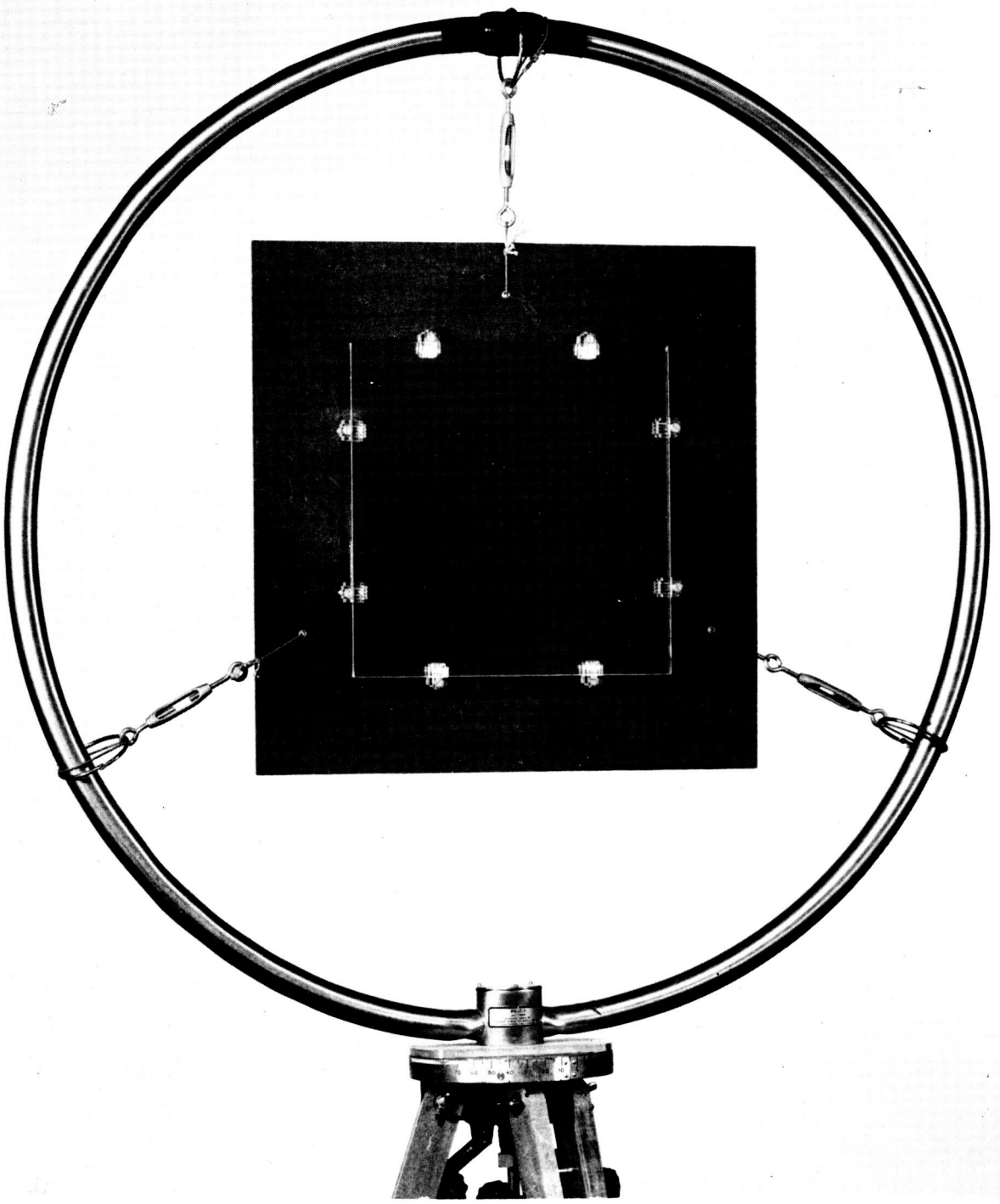

FIG. C.1 ABNORMAL LOOP ANTENNA

$$2 E_1 (1 - \sin \theta)$$

For utmost long-term stability, the normal loop and whip signals should be added employing passive circuitry only; preamplifiers should be employed only after addition.

Experience has shown that aperiodic circuitry is essential prior to the addition because even minor drifting of tuned circuits will introduce phase and amplitude changes which upset the cancellation of E_o.

The technique used for the addition of the normal loop and whip signals is shown in Figure C. 2. The whip is fabricated of thin-wall aluminum tubing to lower its impedance. Allowance has been made for approximately 10 feet of low capacitance cable (RG-62/U) connecting the whip to the phase-shifter and adder circuitry. An electrical ground plane is provided for the whip to ensure stability.

Initially, the loop-whip system is adjusted for a minimum signal at noon when the downcoming skywave amplitude is at a minimum. The phase and amplitude controls are adjusted for a null. This will result in the residual ground wave being approximately equal to the normal skywave vector. With one or two days of data at this setting it is possible to draw a polar (phase-amplitude) diagram of the recorded vector. This is a NORLIL or Normal Loop Induction Locus. It should spiral about the tip of the residual ground wave vector. The apparent center of the NORLIL designates the phase and amplitude of the residual ground wave with respect to the normal skywave.

Final adjustment of the normal loop-whip system is just a matter of adjusting the phase and amplitude controls until the vector recorded is of the same phase and amplitude as that anticipated from the evidence of the NORLIL. Refer to Figure C. 3. Care must be taken to always include the effects of the difference in frequencies of the standard oscillator and the NSS frequency. Experience at Wallops Station has shown that adjustment of the whip phase shifter for 90^o is not sufficient. This has been attributed to the large number of buried conductors in the area (power cables, telemetry wires, runway reinforcements, etc.).

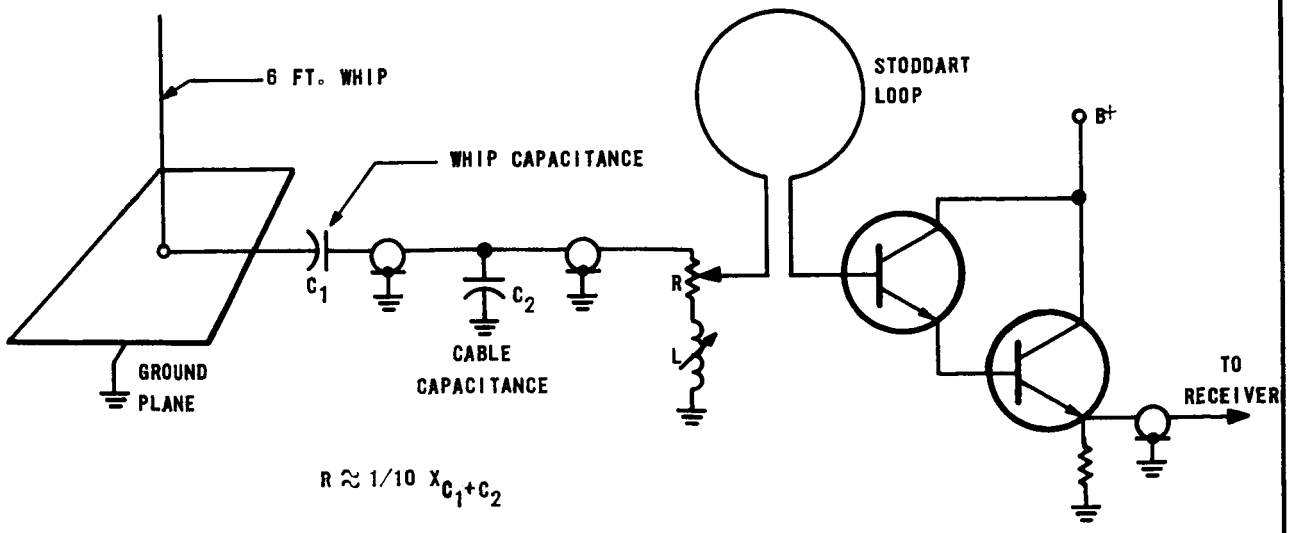

$R \approx 1/10\ X_{C_1+C_2}$

$X_L \approx 1/10\ R$

FIG. C.2 NORMAL LOOP/WHIP ANTENNAS

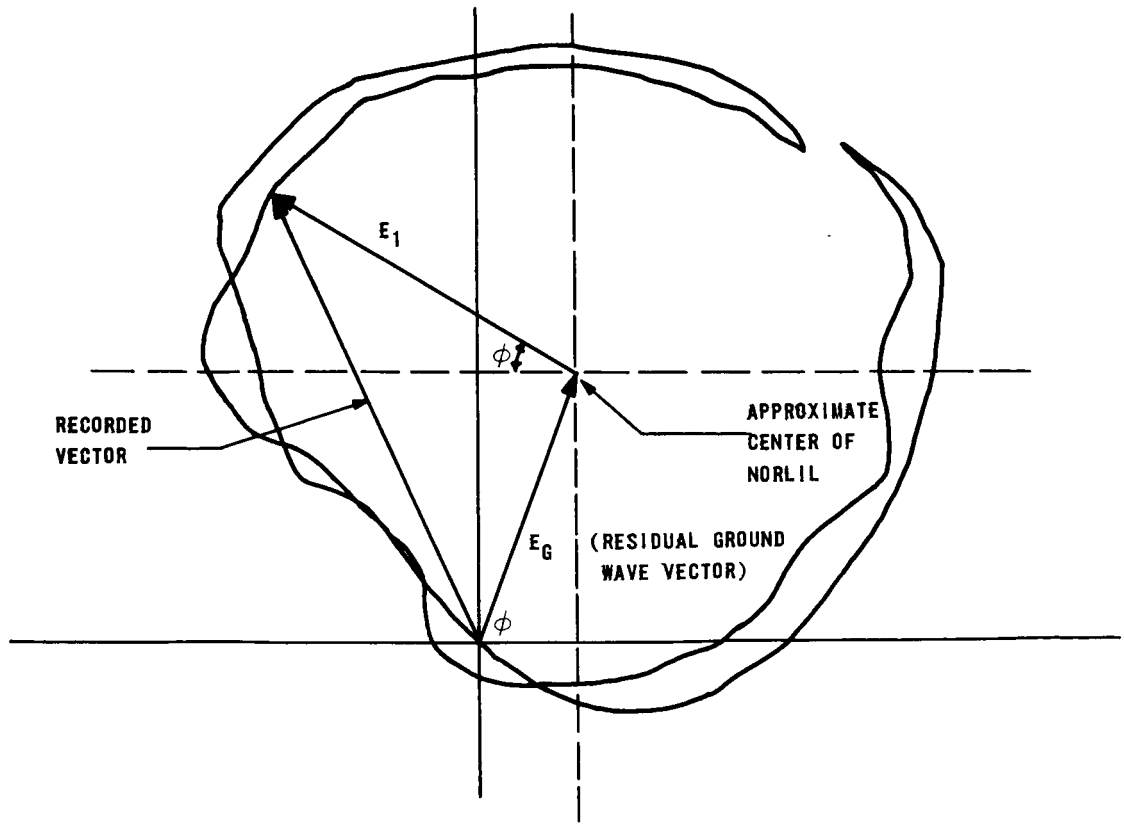

FIG. C.3 POLAR DIAGRAM OF NORMAL LOOP/WHIP SIGNAL

APPENDIX D

PROPAGATION PATH AZIMUTH

The importance of knowing the azimuth of the propagation path at the receiver has already been pointed out in order to adjust the abnormal loop quickly. Finding this azimuth involves using spherical trigonometry. The propagation path is the great circle path from transmitter to receiver.

The solution of this problem is found in Marine and Air Navigation by J. W. Stewart and N. L. Pierce. Given two points A and B (transmitter and receiver) at latitudes and longitudes L_A, Lo_A, L_B, Lo_B, respectively, we are required to find the great circle distance between them, D_{AB} and angle C_B (Fig. D. 1). Introducing an auxiliary angle R defined by

$$\tan R = \cot L_B \cos Lo_{AB}$$

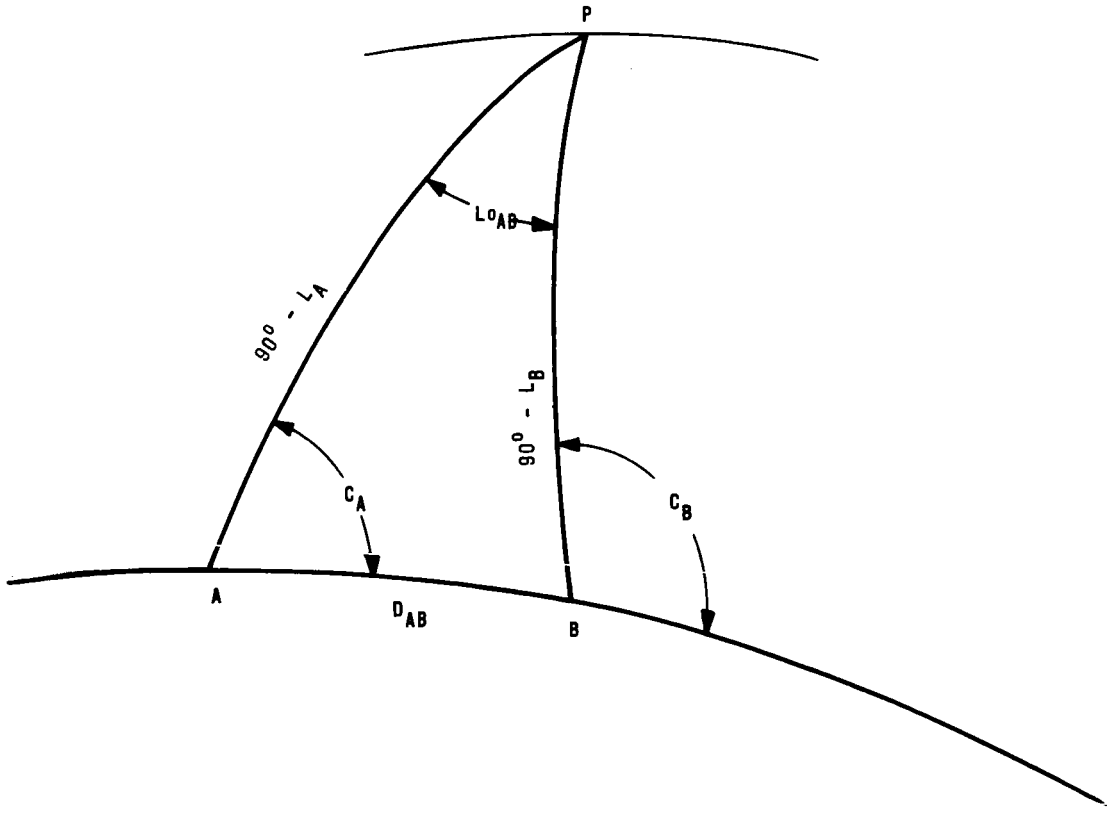

FIG. D.1 GREAT CIRCLE PATH

where Lo_{AB} is the difference in longitudes of A and B. The great circle course at B, the receiver, is then specified by C_B, given by

$$\cot C_B = \cot Lo_{AB} \cos (L_B + R) \operatorname{cosec} R.$$

The great circle distance is then found from

$$\cot D_{AB} = \tan (L_B + R) \cos C_B.$$

C_A is given by the same equation as C_B, i.e.,

$$\cot C_A = \cot Lo_{AB} \cos (L_A + R) \operatorname{cosec} R.$$

In performing all these computations strict regard must be had to the signs of the quantities. If the points of receiver and transmitter are in different hemispheres, the latitude of one must be regarded as negative with respect to the other, and they must be marked with opposite signs.

The coordinates of transmitter and receiver for the NSS-Wallops path are:

Wallops Main Base	37° 55.9' N, 75° 28.3' W
NSS - Annapolis, Md.	38° 59.4' N, 76° 27.8' W

The distance between NSS and Wallops is 1° 18.1' or 145 km, and the bearing at Wallops is N-36° 28.1' - W true.

APPENDIX E

RECEIVING SYSTEM

VLF INSTRUMENTATION IN JULY 1964

The block diagram of the steep-incidence VLF instrumentation utilized in July 1964 is shown in Figure E. 1. The abnormal loop is oriented with its electrical plane perpendicular to the plane of incidence and the earth's surface. The received signal is peak-detected and phase-compared with a standard reference frequency derived by means of a standard oscillator and frequency synthesizer. Outputs of the peak detector and phase meter are then applied to the dual-channel chart recorder. Consequently, relative amplitude and phase of the abnormal skywave component are recorded. Additionally, one-minute timing pulses are applied to the chart paper to facilitate scaling of the data.

VLF INSTRUMENTATION IN NOVEMBER 1964

In November, both the abnormal and the normal skywave components were recorded. As described previously, the normal antenna system responds to the normal skywave reduced by $E_1 \sin\theta$ (θ = angle of incidence). The normal system responds to E_1 (1 - sin θ), where E_1 is the downcoming normal skywave component; this is approximately equal to 0.3 E_1. However, noise which is arriving from all directions is little affected and the signal-to-noise ratio suffers. At times, the low signal/noise ratio makes data scaling difficult. This was overcome by designing and building a gated receiver.

Most VLF stations transmit conventional CW Morse traffic. The keying simply gates the master oscillator so the code elements are phase coherent. Nevertheless, the keying complicates the receiver design. The second complication caused by the Morse code is due also in part to the typically high Q of the VLF transmitting antennas. The Q is so high that the code elements become very rounded or "soft." The result is a shift in the phase of the code pulses during rise and fall times. This effect is shown in Figure E. 2 which is a record of the output of a phase meter during the transmission of conventional Morse code.

A block diagram of the system used in November is shown in Figure E. 3. A whip antenna feeds the ground wave of NSS (plus some normal skywave) to an Eddystone VLF receiver. The IF output is peak detected and clipped to avoid changes in signal amplitude deteriorating system performance. The signal is

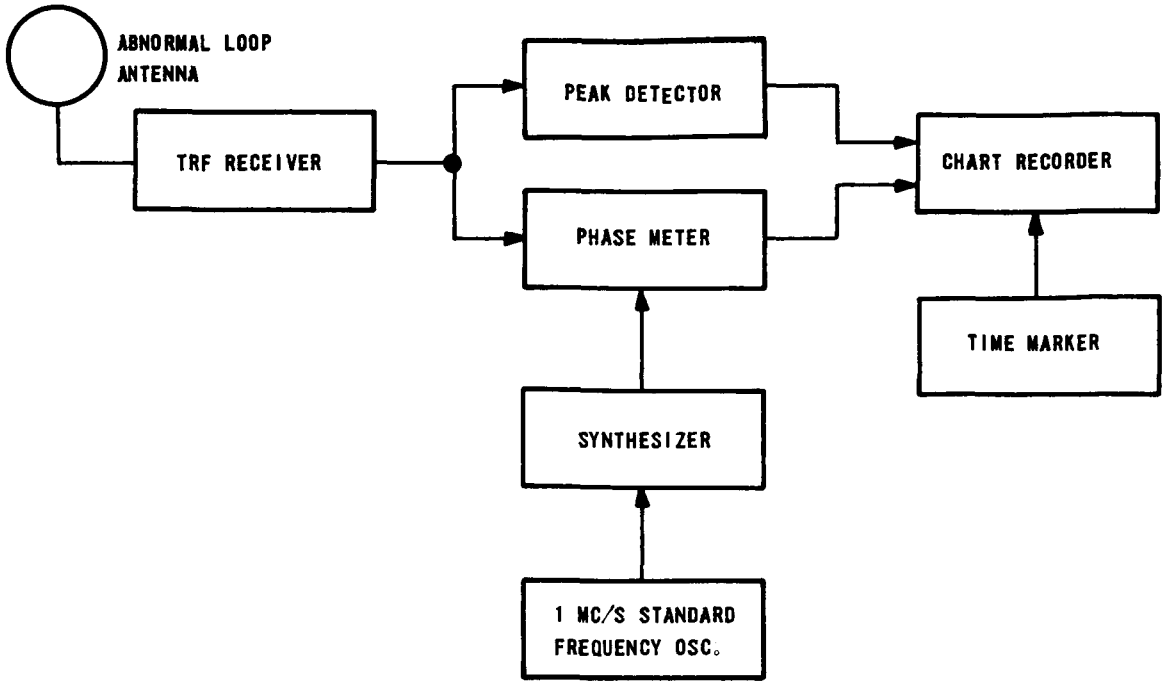

FIG. E.1 BLOCK DIAGRAM OF VLF EXPERIMENT IN JULY 1964

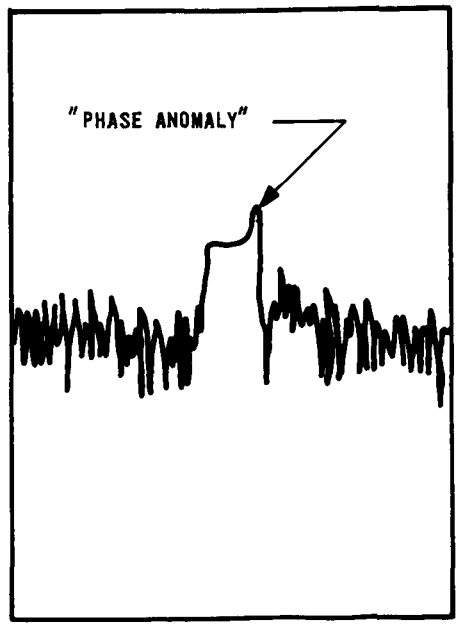

FIG. E.2 RISE AND DECAY TIME PHASE ANOMALY DUE TO HIGH-Q TRANSMITTING ANTENNA

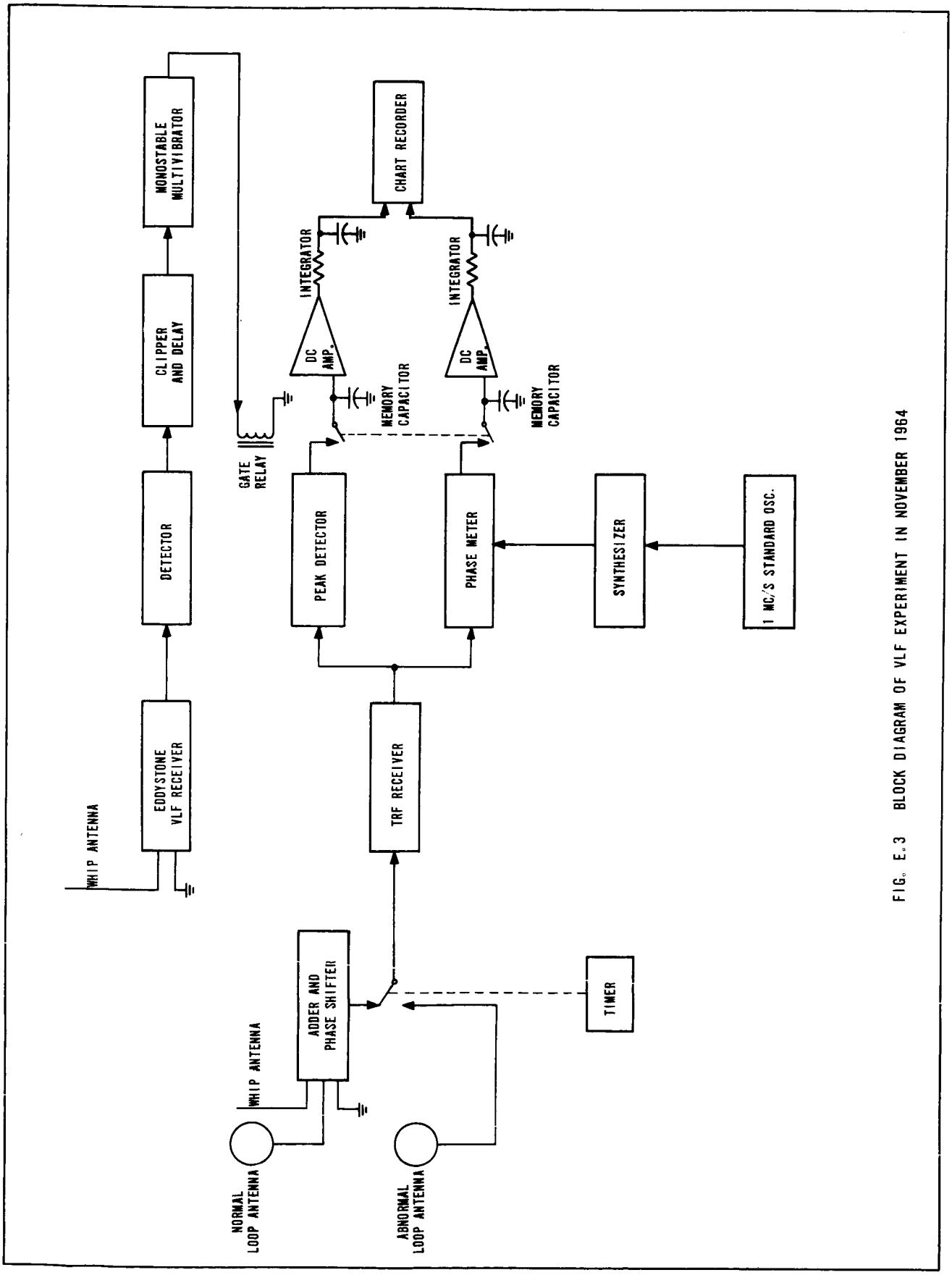

FIG. E.3 BLOCK DIAGRAM OF VLF EXPERIMENT IN NOVEMBER 1964

delayed and then used to fire a monostable multivibrator. The delay and multivibrator ON times are chosen so that the multivibrator is ON only during the constant-phase region of the Morse code elements. These time relations are shown in Figure E.4. Each Morse element is treated as if it were a Morse dot, the shortest element.

A reed relay, controlled by the multivibrator, switches the output of the phase meter across a capacitor only during the times of constant phase. At other times the relay opens and the capacitor holds its charge. The capacitor remembers the phase between those times when it can be read accurately.

The technique for measuring amplitude is very similar. The relay closes during a flat-topped portion of each dot or dash and the capacitor is charged by a peak detector each time. If the amplitude drops, the capacitor will discharge through the switch.

Each capacitor drives a DC amplifier having a high input impedance. Using a 1 μf capacitor results in a 100-second memory. This time constant does not reduce the system time constant; the capacitor can charge or discharge through the switch within the duration of Morse dot. The system response time, at the capacitor, is limited only by the rate at which Morse code is sent.

The DC amplifiers couple the capacitor voltage to a filter. The amplitude filter, which has a one-second time constant, smooths variations due to noise and provides a cleaner, more accurate record. This system responds to the peak-signal level and is not affected by the duty cycle of the transmitter. The phase-output filter also has a time constant of one second. The output of this filter is a DC voltage directly proportional to phase. Since the phase meter is a synchronous detector, the system S/N and resolution is improved by this post-detection integration.

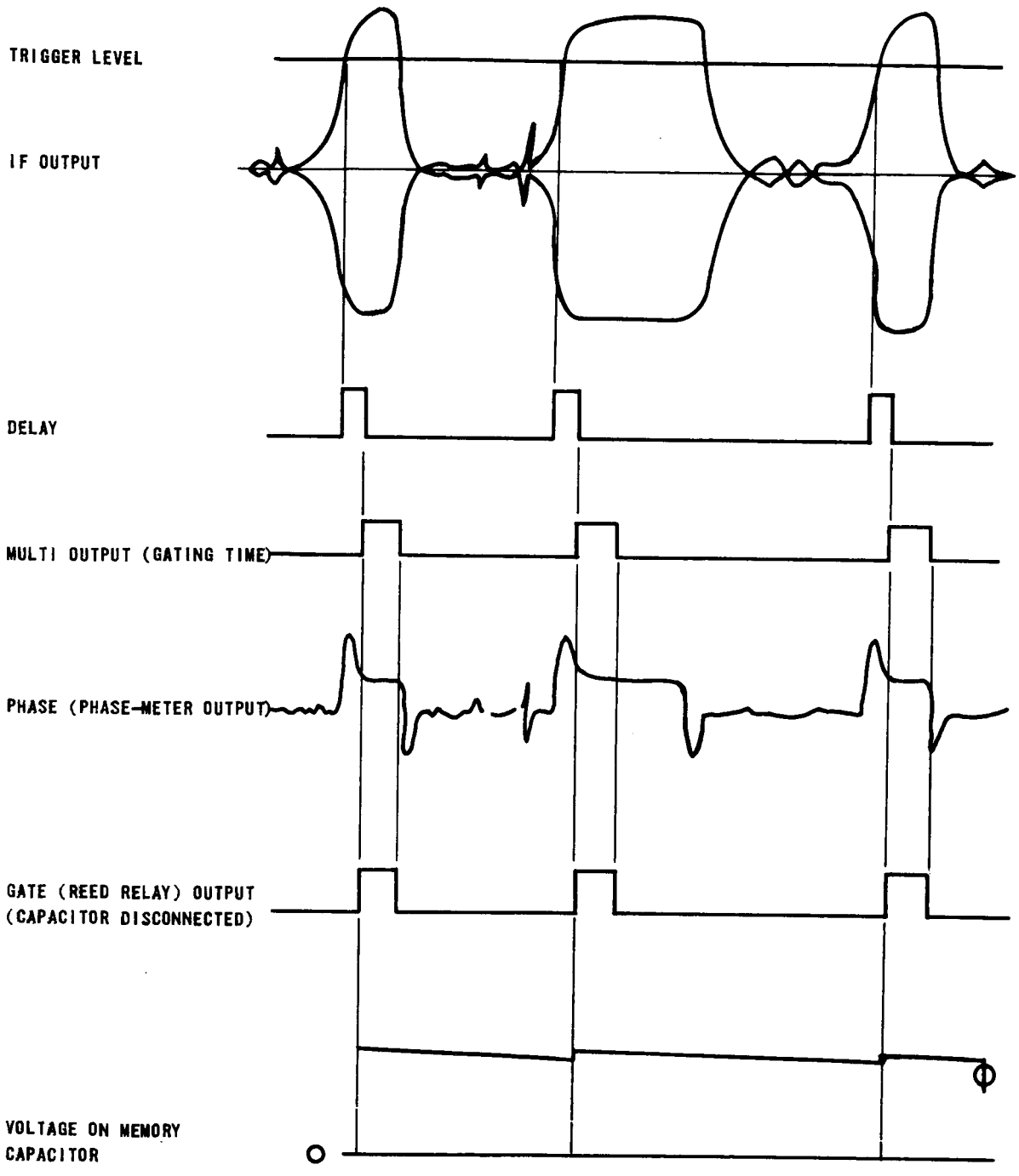

FIG. E.4 TIME RELATIONS FOR GATED RECEIVER PHASE MEASUREMENT

Reverse (Page 64) Blank

APPENDIX F

VLF DATA FOR NOVEMBER 1964

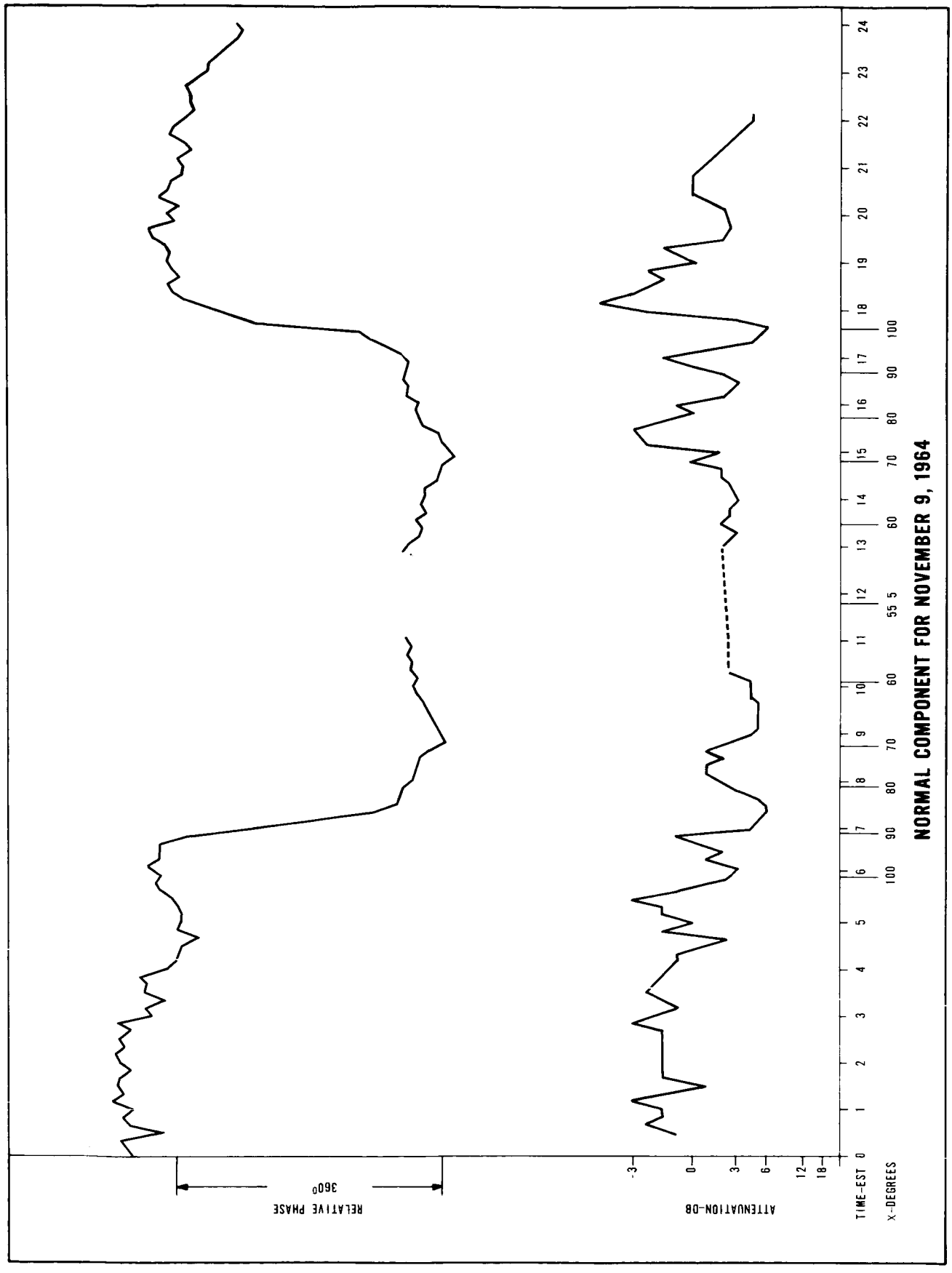

Reverse (Page-68-) Blank

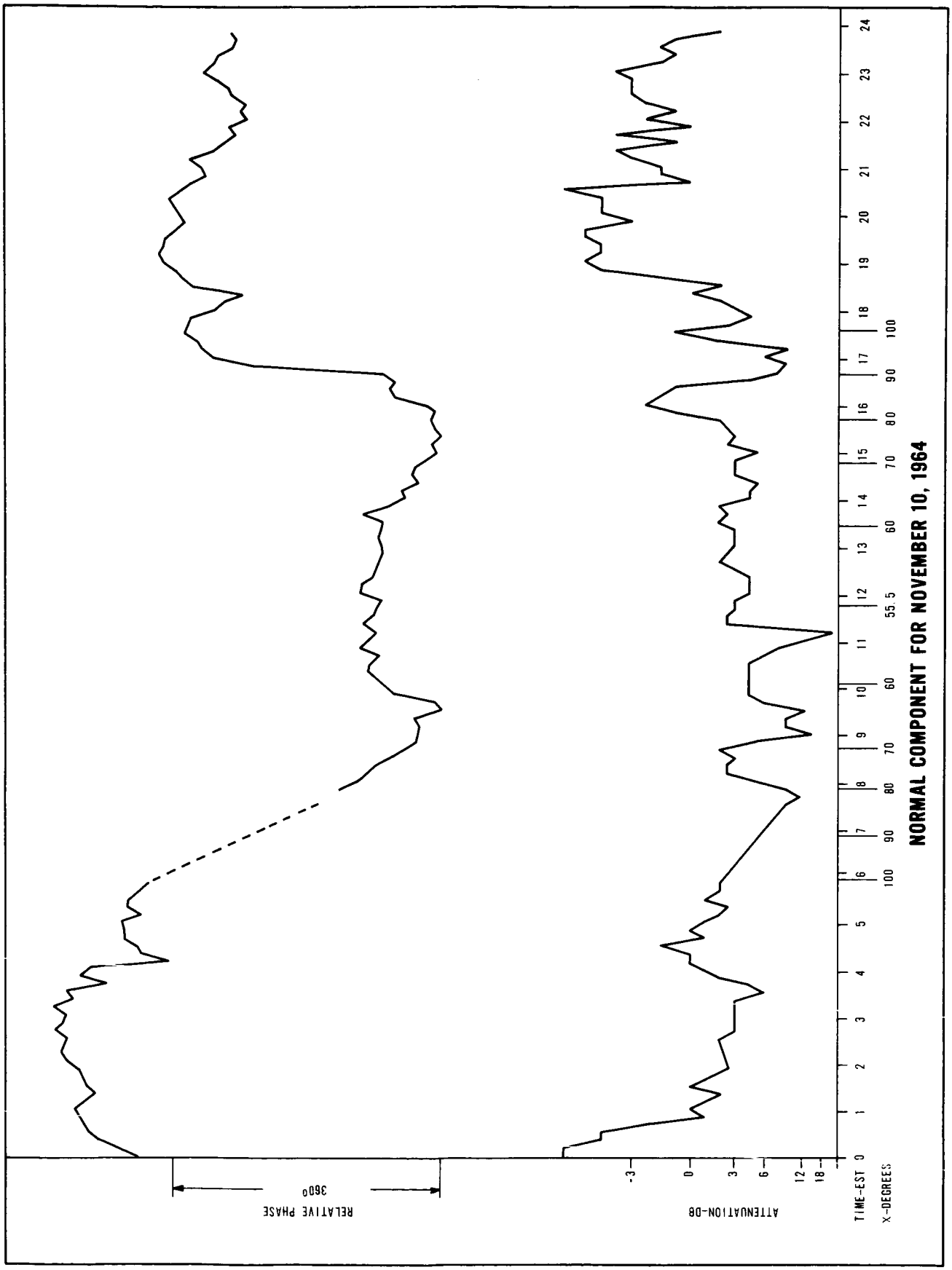

Reverse (Page-70-) Blank

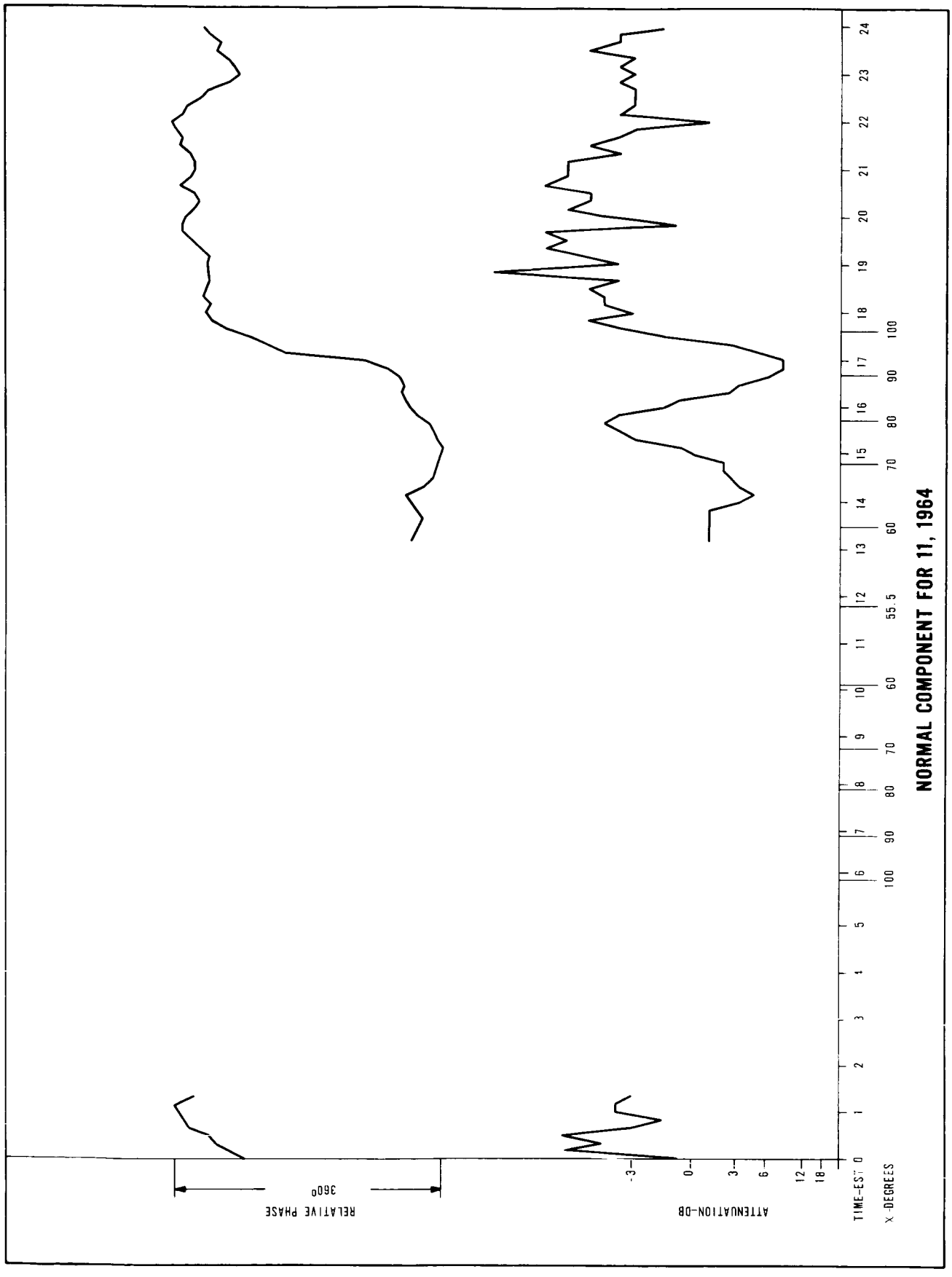

Reverse (Page-72-) Blank

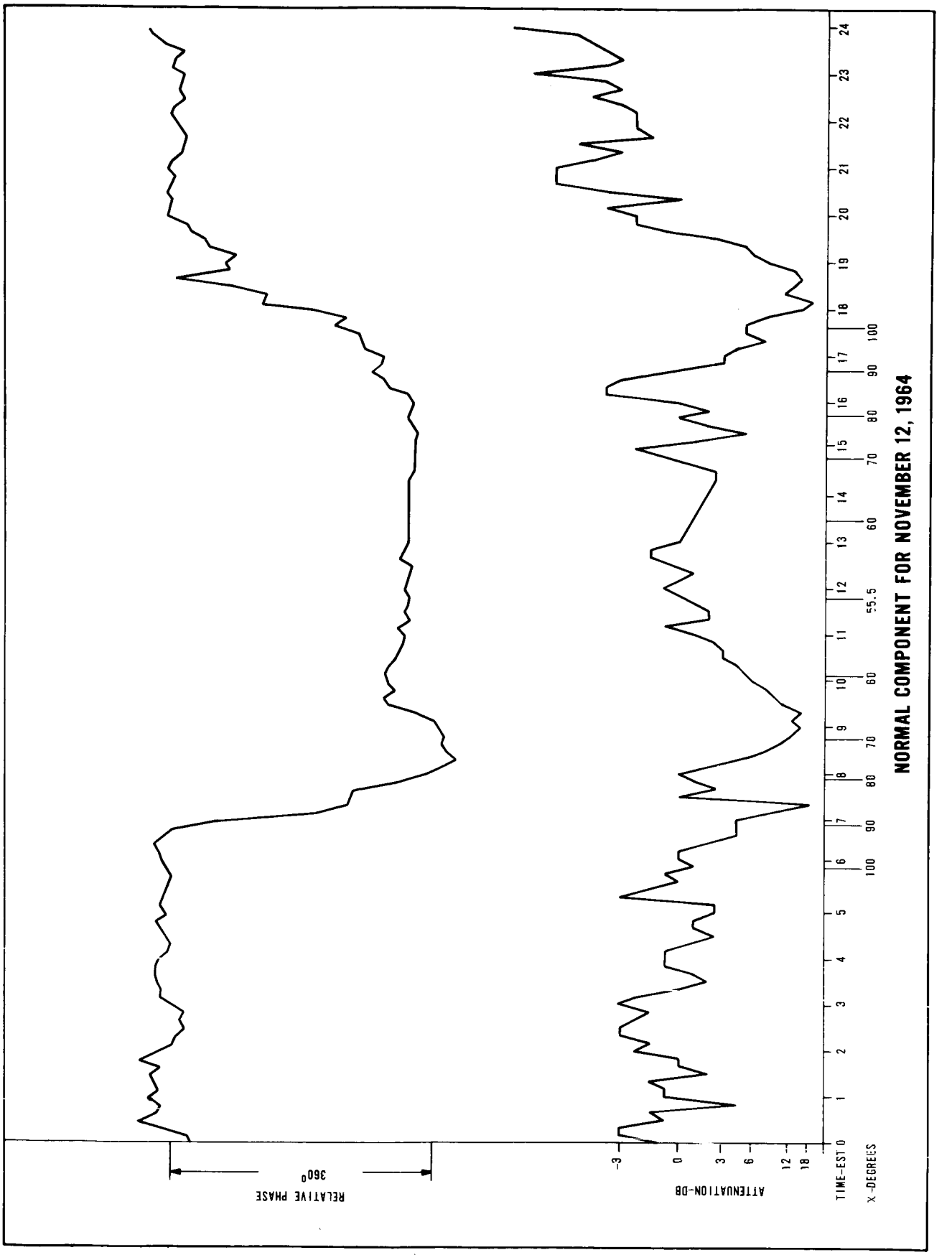

Reverse (Page-74-) Blank

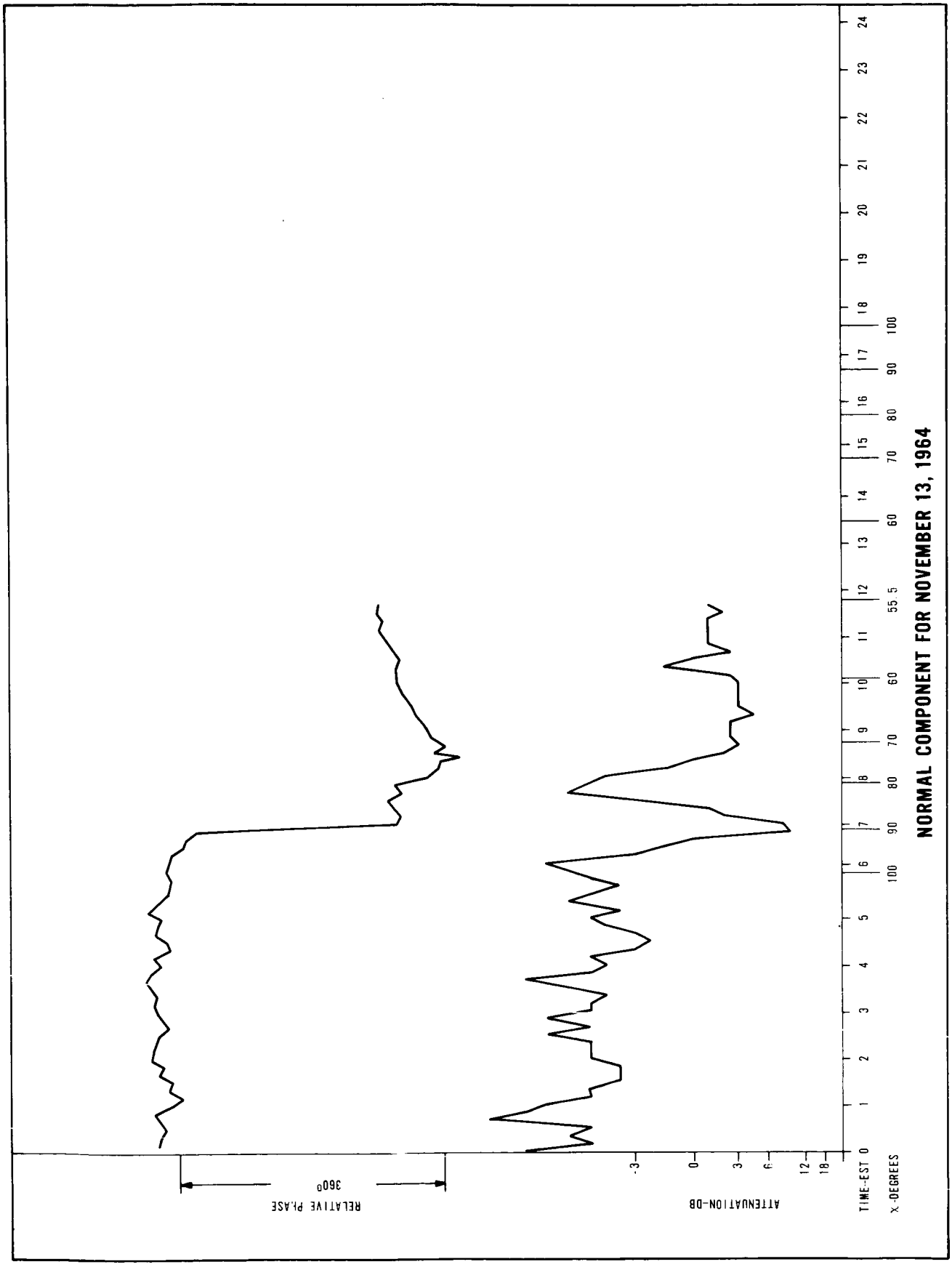

Reverse (Page-76-) Blank

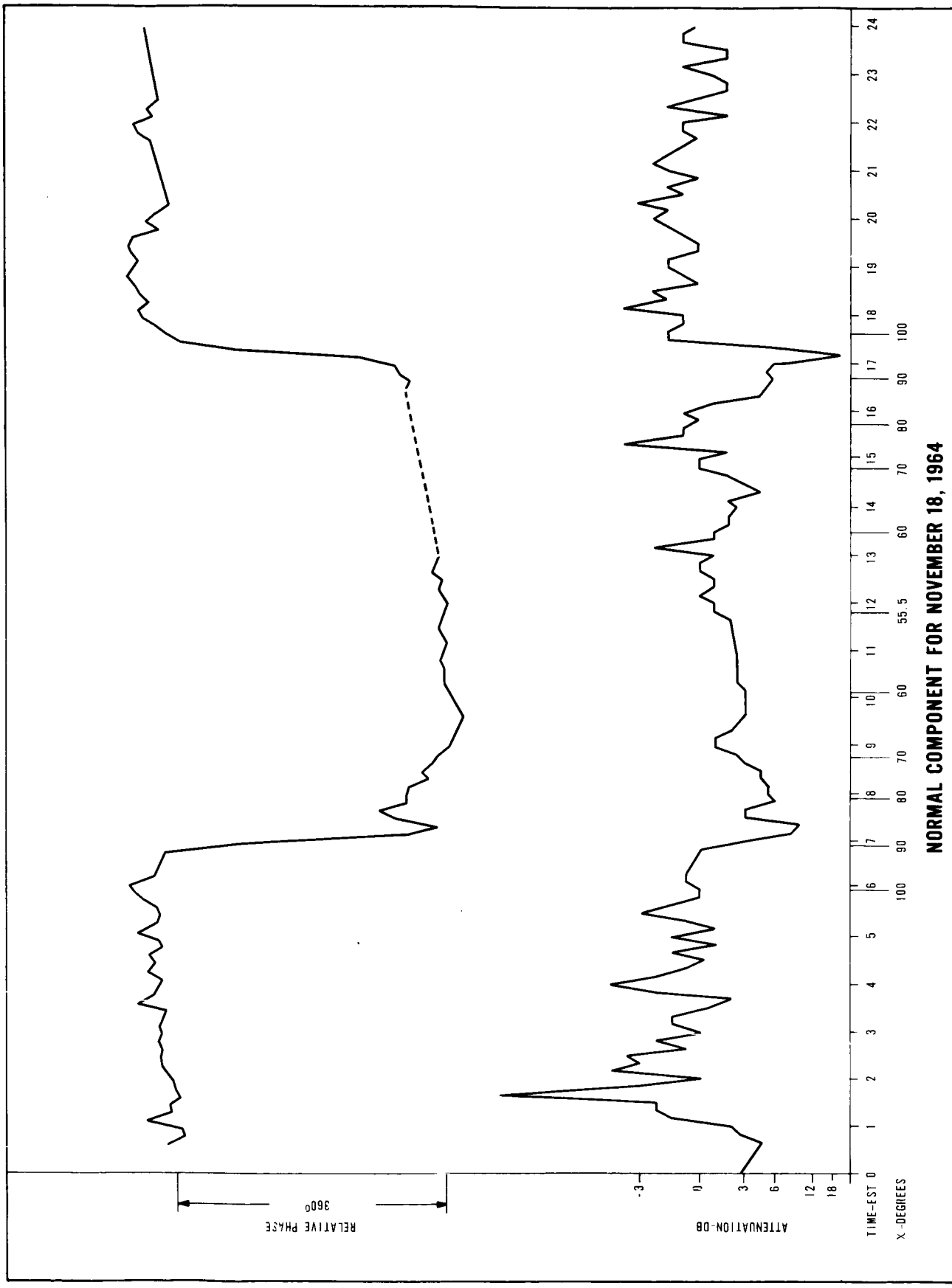

Reverse (Page-78-) Blank

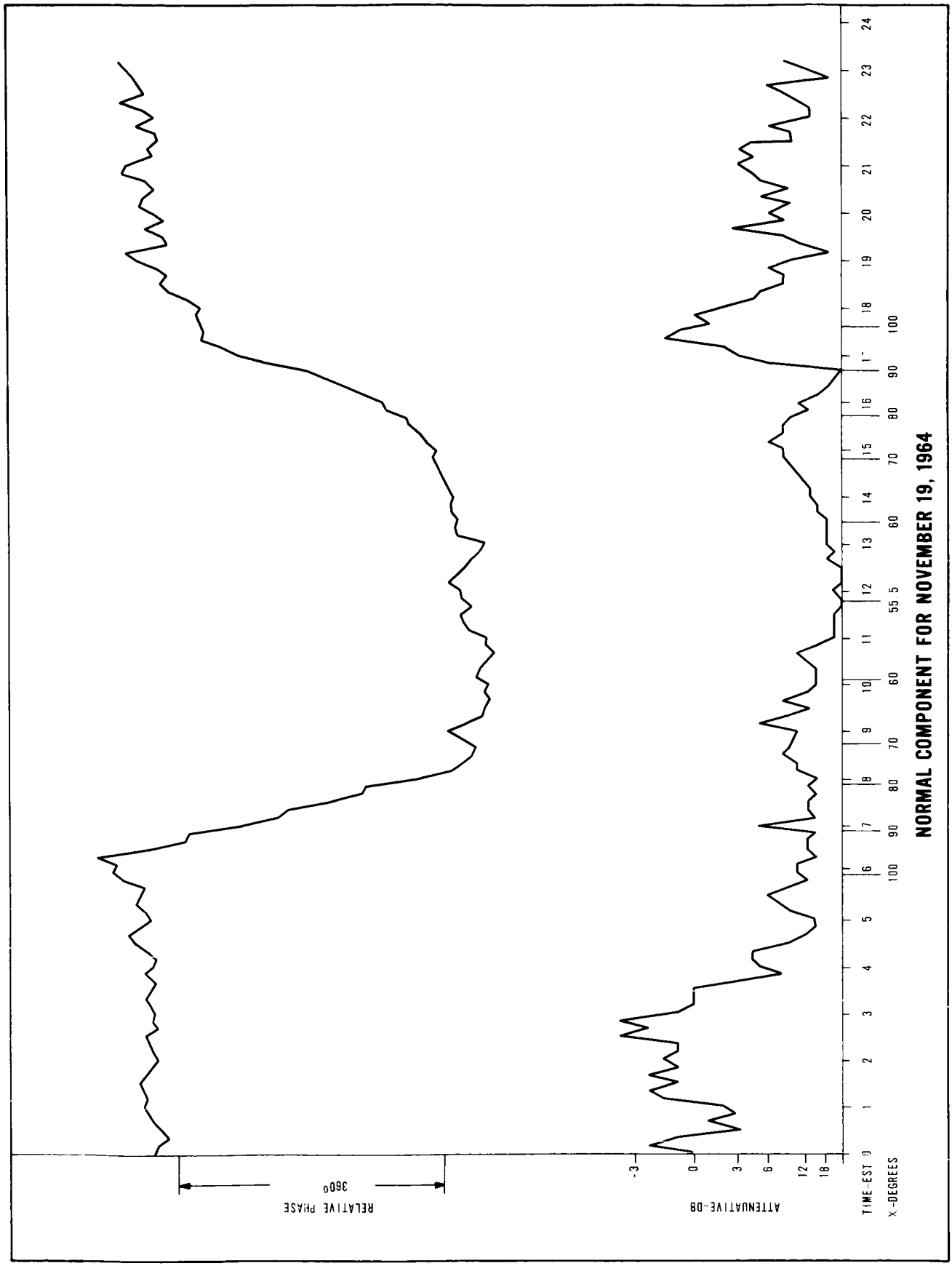
NORMAL COMPONENT FOR NOVEMBER 19, 1964
RELATIVE PHASE
360°
ATTENUATIVE-DB
-3
0
3
6
12
18
TIME-EST
X-DEGREES
1
2
3
4
5
6
7
8
9
10
11
12
13
14
15
16
17
18
19
20
21
22
23
24
100
90
80
70
60
55 5
60
70
80
90
100

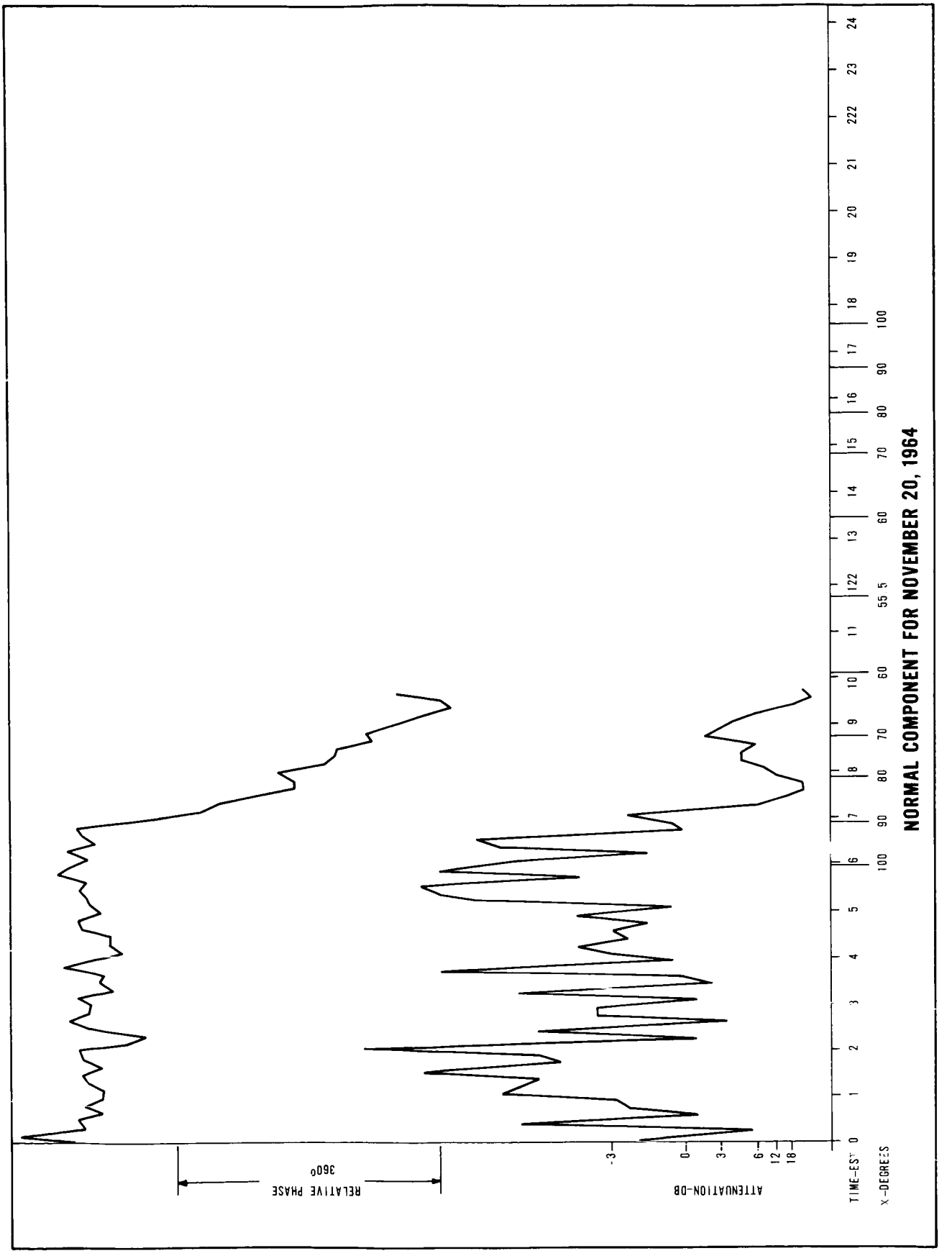

Reverse (Page-82-) Blank

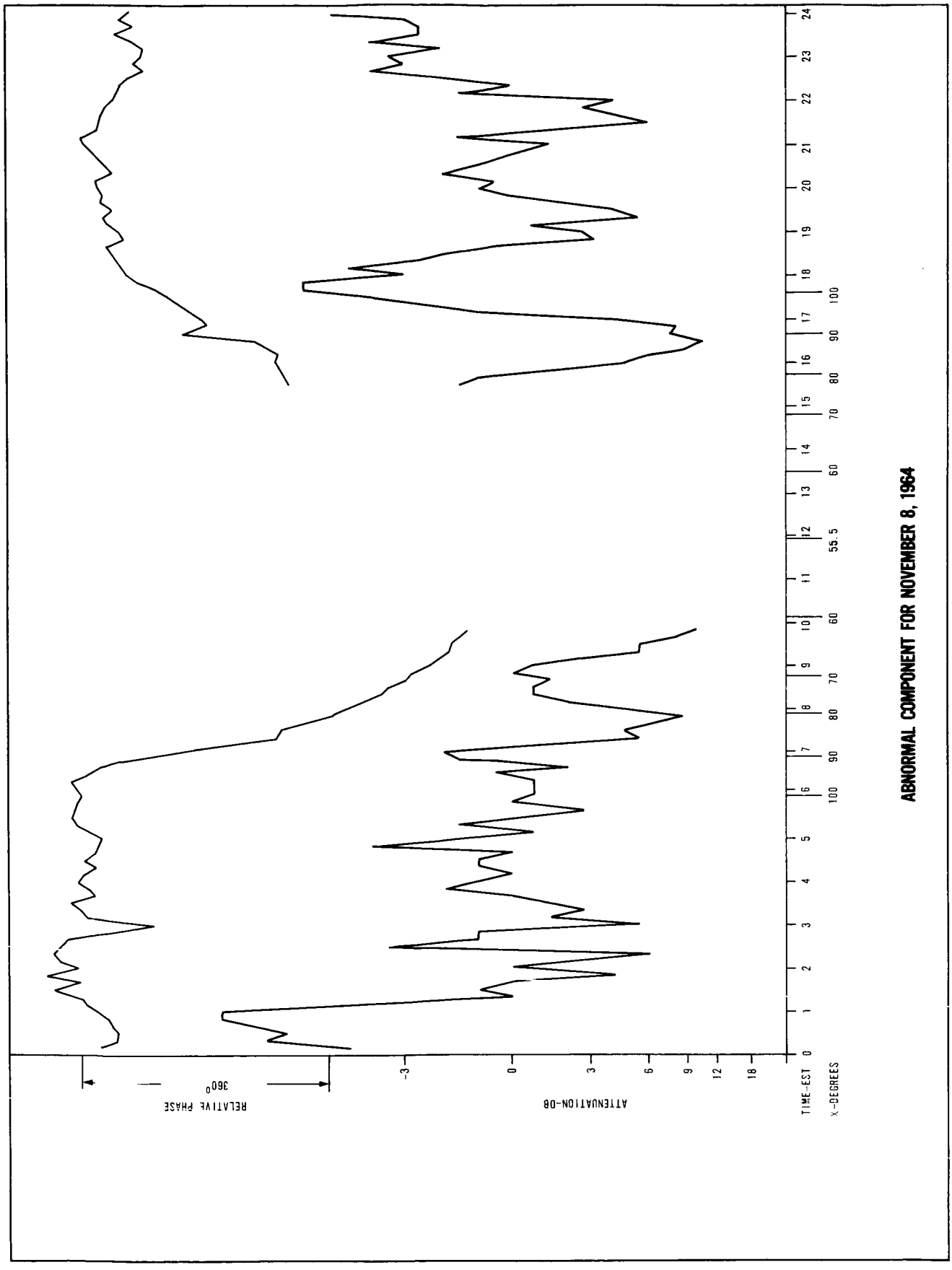

Reverse (Page-84-) Blank

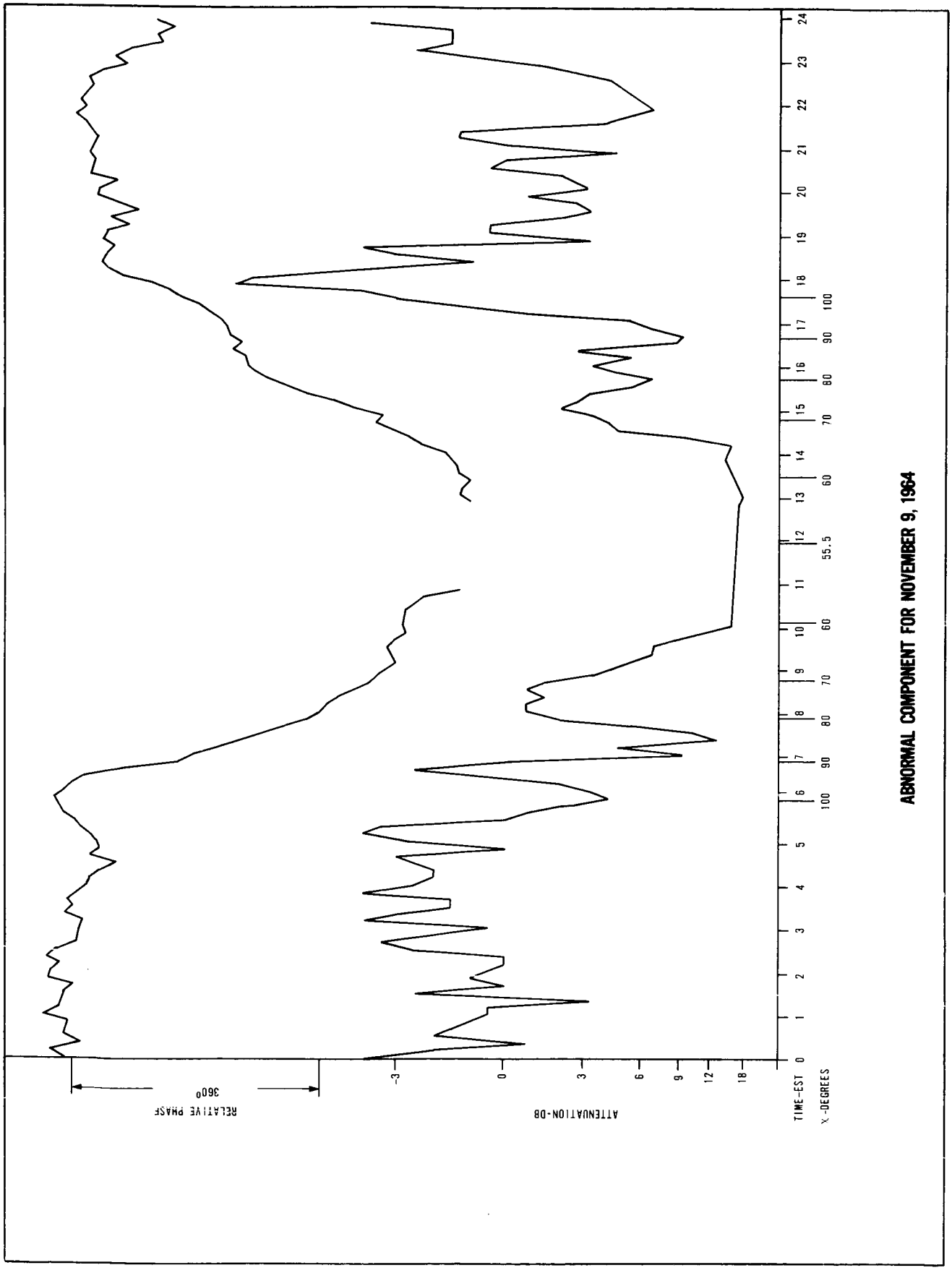

Reverse (Page-86-) Blank

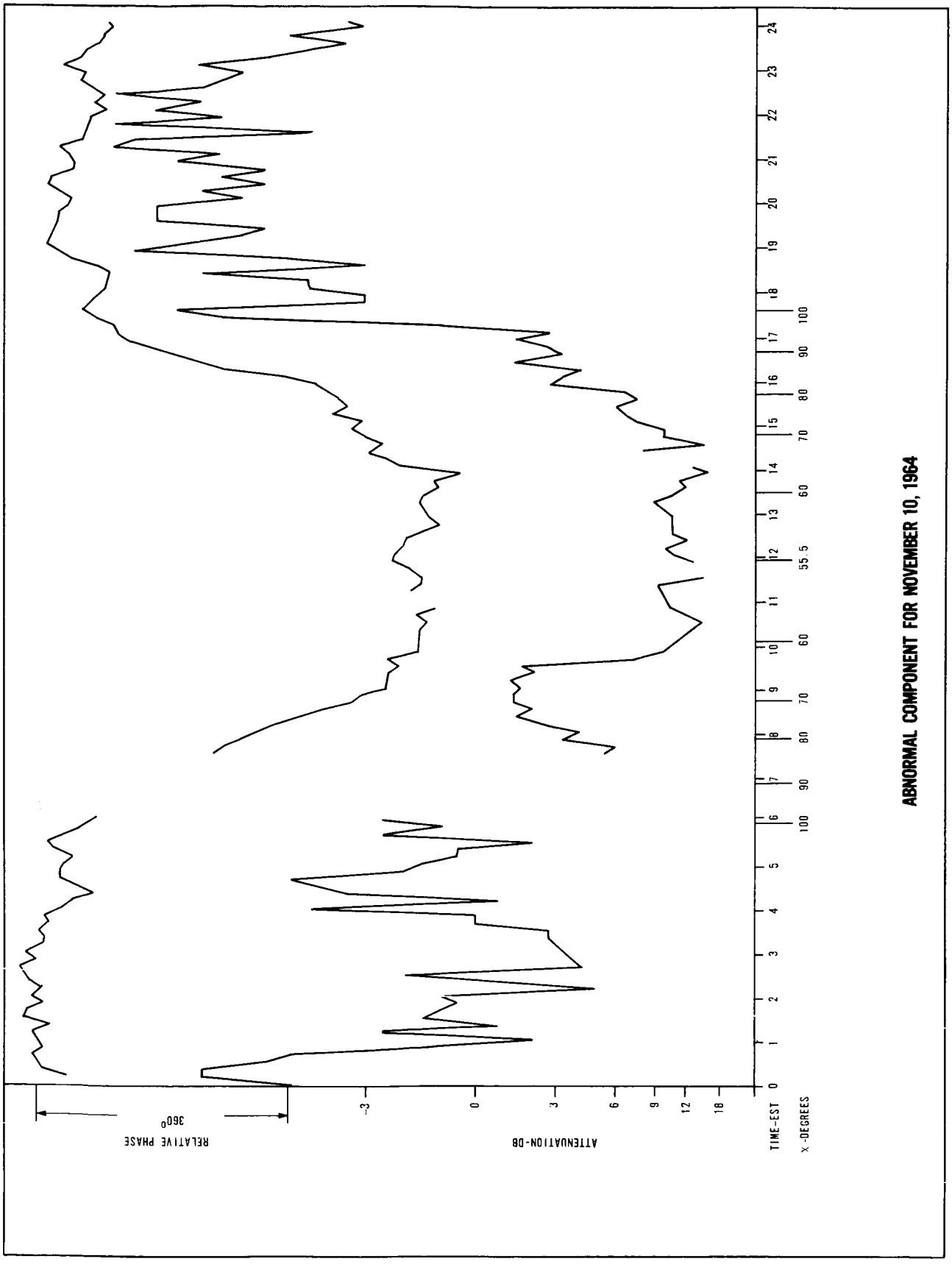

Reverse (Page-88-) Blank

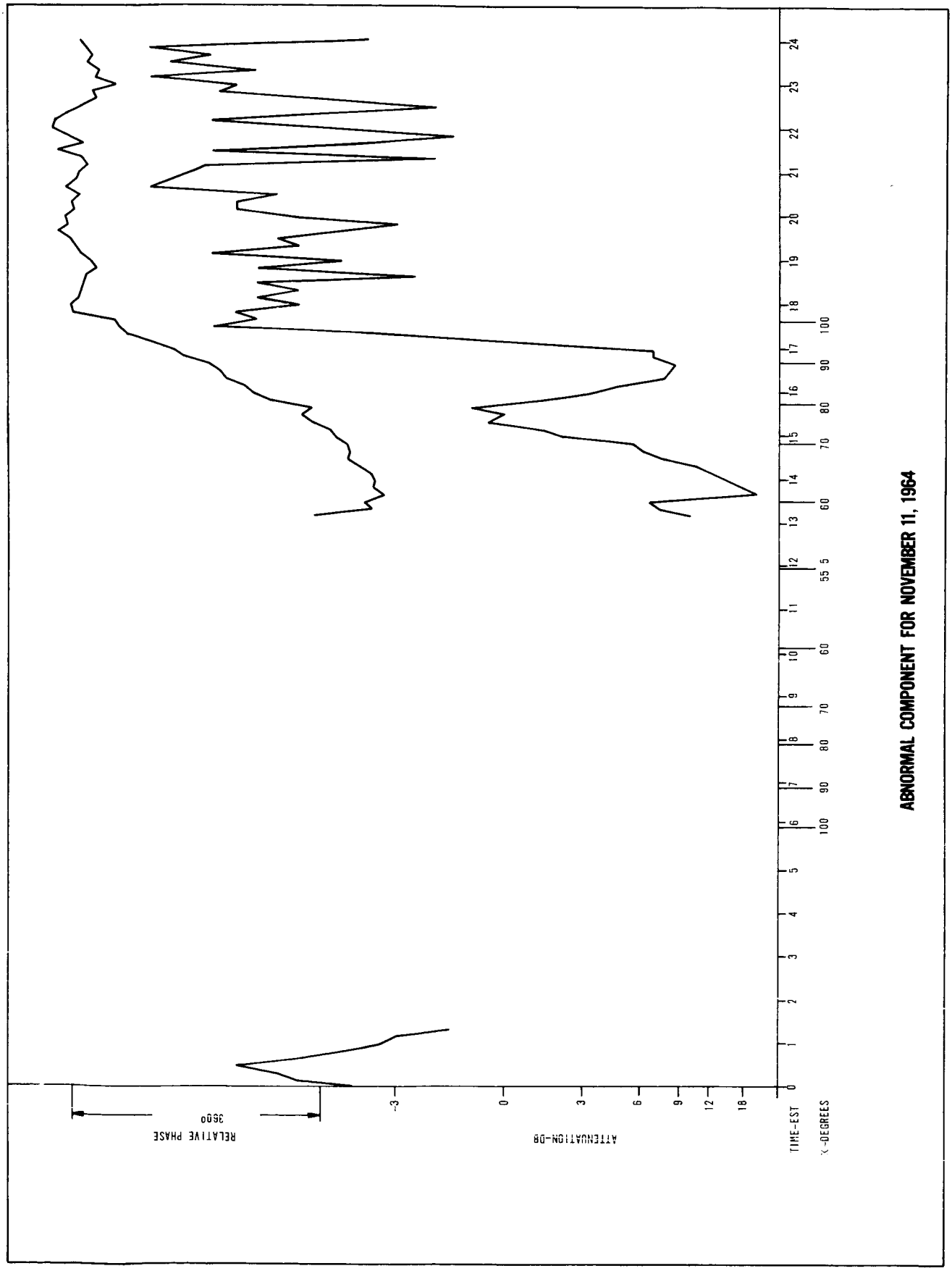
ABNORMAL COMPONENT FOR NOVEMBER 11, 1964
RELATIVE PHASE
360°
ATTENUATION-DB
-3
0
3
6
9
12
18
TIME-EST
X-DEGREES

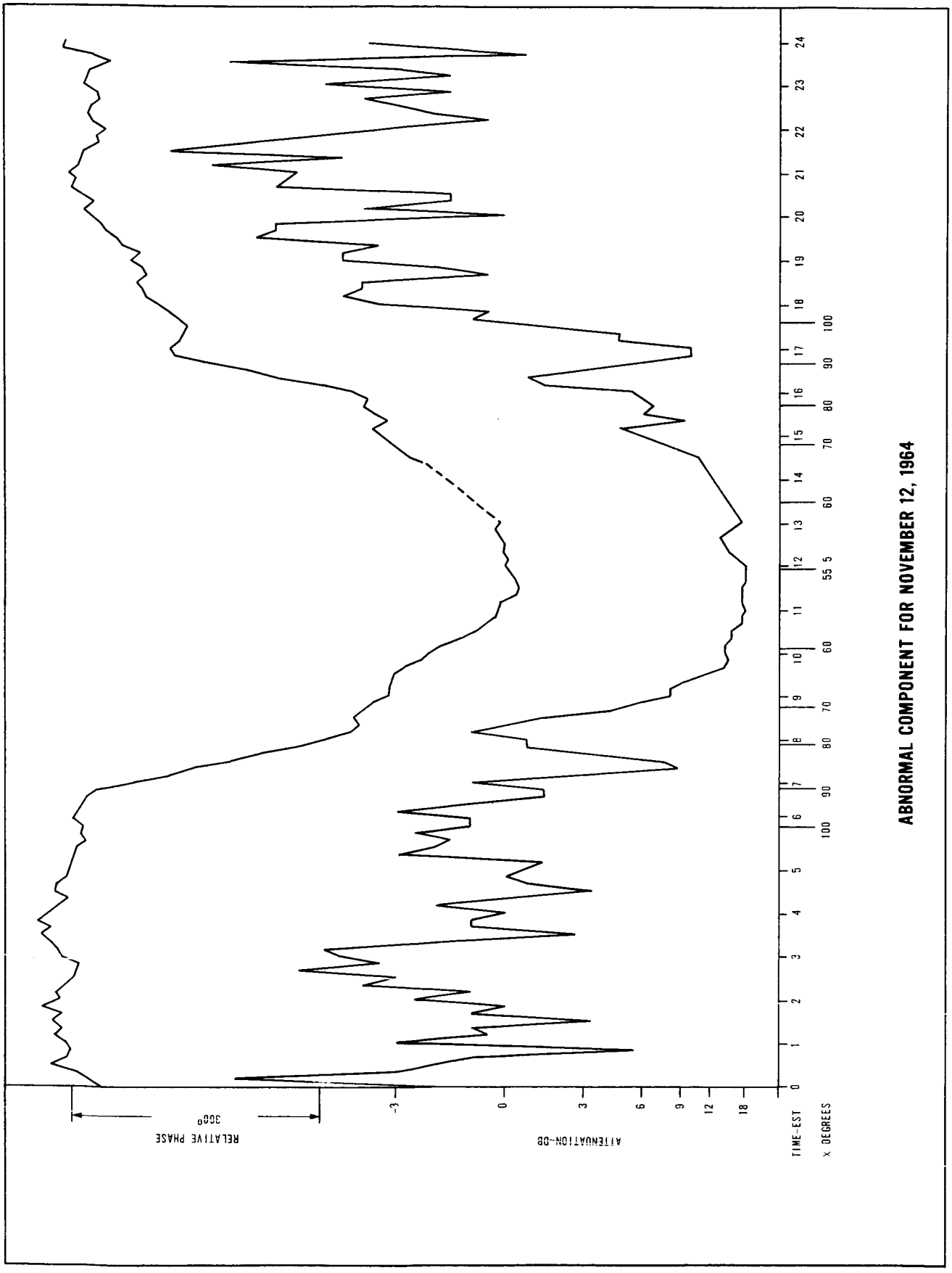

Reverse (Page-92-) Blank

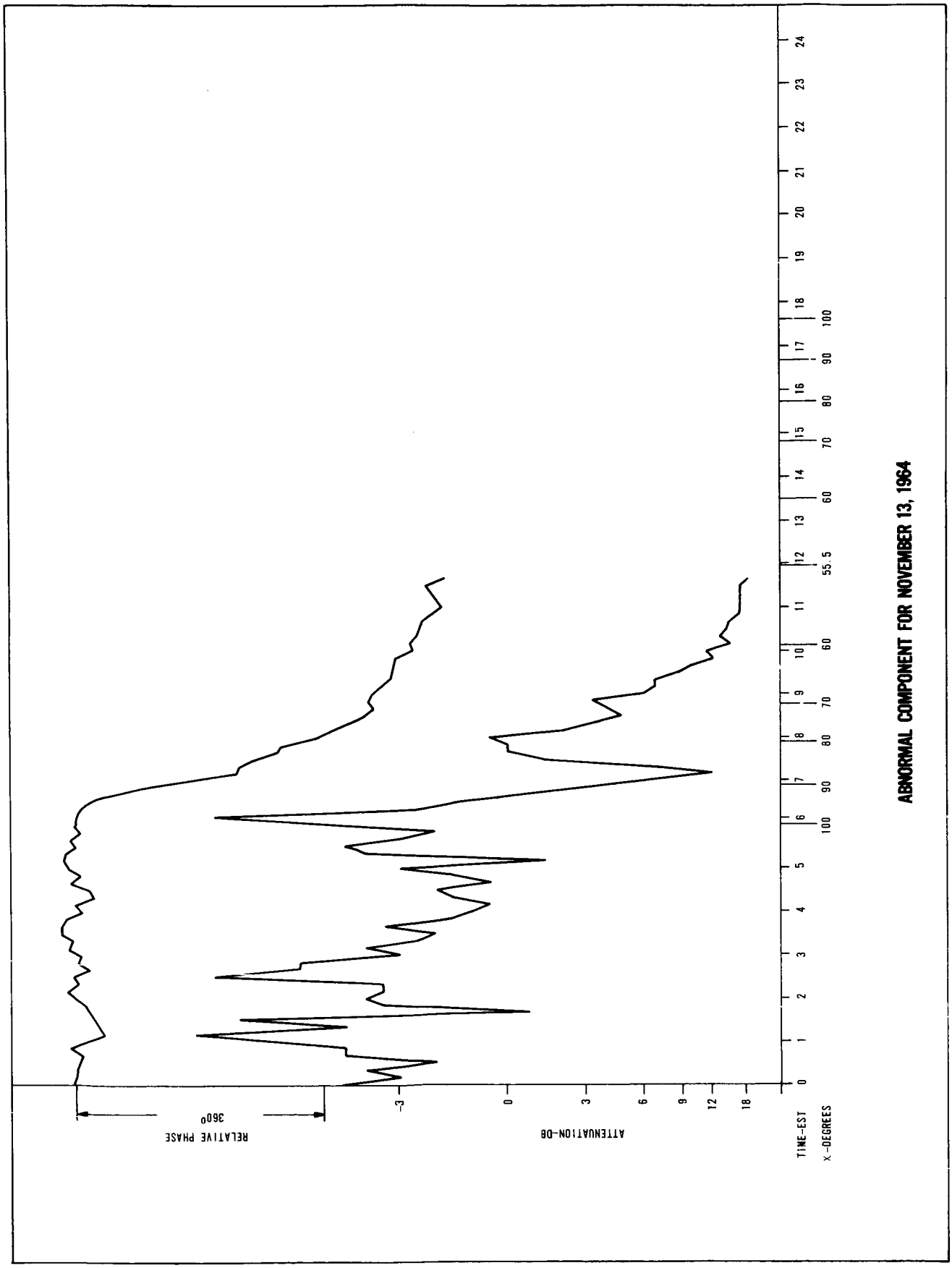

Reverse (Page-94-) Blank

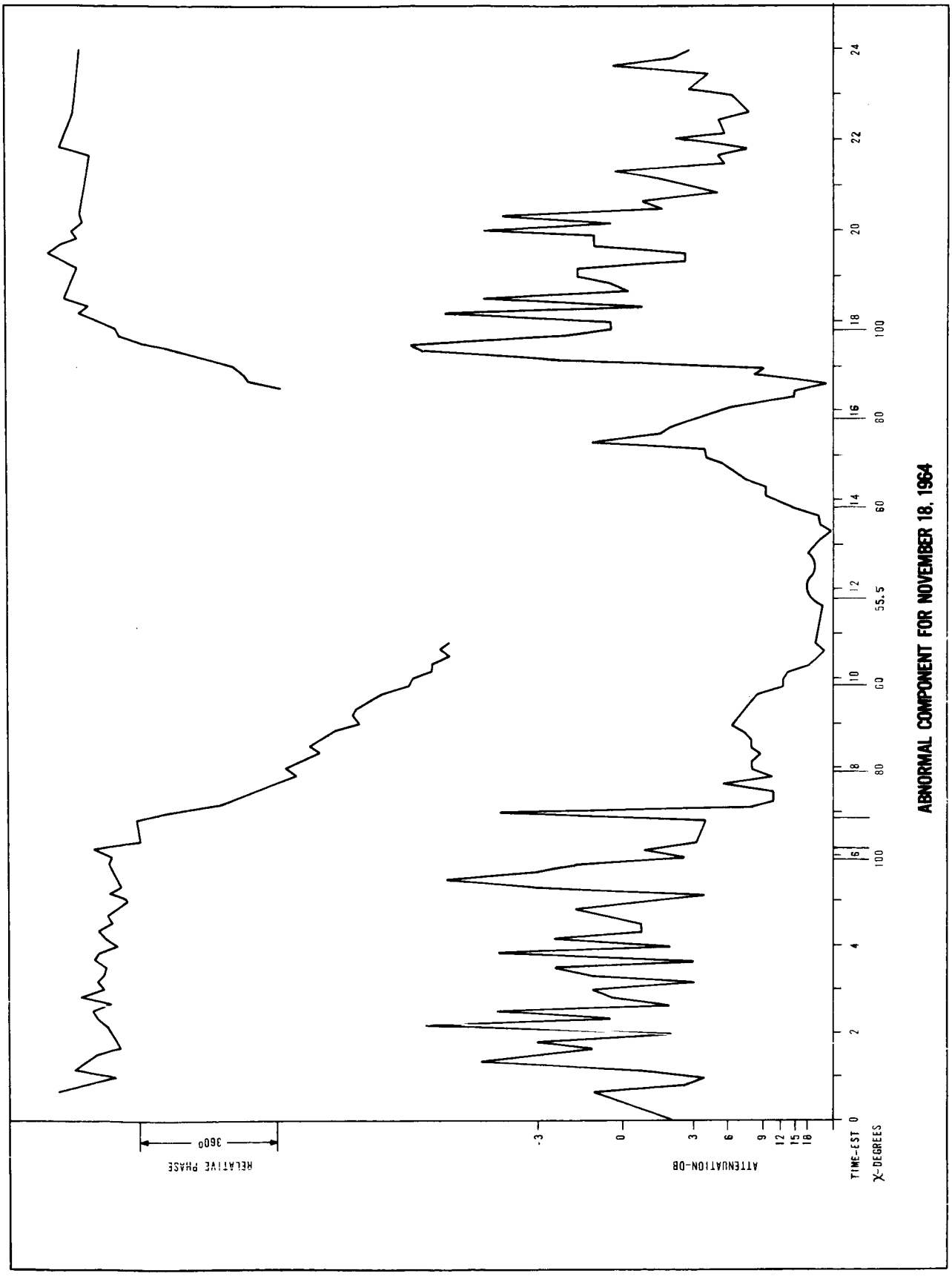

Reverse (Page-96-) Blank

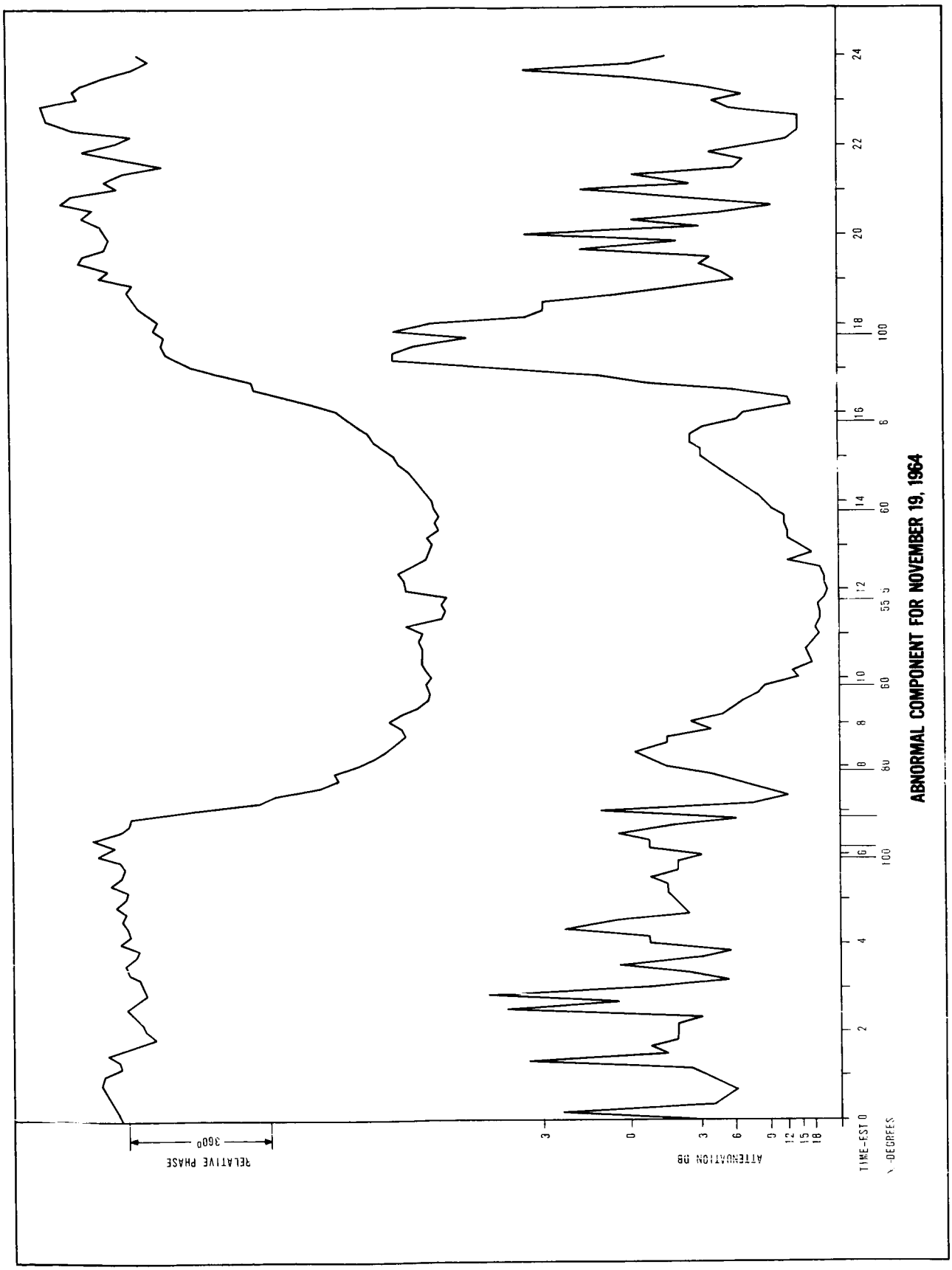
ABNORMAL COMPONENT FOR NOVEMBER 19, 1964
RELATIVE PHASE
360°
ATTENUATION DB
3
0
3
6
9
12
15
18
TIME-EST
DEGREES

REFERENCES

Aikin, A.C., The Sunrise Absorption Effect Observed at Low Frequencies, JATP, 23, 287-300, 1961.

Aikin, A.C., A Preliminary Study of Sunrise Effects in the D-Region, Electron Density Profiles in the Ionosphere and Exosphere, edited by B. Maehlum, The Macmillan Co., New York, 1962.

Aikin, A.C., J.A. Kane and J. Troim, Some Results of Rocket Experiments in the Quite D-Region, JGR, 69, 4621-4628, 1964.

Barrington, R.E., B. Landmark, O. Holt and E. Thrane, Experimental Studies of the Ionospheric D-Region, NDRE Report No. 44, 1962.

Barrington, R.E. and E. Thrane, The Determination of D-Region Electron Densities from Observations of Cross Modulations, JATP, 24, 31-42, 1962.

Barrington, R.E., E.V. Thrane and B. Bjelland, Diurnal and Seasonal Variations in D-Region Electron Densities Derived from Observations of Cross Modulation, Can. J. Physics, 41, 271-285, 1963.

Belrose, J.S. and M.J. Burke, Study of the Lower Ionosphere using Partial Reflection 1. Experimental Technique and Methods of Analysis, JGR, 69, 2799-2818, 1964.

Belrose, J.S. and L.W. Hewitt, the Variability of Electron Number Density in the Lowest Ionosphere Over Ottawa in Winter, presented at the Spring URSI/IEEE Meeting, 20-24 April 1965, Washington, D.C.

Best, J.E., J.A. Ratcliffe and M.V. Wilkes, Experimental Investigations of Very Long Waves Reflected from the Ionosphere, Proc. Roy. Soc. A, 156, 614-633, 1936.

Bowhill, S.A. and G.G. Kleiman, An Integrated Experiment for the Study of the Aeronomy of the D-and E-Regions of the Ionosphere, presented at the Fall URSI/IEEE Meeting, 12-14 October 1964, Urbana, Illinois.

Bowhill, S.A. and L.G. Smith, Rocket Observations of the Lower Ionosphere at Sunrise and Sunset, presented at the 1965 COSPAR meeting, May 1965, Argentina.

Bracewell, R.N., K.G. Budden, J.A. Ratcliffe, T.W. Straker and K. Weekes,

The Ionospheric Propagation of Low and Very Low Frequency Radio Waves Over Distances Less Than 1000 km, Proc. I.E.E. (Part III), 98, 221-236, 1951.

Bracewell, R.N., The Ionspheric Propagation of Radio Waves of Frequency 16 kc/s Over Distances of about 200 km, Proc. I.E.E. (Part IV), 99, 217-228, 1952.

Bracewell, R.N. and W.C. Bain, An Explanation of Radio Propagation at 16 kc/s in Terms of Two Layers below E-Layer, JATP, 2, 216-225, 1952.

Brown, S.B. and W. Petrie, The Effect of Sunrise on the Reflection Height of Low Frequency Waves, Can. Jour. Physics, 32, 90-98, 1954.

Burke, M.J. and E.H. Hara, Tables of the Semiconductor Integrals $C_p(X)$ and Their Approximations for use with Generalized Appleton-Hartree Magneto-Ionic Formulas, DRTE Report No. 1113, May 1963.

Chapman, S., Proc. Phys. Soc., 43, 26-, 1931.

Chapman, S., Proc. Phys. Soc., 43, 483-, 1931.

Deeks, D.G., Some Tentative Suggestions of Electron Density Profiles in the D-Region, Internal Memorandum No. 121, Radio and Space Research Station, Slough, England.

Deeks, D.G., D-Region Electron Distributions in Middle Latitudes Deduced from the Reflection of Long Radio Waves, Internal Memorandum No. 219, Radio and Space Research Station, Slough, England.

Donahue, T.M., A Note on Polar Blackouts, JATP, 20, 76-79, 1961.

Fejer, J.A. and R.W. Vice, An Investigation of the Ionospheric D-Region, JATP, 16, 291-306, 1959.

Gregory, J.B., The Influence of Atmospheric Circulation on Mesospheric Electron Densities in Winter, J. Atmos. Sciences, 22, 18-23, 1965.

Hargreaves, J.K., The Behavior of the Lower Ionosphere near Sunrise, JATP, 24, 1-7, 1962.

Holt, O., Some Experimental Studies of the Ionospheric D-Region at High Latitudes, NDRE Report No. 46, 1963.

REFERENCES (Cont'd)

Hopkins, H. G. and L. G. Reynolds, An Experimental Investigation of Short-Distance Ionospheric Propagation at Low and Very Low Frequencies, Proc. I. E. E. (Part III), 101, 21-34, 1954.

Hultqvist, B., On the Height Distribution of the Ratio of Negative Ion and Electron Densities in the Lowest Ionosphere, JATP, 25, 225,-240, 1963.

Hultqvist, B., Reply to "On the Height Distribution of the Ratio Negative Ion and Electron Densities in the Lowest Ionosphere," JATP, 26, 145-150, 1964.

Hultqvist, B., Studies of Ionospheric Absorption of Radio Waves by the Cosmic Noise Method, Radio Astronomical and Satellite Studies of the Atmosphere, edited by Jules Aaons, North-Holland Publishing Co., Amsterdam, 1963.

Kane, J. A., Re-evaluation of Ionospheric Electron Densities and Collision Frequencies Derived from Rocket Measurements of Refractive Index and Attenuation, JATP, 23, 338-347, 1961.

Landmark, B., and F. Lied, Observation of the D-Region from a Study of Ionospheric Cross Modulation, JATP, 23, 92-100, 1961.

Moler, W. F., VLF Propagation Effects of a D-Region Layer Produced by Cosmic Rays, JGR, 65, 1459-1468, 1960.

Nicolet, M. and A. C. Aikin, The Formation of the D-Region of the Ionosphere, JGR, 65, 1469-1483, 1960.

Reid, G. C., A Study of the Enchanced Ionization Produced by Solar Protons during a Polar Cap Absorption Event, JGR, 66, 4071-4085, 1961.

Reid, G. C., and H. Leinbach, Morphology and Interpretation of the Great Polar Cap Absorption Events of May and July 1959, JATP, 23, 216-228, 1961.

Reid, G. C., Physical Processes in the D-Region of the Ionosphere, Reviews of Geophysics, 2, 311-333, May 1964.

Reid, G. C., D. K. Bailey and H. Leinbach, On the Height Distribution of the Ratio of Negative Ion and Electron Densities in the Lowest Ionosphere, JATP, 26, 145-147, 1964.

Sechrist, C. F. and J. M. Musser, Variation of the VLF Conversion Coefficient During the Sunrise Transition, presented at the Fall URSI/IEEE Meeting, 12-14 October 1964, Urbana, Illinois.

REFERENCES (Cont'd)

Sechrist, C. F. and J. M. Musser, Sunrise and Sunset Changes in VLF Radio Waves Ionospherically Reflected Near Vertical Incidence, presented at the Spring URSI/IEEE Meeting, 20-24 April 1965, Washington, D. C.

Sen, H.K. and A. A. Wyller, On the Generalization of the Appleton-Hartree Magnetoionic Formulas, JGR, 65, 3931-3950, 1960.

Stewart, J. Q. and N. L. Pierce, Marine and Air Navigation, Ginn and Co., New York, 1944.

Straker, T. W., The Ionospheric Propagation of Radio Waves of Frequency 16 kc/s Over Short Distances, Proc. I. E. E. (Part C) 102, 122-133, 1955.

Swider, W., Sunrise Geometry and the Optical Depth Factor, Sci. Report No. 164, Ionos. Res. Lab., The Penna. State Univ., 1962.

Wagner, K. U., Investigation of the State of the Lower Ionosphere During Sunrise, Geomagnetizm i Aeronomiya, 4, 90-101, 1964.

Weekes, K. and R. D. Stuart, The Ionospheric Propagation of Radio Waves with Frequencies Near 100 kc/s Over Short Distances, Proc. I. E. E. (Part IV), 99, 29-37, 1951.